UNCLASSIFIED

AD NUMBER

AD234776

NEW LIMITATION CHANGE

TO

Approved for public release, distribution unlimited

FROM

Distribution authorized to U.S. Gov't. agencies and their contractors; Administrative/Operational Use; May 1959. Other requests shall be referred to Director, Wright Air Development Center, Wright-Patterson AFB, OH 45433.

AUTHORITY

AFAL ltr, 17 Aug 1979

THIS PAGE IS UNCLASSIFIED

WADC TECHNICAL REPORT 53-173
PART VI

A STUDY OF RAIN EROSION TESTING METHODS FOR SUPERSONIC SPEED

Donald E. Hurd
Roy F. Holmes

Thermodynamics Laboratories
Convair, A Division of General Dynamics Corporation

JANUARY 1960

This report is not to be announced or distributed automatically to foreign governments (AFR 205-43A, paragraph 6d).

Statement A
Approved for Public Release

WRIGHT AIR DEVELOPMENT CENTER

NOTICES

When Government drawings, specifications, or other data are used for any purpose other than in connection with a definitely related Government procurement operation, the United States Government thereby incurs no responsibility nor any obligation whatsoever; and the fact that the Government may have formulated, furnished, or in any way supplied the said drawings, specifications, or other data, is not to be regarded by implication or otherwise as in any manner licensing the holder or any other person or corporation, or conveying any rights or permission to manufacture, use, or sell any patented invention that may in any way be related thereto.

- - - - -

Qualified requesters may obtain copies of this report from the Armed Services Technical Information Agency, (ASTIA), Arlington Hall Station, Arlington 12, Virginia.

- - - - -

Copies of WADC Technical Reports and Technical Notes should not be returned to the Wright Air Development Center unless return is required by security considerations, contractual obligations, or notice on a specific document.

WADC TECHNICAL REPORT 53-173
PART VI

A STUDY OF RAIN EROSION TESTING METHODS FOR SUPERSONIC SPEEDS

Donald E. Hurd
Roy F. Holmes

Thermodynamics Laboratories
Convair, A Division of General Dynamics Corporation

JANUARY 1960

Materials Laboratory
Contract No. AF 33(616)-3421
Project No. 7340

WRIGHT AIR DEVELOPMENT CENTER
AIR RESEARCH AND DEVELOPMENT COMMAND
UNITED STATES AIR FORCE
WRIGHT-PATTERSON AIR FORCE BASE, OHIO

500 – February 1960 – 23-648

FOREWORD

This report was prepared by the Convair Division of General Dynamics under United States Air Force Contract No. AF 33(616)-3421. This contract was initiated under Project No. 7340, "Non-Metallic and Composite Materials," Task No. 73400, "Organic and Inorganic Plastics." The Materials Laboratory, Directorate of Laboratories, Wright Air Development Center, directed the project with Mr. S. A. Marolo as Project Engineer. Work at the Convair Thermodynamics Laboratories was under the direction of Mr. R. F. Holmes.

This report covers the work period of October 1957 through May 1959.

ABSTRACT

To better understand the mechanism by which materials passing through rain at supersonic speeds are damaged, the results of numerous types of impacts on metals were analyzed.

An equation which relates total energy of impact to the volume of metal displaced was derived and found adequate to explain damage in the velocity range from less than one foot per hour to greater than Mach 3. This equation together with results of incidence angle tests led to an overall damage equation which was successfully applied to the problem of multiple drop rain damage. Principal parameters are target material tensile strength; impacting material shape and mass; angle of incidence; and the velocity of impact.

Facility improvements and test method refinements are described.

PUBLICATION REVIEW

This report has been reviewed and is approved.

FOR THE COMMANDER:

W E Dirkes

W. E. DIRKES
Chief, Plastics Branch
Non-Metallic Materials Division

TABLE OF CONTENTS

		Page
OBJECTIVE		1
INTRODUCTION		2
I.	IMPROVEMENT OF THE SINGLE DROP CAPTURED PROJECTILE FACILITY	3
II.	DAMAGE CONTOUR STUDY	5
III.	ANGLE STUDY	7
IV.	DAMAGE EQUATION DEVELOPMENT	8
V.	INFLUENCE OF HIGH STRAIN RATES ON THE EFFECTIVE TARGET YIELD STRENGTH	23
VI.	MULTIPLE DROP RAIN DAMAGE STUDY	26
VII.	SUMMARY	29
VIII.	BIBLIOGRAPHY	30
	APPENDIX I - ANGLE STUDY DATA AND CALCULATIONS	93
	APPENDIX II - DERIVATION OF EQUATIONS USED IN THE COMPUTATION OF ENERGIES AND VOLUMES	94

LIST OF TABLES

Table		Page
I.	Low Velocity Data - Steel Ball Brinell Tests on Lead	31
II.	Low Velocity Data - Steel Ball Brinell Tests on Polyethylene	34
III.	Moderate Velocity Data - Steel Indenter Drop Tests on 1100-0 Aluminum	36
IV.	High Velocity Impact Data - Mercury Drops	39
V.	High Velocity Impact Data - Steel Balls and Water Drops. . .	49

LIST OF ILLUSTRATIONS

Figure		Page
1.	Time Delay Generator and Drop Release System	50
2.	Schematic Diagram	51
3.	Drop Tester	52
4.	Damage Mark Contour - Cylindrical Indenter	53
5.	Normalized Damage Mark Contour - Cylindrical Indenter . . .	54
6.	Normalized Damage Mark Contour - Conical Indenter - 90° Included Angle	55
7.	Depth vs $\frac{\text{Travel}}{\text{Cylinder Radius}}$	56
8.	Drop Height vs Penetration Depth for Drop Tester - Cylindrical Indenter	57
9.	Drop Height vs Penetration Depth for Drop Tester - Conical and Spherical Indenters	58
10.	Impact Energy vs Volume Displaced for Drop Tester - Cylindrical Indenter	59
11.	Impact Energy vs Volume Displaced for Drop Tester - Conical and Spherical Indenters	60
12.	Slope M of "Energy vs Displace Volume Curve" vs Target Tensile Strength	61
13.	$v_o^2 - v^2$ vs An Expression Containing Gamma	62
14.	Energy vs Volume - Low Velocity - Lead No. 1	63
15.	Energy vs Volume - Low Velocity - Lead No. 2	64
16.	Energy vs Volume - Low Velocity - Polyethylene	65
17.	Energy vs Volume - 1100-0 Aluminum - 1.0 mm Mercury . . .	66

LIST OF ILLUSTRATIONS (Continued)

Figure		Page
18.	Energy vs Volume - 1100-0 Aluminum - 1.5 mm Mercury . . .	67
19.	Energy vs Volume - 1100-0 Aluminum - 1.6 mm Mercury . . .	68
20.	Energy vs Volume - 1100-0 Aluminum - 1.0 mm Steel Ball . .	69
21.	Energy vs Volume - 2024 Aluminum - 1.0 mm Mercury . . .	70
22.	Energy vs Volume - 2024 Aluminum - 2.0 mm Mercury . . .	71
23.	Energy vs Volume - 2024 Aluminum - 2.0 mm Water	72
24.	Energy vs Volume - 7075-T4 Aluminum - 1.5 mm Mercury . .	73
25.	Energy vs Volume - Copper - 1.0 mm Mercury	74
26.	Energy vs Volume - Copper - 2.0 mm Mercury	75
27.	Energy vs Volume - Lead - 1.5 mm Mercury	76
28.	Energy vs Volume - Lead - 2.85 mm Mercury.	77
29.	Energy vs Volume - Lead - 2.0 mm Water	78
30.	Energy vs Volume - Cold Rolled Steel (Annealed) 1.5 mm Mercury	79
31.	Energy vs Volume - Stainless Steel - 1.50 mm Mercury . . .	80
32.	Gamma vs Impact Velocity - 1100-0 Aluminum - 1.6 mm Mercury	81
33.	Gamma vs Impact Velocity - 1100-0 Aluminum - 1.0 mm Stainless Steel Sphere	82
34.	Gamma vs Impact Velocity - 2024 Aluminum - 1.0 mm Mercury.	83
35.	Gamma vs Impact Velocity - 2024 Aluminum - 2.0 mm Mercury.	84

LIST OF ILLUSTRATIONS (Continued)

Figure Page

36. Gamma vs Impact Velocity - 2024 Aluminum 2.0 mm Water. . . 85

37. Gamma vs Impact Velocity - Copper - 1.0 mm Mercury 86

38. Gamma vs Impact Velocity - Copper - 2.0 mm Mercury 87

39. Gamma vs Impact Velocity - Lead - 1.5 mm Mercury. 88

40. Gamma vs Impact Velocity - Lead - 2.85 mm Mercury 89

41. Gamma vs Impact Velocity - Cold Rolled Steel (Annealed) - 1.5 mm Mercury 90

42. Gamma vs Impact Velocity - 321 Stainless Steel - 1.5 mm Mercury 91

43. Dynamic Yield Stress/Static Yield Stress vs Average Rate of Strain - Mild Steel 92

OBJECTIVE

This study was undertaken to develop practical methods for testing materials for rain erosion resistance at supersonic speeds, to determine the mechanisms through which this erosion takes place, and to conduct an evaluation of materials and specimen shapes using the methods developed.

Manuscript released by the authors 9 June 1959 for publication as a WADC Technical Report.

INTRODUCTION

A program of study of supersonic rain erosion testing techniques and material evaluation has been active at the Convair Thermodynamics Laboratories since 1952. This program has for the past three years concentrated on the free ballistics method for material evaluation; the captured projectile method for single drop impacts; and the rocket sled method for full scale radome erosion studies.

This report describes the activity on the captured projectile single drop impact phase and certain theoretical free ballistics tests during the period of October 1957 through July 1958.

I. IMPROVEMENT OF THE SINGLE DROP CAPTURED PROJECTILE FACILITY

To improve the accuracy with which single drop impacts were made and to improve the reliability of the data obtained therewith, several changes were made in the facility[5] and testing method. First, to obtain specimen recovery over a greater velocity range, the length of the steel capture tube was increased from 100 to 200 feet in length. In addition, the projectile design was changed so that weight was minimized by both projectile construction and material. The projectiles are now of 7075-T6 aluminum instead of steel with washers made of the same material instead of copper. Nitrocellulose rifle power (Dupont No. 4227) was found to increase the velocity range to greater than 5000 feet per second. To increase timing accuracy of the magnetic pickups used to determine velocities, it was necessary to use a Berkley counter which measured time to 10^{-6} second - one significant figure greater than had been used formerly.

All the above improvements were made to increase the velocity range and velocity measuring capabilities of the system. To obtain usable data, however, it was now necessary to develop a method for producing large numbers of accurately measured drops to be hit by the passing projectile. After many tries at developing a multiple drop system for obtaining accurately measured and rigorously controlled drop sizes, the conclusion was drawn that this system would not be possible without adding extreme complexity and additional expense. Even when individual drop sizes could be detected by various pressure pickup means, the sizes were not reproducible to the extent that the drops could be used on the firing range without a large probability of size variance. The decision was made to utilize a single drop method which employed the use of a cadmium selenide photo cell. The single drops are individually weighed in small test tubes on an analytical balance and dropped in the path of a sample tipped projectile. To coordinate the position of the drop at any given instant, and the point at which the drop would be hit by the projectile, a time delay generator was developed. During a firing sequence, a test tube containing one of the weighed drops is allowed to tilt allowing its drop to fall through a tube containing a light source and cadmium selenide photo cell. When the light beam is interrupted by the passing drop, an electrical pulse is sent to the time delay generator. This generator then waits for a set time delay period, and introduces a firing pulse to the gun. The time delay necessary to fire the gun at just the proper moment so that the sample will strike the passing mercury drop can be determined by calibrating the system.

Summarizing, therefore, the equipment was designed to, first, detect the passing of a falling particle through a given point; and second, to generate a delay equal to the time required for the droplet to reach a second given point and then to cause the firing of a squib so that the fired projectile and the particle collide at the second given point.

The time delay generator, designed in Convair's Electronic Laboratories, is housed in a 5" x 3" x 9" cabinet, and is sturdily built for the rigorous conditions on a firing range. The generator is completely self-contained with lights to indicate the state of charge of internal capacitors, safety switches, calibration charts and time delay controls. One switch is available which completely isolates the firing circuit from the photo cell tripping circuit so that the apparatus may be operated safely until such time as it is desired to fire the gun. Electronic circuitry consists of a two stage amplifier for raising the level of the photo cell signal, a screen-coupled phantastron tube for generating the linear time delay and a thyratron for firing the squib. A power transformer, silicon rectifiers, and gas tube regulator comprise the power supply. A picture showing the photo cell dripper system and electronic "black box" will be found in Figure 1. Figure 2 is a schematic circuit diagram of the box.

II. DAMAGE CONTOUR STUDY

Study of the shape or contour of damage marks was desired to provide a basis for later statistical analysis of multiple drop impacts within a given small area. A volcano-shaped contour was obtained in every case of solid spherical drop impacts, even at low velocities. Tests were made with solid indenters of varying shapes in the drop tester shown in Figure 3. By means of an optical micrometer, it was possible to take readings of depth and distance traveled along the surface of a given sample and thereby plot the exact contour of a given damage site. Such contours are shown in Figure 4. The volcanoes in some cases are actually at a slight angle to the original planar surface. By taking careful note of the scales to which these contours are plotted, this inclined angle is seen to be extremely small - only about 20 minutes for most. These curves could be changed to make an equivalent damage mark perpendicular to the planar surface by means of a combination of rotations and translations of the optical micrometer data (see Figures 5 and 6). These transformation equations may be given in the following form:

$$x = x_o \cos \Theta - y_o \sin \Theta + p \sin \Theta - p \sin 2\Theta$$

$$y = y_o \cos \Theta + x_o \sin \Theta - p \cos \Theta + p \cos 2\Theta$$

where (x, y) = transformed coordinates, (x_o, y_o) = original "tilted" coordinates, Θ = angle of tilt, and p = vertical distance of volcano surface to the undamaged sample planar surface.

From these normalized curves, some suitable correlation was hoped to be found between the volcano shape and the indenter shape as well as with depth and penetration.

A brief study was made of the contour of impact marks made by cylindrical indenters in the drop test machine. The overall appearance of these damage marks was a cylindrical hole in the target metal with a volcano-like rim of displaced metal. From the two samples tested the volcano shape could be plotted as a straight line function on a semi-log paper, i.e., the logarithm of the height from the original planar surface was directly proportional to the ratio of the distance from the impact center to the radius of the impact mark. As shown in Figure 7, the slope of this straight-line logarithmic relation was the same for impact sites created by two cylindrical indenters of widely differing radii. This slope is undoubtedly proportional to the target material strength and/or the shape of the indenter. Further work should be done to establish this relation. When this particular volcano shape (now known from this curve) was integrated around the hole to obtain the volume of metal "pushed up," this volume was found to be nearly equal to the volume displaced from the cylindrical holes in the metal. There is, therefore, only a small amount of material compression indicated in the damage process. From this and other relations,

not only the depth of penetration, but also the exact contour of the damage mark (data actually restricted to cylindrical indenters used on 1100-0 aluminum) can be determined.

If we denote y_o as the peak height of the volcano, "r" as the radius of the hole in question and "m" the slope of the curve, we may write the relation for the volume of material in this volcano shape as follows:

$$V = \frac{\pi y_o'}{r^2} \left\{ \frac{e^{kr}}{K^2} \left[1 - e^{-Ky_o'} \right] \left[(Kr - 1)^2 + 1 \right] + \frac{e^{Kr - Ky_o'}}{K^2} \left[(Ky_o' - 1)^2 - 1 \right] \right\}$$

where $K = \frac{mr}{0.4343}$

We have utilized a convenient variable which may prove important in a further study. This variable is the maximum height, y_o', of the volcano above the planar surface. Equations of the form

$$y = k^{mx}$$

were also found, when semi-log graphs were made for conical and spherical indentations. Although the equations obtained for the three indenter shapes were of the same general form, the exact correlation of plotting parameters was not evident after brief investigation.

III. ANGLE STUDY

To study the effect of change in incidence angle on impact damage severity, several copper samples were fabricated in conical configurations of from 30° to 150° included angle. An attempt was made to fire these at 1.50 mm mercury drops; however, due to the excess weight of the copper specimens, they continually broke away from the adapter when it decelerated in the capture tube. Most of the specimens continued through the capture tube and were either lost or damaged so badly that impacts could not be measured. Work was temporarily suspended on these copper cones until a suitable adapter could be developed.

A better approach to the problem was then tried by using 1100-0 aluminum wedges of various included angles. The configurations used in these tests were 15°, 30°, 45°, 60°, 75° half-angle wedges together with some 90° (i.e., flat plate) aluminum samples. These tests utilized both 1 mm steel ball bearings of close tolerance and accurately measured mercury drops of about 1.50 mm diameter. Complete data on these tests will be found in Appendix I. Damage received by the angled specimens was found to be exactly that which would correspond to a flat plate impact at the normal component velocity. To do a proper analysis of this damage, it was necessary to determine what the damage would be at this component velocity. Such damages were taken from previously worked out depth versus velocity curves. Such velocities should be calculable from energy-volume theory (see "Damage Equation Development," Section IV). Up to this time, however, the energy-volume work has not been extended to cover angle study implications.

IV. DAMAGE EQUATION DEVELOPMENT

During the period October 1957 to August 1958, primary emphasis was placed on theoretical studies of single drop impacts. At the end of the previous contractual period, several theoretical problems remained to be sclved. These problems included the effect of varying the impact incidence angle on severity of erosion and many aspects concerning the prediction of erosion damage from known physical parameters. In addition, the comparison between liquid and solid drop impacts was still to be made.

To gain a full understanding of the mechanisms involved, some brief physical tests were made using solid steel indenters. An apparatus similar to that shown in Figure 3 was used together with two steel weights which held various sizes of cylindrical, conical and spherical indenter tips. By means of this machine, it was possible to drop a given shape and weight of indenter from heights up to 30 centimeters. One of the weights used was 447.1 grams, the other 1125 grams. Most of the tests were done on 1100-0 aluminum which had formerly been prepared for 20 mm single drop impacts. The points shown in Figures 8 and 9 were obtained by carefully measuring the penetration depth and the drop height of the indenter. These curves indicate that when cylindrical indenters were used, a different "drop height versus penetration depth" slope was obtained for each radius; when conical or spherical indenters were used, a characteristic slope was found for each shape. Parallel lines were obtained from the data of the two indenter weights. Considerable calculation led to the conclusion that the volume of material displaced was directly proportional to the impact energy. Although the curves obtained (see Figures 10 and 11) do not exhibit perfectly straight lines, the indenter "bounce" is assumed to be responsible for varying small amounts of energy loss and resultant deviations from straight line curves.

In our former analysis of damage parameters, (WADC TR 53-173 Part IV) we considered such variables as the impact velocity, depth of penetration, drop size, drop liquid density, and the density of the target material as well as its tensile strength. Energy versus volume type curves, presently being studied, inherently include such variables as impact velocity, drop density (to obtain drop mass), depth of penetration and original drop radius. This energy versus displaced volume relation encompasses a much larger field of impact shapes than the former equations which assumed perfectly spherical impacting drops. Measurements indicate that although liquid drops remain nearly spherical under high velocity impact conditions, they do deform slightly into approximately ellipsoidal shapes. Even steel ball bearings under high-impact conditions are known to deform to a certain extent through natural elastic processes. This ellipsoidal damage shape may be seen in cross-sectional photos appearing in WADC TR 53-192 Part XII, by Dr. Olive Engel of the National Bureau of Standards. The pictures, which are magnified ten times and show mercury drop damage marks in lead, 1100 aluminum and copper clearly indicate that the craters have approximately ellipsoidal bottoms with nearly straight

sides. The 1100-0 aluminum exhibits the unusual property of allowing the mercury liquid to form a subsurface cavity of larger diameter than the entrance holes. For calculation purposes, however, it is believed that only slight errors would result in assuming the damage shape previously mentioned.

Due to these effects, a damage equation which takes into account such variations in drop shape or solid particle shape to predict "erosion" damage is highly desirable. Such an extension could conceivably lead to the prediction of damage from irregularly shaped meteorites on ballistic missiles, satellites, etc.

Because this energy-volume relation worked so well with solid indenter impacts, the relation was also applied to the mercury and water drop impact data. The equations worked exceedingly well on this data. Because of the extensive calculations which had to be done in order to properly present these data, they were not included in previous reports. In this energy-volume relation, we use "total energy." The change in potential energy plus the change in kinetic energy is equal to the "total energy" transferred in displacing a given volume of metal. In the case of most mercury drop impacts, we have extremely high velocities, i.e., extremely large changes in kinetic energy and a relatively insignificant change in potential energy. In the case of the drop testing techniques using the solid indenters, we had much lower velocities -- about 8 feet per second. Several tests were made to determine a Brinell hardness of lead. The method used was such that a considerable amount of data could be applied to this study of energy versus volume displaced. Low velocities of about 0.002 mm per second were involved. In this case, kinetic energy was negligible compared to the potential energy contribution. Correlation of all this data was found to be excellent, and that the energy-volume relation holds equally well through the entire velocity range to Mach 3.

Discovery was made during remeasurement with our optical micrometer that many of the damage depths and diameters formerly measured for mercury drop impacts were erroneous. The micrometer makes possible the measurement of depths to within ± 0.0001 inch. A recalculation of a large mass of this data was done by the Convair Computer Lab. Also found was that the method used for drop size measurement was somewhat crude in 1955. At that time, a large number of drops were counted and weighed and an average drop size was taken for calculation purposes. These statistically determined sizes were not representative for individual impacts, however, because the size varied widely from drop to drop and with testing conditions. At present, mercury drop sizes to within ± 0.0001 mm can be determined because the drops are individually weighed on an analytical balance. Specimens for which the least precisely determined values of drop size and impact velocity are available are given an accuracy index of 3. Data obtained while using the latest control techniques are given a measurement accuracy index rating of 1.

In continuing the analytical study of damage, relation of the energy-volume slope with some target material property such as tensile strength was desired. This strength property may or may not be the one of absolute physical significance. In former work (WADC TR 53-173 Pt IV) with mercury drops, however, it was found that tensile strength measurements gave reasonable correlation with the apparent dynamic molecular bond strengths. On plotting the slopes of the energy versus volume curves versus the tensile strength of test materials, a straight line was obtained which passed through the origin (Figure 12). We are now led to the relation that the impact energy divided by the volume displaced and by the material tensile strength is constant. Although dimensionless, this constant appears not to be equal to one. The value of the constant possibly depends upon the drop liquid (or solid) physical properties or even upon the apparent increase in target material yield strength due to high rates of strain (see Section V).

Inasmuch as it has been determined that impact energy is proportional to volume displaced, it would be desirable, in a theoretical instance, to know the damage area shape in order to determine what the displaced volume should be. (Actually, the E versus V line does not pass through the origin when plotting high velocity impact data - the reason will be shown in the coming section.) As formerly stated, an impacting sphere, whether of steel, mercury, water, etc., will not remain spherical during these high velocity impacts. On examining the impact marks of many samples, the bottom of the "crater" is found to be approximately ellipsoidal. We shall, therefore, assume a hypothetical impact process wherein a spherical drop hits the target material and is deformed into a perfectly ellipsoidal drop which then proceeds through the material until coming to rest. To find a relationship between drop shape and some function of energy or volume, the ratio of "a" (ellipse major axis) to "b" (ellipse minor axis) was defined as a drop shape parameter.

The following derivation shows that the energy-volume equation outlined above may be broken down into a form which includes the impact velocity (v_o), material tensile strength (S_t), liquid drop density (ρ_ℓ), and this new shape parameter (γ) as well as the depth of penetration (x), and the damage radius (r), drop mass (m_o), drop diameter (δ).

Starting with the basic energy-volume equation:

(1) $E_\alpha = k S_t V$

where E_α = kinetic deformation energy,

k = proportionality constant,

V = volume of displaced target material, and

$$E_o - E_A = \frac{m_o}{2} (v_o^2 - v_A^2)$$

$$E_\alpha = \frac{m_o}{2} (v_\alpha^2 - v^2)$$

where E_o = total impact kinetic energy,

E_A = elastic potential energy,

v_A = minimum velocity necessary for permanent deformation

v = velocity of drop at any point in the damage process

v_α = drop velocity at time of first permanent deformation.

For all cases of practical interest, $v = 0$.

$$\therefore \quad E_\alpha = \frac{m_o v_\alpha^2}{2}$$

In addition to the above energies, some kinetic energy, E', is imparted to the target material.

$$E' = -\int_{m' v_\alpha}^{o} v' \, d(m' v') = -m' \int_{v_\alpha}^{o} v' \, dv' = \frac{m' v_\alpha^2}{2}$$

where m' = effective target mass at $v = v_\alpha$ (the mass of target material enclosed by the initial impact shock wave at time of first permanent deformation).

$$E_o = E_A + E_\alpha + E' = E_A + E_\alpha \left(1 + \frac{m'}{m_o}\right)$$

$$\therefore \quad E_\alpha = (E_o - E_A) \frac{m_o}{m_o + m'}$$

As would be expected, m' increases and E_α decreases with the target material sound velocity.

$$m_o = \frac{\pi}{6} \delta^3 \rho_\ell$$

when $x \leqslant b$:

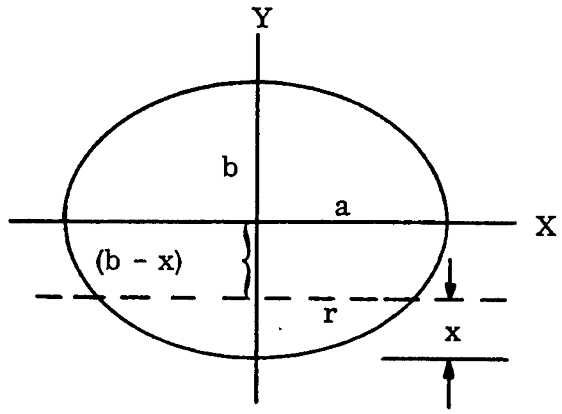

$$V = \pi \int_{b-x}^{b} X^2 \, dY$$

$$\frac{X^2}{a^2} + \frac{Y^2}{b^2} = 1$$

$$X^2 = a^2 \left(1 - \frac{Y^2}{b^2}\right)$$

$$\therefore \quad V = \pi a^2 \int_{b-x}^{b} \left(1 - \frac{Y^2}{b^2}\right) dY$$

$$= \pi a^2 \left[Y - \frac{Y^3}{3b^2} \right]_{b-x}^{b}$$

$$V = \frac{\pi a^2 x^2}{b} - \frac{\pi a^2 x^3}{3 b^2}$$

but $R^3 = a^2 b$

$$\therefore \quad V = \pi R^3 \frac{x^2}{b^2} - \pi R^3 \frac{x^3}{3 b^3}$$

Now $\quad b^3 = \dfrac{R^3}{\gamma^2}$

and $\quad V = \pi R \gamma^{4/3} x^2 - \dfrac{\pi}{3} \gamma^2 x^3 \qquad (x \leqslant b)$

Substituting ~

$$\frac{2}{3}\,\pi R^3\,\rho_\ell\,(v_\alpha^{\,2} - v^2) = \frac{\pi}{3}\,k\,S_t\,(3R\gamma^{4/3}x^2 - \gamma^2 x^3)$$

(2) or $$v_\alpha^{\,2} - v^2 = \frac{2\,k\,S_t}{\delta^3\rho_\ell}\,x^2\,(3\,\delta\,\gamma^{4/3} - 2\,\gamma^2 x)$$

for $x \leqslant b$

When $x \geq b$:

$$V = \frac{2}{3}\,\pi\,R^3 + \pi\,a^2\,(x - b)$$

but $R^3 = a^2 b$ and $a = r$

$\therefore$ $$V = \frac{2}{3}\,\pi R^3 + \pi r^2 x - \pi R^3$$

and $$V = \pi r^2 x - \frac{\pi}{3}\,R^3 \qquad (x \geqslant b)$$

Substituting ~

(3) $$\frac{2\pi}{3}\,R^3\,\rho_\ell\,(v_\alpha^{\,2} - v^2) = \frac{k\,\pi\,S_t}{3}\,(3r^2 x - R^3)$$

also $r^2 = \gamma^{2/3} R^2$

$\therefore$ $$v_\alpha^{\,2} - v^2 = \frac{k\,S_t}{2R^3\,\rho_\ell}\,(3\,\gamma^{2/3}R^2 x - R^3)$$

(4) or $$v_\alpha^{\,2} - v^2 = \frac{k\,S_t}{2\,\delta\,\rho_\ell}\,(6\,\gamma^{2/3} x - \delta)$$

for $x \geqslant b$

In Figure 13 is shown a plot of velocity squared versus a term including gamma. The points on this curve include 1.0 mm, 1.5 mm and 2 mm sized mercury drop impacts on copper and indicate a straight line slope exactly equal to the energy-volume constant times the material tensile strength divided by twice the liquid density. The copper specimens used were of two different tensile strengths -thus the two slopes, see equation page 14.

To physically determine the γ obtained in any given damage site, it was necessary to make the assumption that the drop volume remained the same. From the following derivation, an equation may be obtained which relates γ to the depth of penetration, original drop radius and measured damage radius. The equation, though somewhat complex may be solved for γ readily by Newton's method in only two approximations (see Figures 32-42).

By assuming that the volume of the drop remains constant and the shape changes to a perfect ellipsoid:

$$V = \frac{4}{3}\pi a^2 b = \frac{4}{3}\pi R^3$$

or $$a^2 b = R^3$$

again a = ellipsoid major axis

b = ellipsoid minor axis

R = original sphere drop radius

$$\gamma = \frac{a}{b} \qquad a = \gamma b$$

$$R^3 = \gamma^2 b^3 \quad \text{or} \quad b = \gamma^{-2/3} R$$

Now $$\frac{X^2}{a^2} + \frac{Y^2}{b^2} = 1$$

At a point $X = r$ and $Y = b - x$,

$$\frac{r^2}{\gamma^2 b^2} + \frac{(b - x)^2}{b^2} = 1$$

$$\gamma^2 x^2 - 2\gamma^2 b x + r^2 = 0$$

$$(5) \quad \therefore \quad \gamma^2 x^2 - 2\gamma^{4/3} R x + r^2 = 0 \qquad \text{for } x \leqslant b$$

When $x \geqslant b$, $a = r$

$$a^3 = \gamma R^3 = r^3$$

$$(6) \quad \text{or} \quad \gamma = \left(\frac{r}{R}\right)^3$$

This relation can be used to rearrange equation (3) — $x \geqslant b$

$$r^2 = \frac{\gamma R^3}{r}$$

$$2\rho_\ell (v_\alpha^2 - v^2) = k S_t \left(\frac{3\gamma x}{r} - 1\right)$$

$$\text{or} \quad \frac{v_\alpha^2 - v^2}{\left(\frac{3\gamma x}{r} - 1\right)} = \frac{k S_t}{2\rho_\ell}$$

When $x \geqslant b$, $v_\alpha \cong v_o$

The slope, M, of the "energy versus displaced volume" curve is equal to $k S_t$ (equation 1). The slope of $(v_\alpha^2 - v^2)$ vs $\left(\frac{3\gamma x}{r} - 1\right)$, plotted in Figure 13, equals $M/2\rho_\ell$ as predicted and illustrates the agreement between test data and theory.

Although an equation was given which relates v_α (not directly measurable) to the impact velocity, v_o, and the velocity of minimum deformation, v_A, it was not used in the above damage equations. This relation,

$$E_\alpha = (E_o - E_A) \frac{m_o}{m_o + m'}$$

or $$v_\alpha^2 = (v_o^2 - v_A^2)\ \frac{m_o}{m_o + m'}\ ,$$

only developed recently, adds a great deal of complexity to the otherwise straightforward damage equations. It should not be inferred that the relation is not practical - the true damage equation is incomplete without the relation. The combined form of damage equation has not been analyzed sufficiently to allow a simplified expression. The linear equation in x (when $x \geqslant b$) may be used to demonstrate the application.

$$v_\alpha^2 = \frac{k\,S_t}{2\,\rho_\ell}\left(\frac{3\,\gamma^{2/3}x}{R} - 1\right)$$

$$\therefore \quad v_o^2 = v_A^2 + \left(1 + \frac{m'}{m_o}\right)\frac{k\,S_t}{2\,\rho_\ell}\left(\frac{3\,\gamma^{2/3}x}{R} - 1\right)$$

but $$m_o = \frac{4}{3}\ \pi R^3 \rho_\ell$$

$$m' = \frac{2}{3}\ \pi\ (x'^3 - x_\alpha^3)\ \rho_m$$

where x' = depth of the impact shock wave in the target material when $v = v_\alpha$

x_α = depth of drop when $v = v_\alpha$

ρ_m = target material density

It will later be shown that $v_A^2 = \frac{S_o}{\rho_\ell}$ for liquid drop impacts and $v_A^2 = 9\,\frac{S_o^3}{\rho_\ell\,Y}$ for solid drop impacts (S_o = dynamic yield strength of target material, and Y = elastic modulus of target material). For a liquid drop, therefore, the damage equation for the region $x \geqslant b$ may be given by the following:

$$v_o^2 = \frac{S_o}{\rho_\ell} + \left[1 + \frac{(x'^3 - x_\alpha^3)}{2\,R^3}\ \frac{\rho_m}{\rho_\ell}\right]\left[\frac{3\,\gamma^{2/3}x}{R} - 1\right]\frac{k\,S_t}{2\,\rho_\ell}$$

It is obvious that the damage equation, $E = k\, S_t\, V$, is not strictly linear when dealing with impact velocities. Deviations from linearity will be noted on many of the E vs V curves of the accompanying figures (14-31). Other mechanisms may be partially responsible for this nonlinear behavior, for example, interaction of shock waves within the target.

INITIAL DAMAGE VELOCITY - LIQUID SPHERES

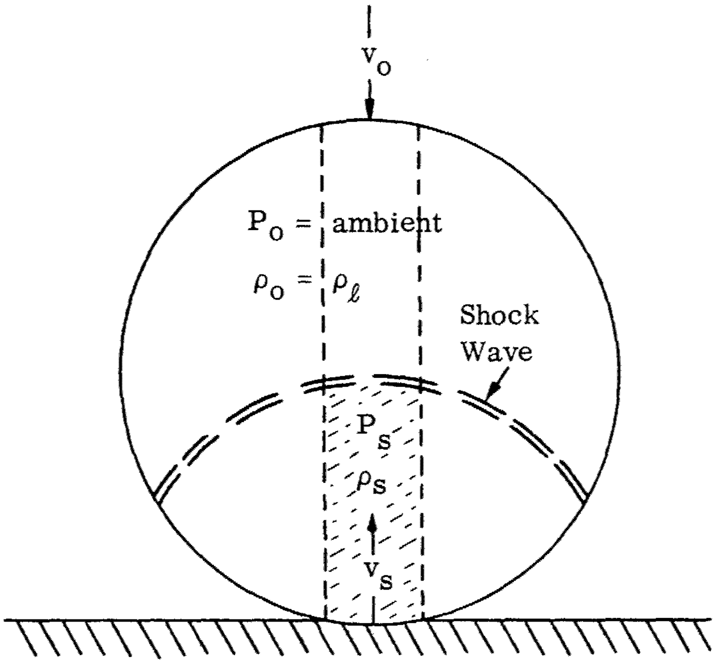

At the damage initiating velocity, v_A, the contact area between sample and liquid drop is small. For this reason the shock may be considered as planar across the cylinder (shown by dotted lines) extending from the contact area.

$$P_o - P_s - \rho_o v_o (v_s - v_o) = 0$$

From continuity:

$$\rho_o v_o = \rho_s v_s$$

$$\therefore \; P_o + \rho_o v_o^2 = P_s + \rho_s v_s^2$$

On the assumption that initial damage occurs through a total transfer of momentum, we shall let the liquid behind the shock (in contact with the sample) come to rest - i.e. $v_s = 0$.

Thus $$v_A^2 = \frac{P_s - P_o}{\rho_o}$$

But since this pressure behind the shock caused the initial yielding, we shall set pressure equal to the dynamic yield strength, S_o. Because any tensile or yield strength values are normally reported in terms of "gauge pressure" rather than "absolute pressure,"

$$P_s - P_o = S_o$$

$$\therefore \quad v_A^2 = \frac{S_o}{\rho_\ell} \quad \text{or} \quad v_A = \sqrt{\frac{S_o}{\rho_\ell}}$$

Target Material	Liquid Drop (Dia. not) Specified	S_o (psi)	S_t (psi)	v_A (Calculated) (ft/sec)	v_A (Observed) (ft/sec)
1100-0 Al	Hg	16,700	18,500	303	200-430
Cu	Hg	31,000	31,000	414	375-425
Pb	Hg	5,600	2,700	175	130-210
Mild C.R. Steel	Hg	120,000	46,500	813	600-950
Pb	H_2O	5,600	2,700	646	400-800

INITIAL DAMAGE VELOCITY - SOLID SPHERES

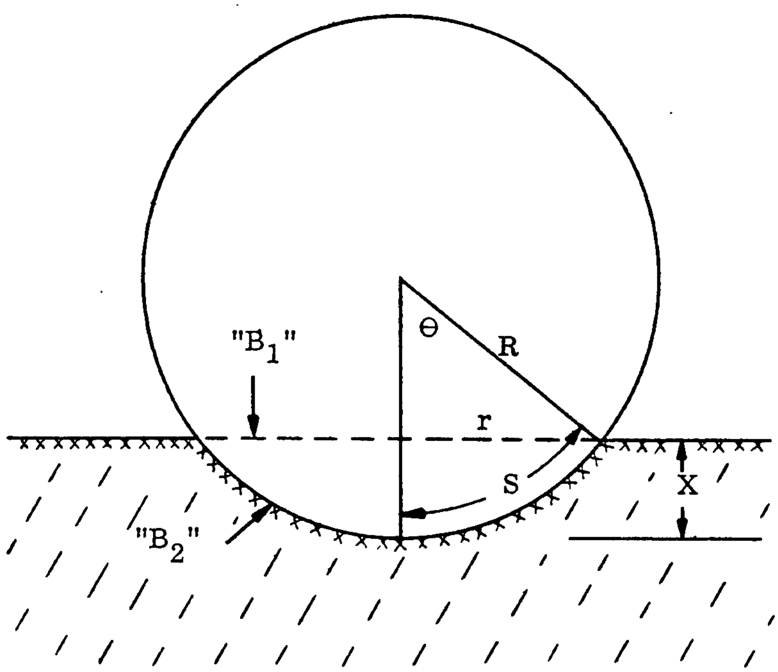

Assume the surface molecules of target material were stretched from position "B_1" to position "B_2" thereby increasing the chain length from r to s.

$$\text{Strain} = \frac{\Delta L}{L} = \frac{s - r}{r} = \frac{R\,\Theta - r}{r} = \left(\frac{R}{r}\right)\Theta - 1$$

Since we shall operate entirely in the elastic region (until first permanent deformation), Hooke's law should be obeyed. In addition, elastic penetration will be very small and the ball should remain very nearly spherical.

$$Y = \text{Youngs Modulus} = \frac{\text{Stress}}{\text{Strain}}$$

Because we are primarily interested in the point at which the first permanent deformation takes place, the stress may be taken as the dynamic yield strength, S_o. At this point, $r = r_o$,

$$\text{Strain} = \frac{\text{Stress}}{Y} = \frac{S_o}{Y} = \left(\frac{R}{r_o}\right)\Theta_o - 1$$

But $$\Theta_o = \sin^{-1}\left(\frac{r_o}{R}\right) = \left(\frac{r_o}{R}\right) + \frac{1}{6}\left(\frac{r_o}{R}\right)^3 + \frac{3}{40}\left(\frac{r_o}{R}\right)^5 + \cdots\cdots\cdots$$

$$\left(\frac{R}{r_o}\right)\Theta_o - 1 = 1 + \frac{1}{6}\left(\frac{r_o}{R}\right)^2 + \frac{3}{40}\left(\frac{r_o}{R}\right)^4 + \cdots\cdots\cdots -1$$

$$\therefore \quad \frac{S_o}{Y} = \frac{1}{6}\left(\frac{r_o}{R}\right)^2 + \frac{3}{40}\left(\frac{r_o}{R}\right)^4 + \cdots\cdots\cdots$$

However, for these small elastic penetrations, $r_o \ll R$.

$$\therefore \quad \frac{S_o}{Y} \cong \frac{1}{6}\left(\frac{r_o}{R}\right)^2 \text{ at the point of permanent deformation}$$

$$\text{or} \quad \frac{F/A}{Y} \cong \frac{1}{6}\left(\frac{r}{R}\right)^2 \text{ in general.}$$

F = total force acting on the indented surface area, A, at the depth, x (corresponding to radius, r). It may be seen from the diagram that

$$R^2 = (R - x)^2 + r^2 = R^2 - 2R\,x + x^2 - r^2$$

or $\quad x^2 - 2R\,x + r^2 = 0$

$$\therefore \quad \frac{r^2}{R^2} = \left(\frac{r}{R}\right)^2 = \frac{2\,R\,x - x^2}{R^2}$$

Since the surface area

$$A = 2\,\pi\,R\,x,$$

$$F = \frac{A\,Y}{6}\left(\frac{r}{R}\right)^2 = \frac{2\,\pi\,R\,x\,Y}{6}\left(\frac{2\,R\,x - x^2}{R^2}\right) = \frac{\pi}{3}\,R^3 Y\left[\frac{2\,R\,x^2 - x^3}{R^4}\right]$$

The energy, E, expended in stopping the drop follows:

$$E = \int_0^{x_o} F\,d\,x = \frac{m_o\,v_A^{\,2}}{2} = \frac{2}{3}\,\pi\,R^3\,\rho_\ell\,v_A^{\,2}$$

where $\quad x_o$ = critical depth (when first permanent deformation is made)

m_o = drop mass

v_A = critical velocity

ρ_ℓ = density of drop material

Then $\quad E = \dfrac{\pi\,R^3 Y}{3}\displaystyle\int_0^{x_o} \frac{2\,R\,x^2 - x^3}{R^4}\,d\,x$

$$= \frac{\pi\,R^3 Y}{3}\left[\frac{2\,x_o^{\,3}}{3\,R^3} - \frac{x_o^{\,4}}{4\,R^4}\right]$$

From the equation $x^2 - 2R\,x + r^2 = 0$, we find that

$$x_o = R\left[1 - \sqrt{1 - \left(\frac{r_o}{R}\right)^2}\,\right]$$

which on expansion becomes:

$$x_o = R\left[\frac{1}{2}\left(\frac{r_o}{R}\right)^2 + \frac{1}{8}\left(\frac{r_o}{R}\right)^4 + \dots\dots\dots\right]$$

But $r_o << R$

$$\therefore \qquad x_o \cong \frac{R}{2}\left(\frac{r_o}{R}\right)^2 = \frac{r_o^2}{2R}$$

Substituting this value into the energy equation above:

$$E = \frac{\pi R^3 Y}{3}\left[\frac{r_o}{R}\right]^6\left[\frac{1}{12} - \frac{1}{64}\left(\frac{r_o}{R}\right)^2\right]$$

By equating this energy to the kinetic energy and substituting $\left(\frac{r_o}{R}\right)^2 = \frac{6 S_o}{Y}$, one obtains the damage initiating velocity, v_A:

$$\frac{2}{3} \pi R^3 \rho_\ell v_A^2 = \frac{\pi R^3}{3} Y \left[216 \frac{S_o^3}{Y^3}\right]\left[\frac{1}{12} - \frac{1}{64} \times \frac{6 S_o}{Y}\right]$$

$$v_A^2 = \frac{S_o^3}{Y^2 \rho_\ell}\left[9 - \frac{81}{8}\frac{S_o}{Y}\right]$$

We may assume for most metals that $S_o << Y$ and simplify the velocity expression:

$$v_A^2 = 9\frac{S_o^3}{Y^2 \rho_\ell}$$

or $\quad v_A = \frac{3 S_o}{Y}\sqrt{\frac{S_o}{\rho_\ell}}$ in any consistent units.

Alternately, for v_A in ft/sec, S_o and Y in psi and ρ_ℓ as specific gravity (dimensionless):

$$v_A = 25.8 \frac{S_o}{Y} \sqrt{\frac{S_o}{\rho_\ell}}$$

To provide a rough check of this relationship, a one millimeter diameter steel ball bearing was dropped on a specimen of 1100-0 aluminum from various heights. The values S_o = 17,450 psi, Y = 10.0 x 10^6 psi, and ρ_ℓ = 7.86 indicated that v_A should equal 2.12 ft/sec. The ball was dropped from as low as 1.00 to 1.25 inches above the sample corresponding to 2.31 to 2.58 ft/sec impact velocities. Slight indentations were detected under the microscope.

V. INFLUENCE OF HIGH STRAIN RATES ON THE EFFECTIVE TARGET YIELD STRENGTH

For some time it has been known that the apparent strength of certain materials, particularly body centered cubic metals, is increased when they are strained rapidly. To the author's knowledge, a complete theoretical treatment of the mechanism of this phenomenon has not been done although both empirical and theoretical studies have been made. For purposes of this report, however, it is desired to show only that the high velocity impact data obtained with mercury drops, etc. yield dynamic strength values similar to those of other investigators. In addition, the damage data for mild cold rolled steel is brought into full accord with the predicted values.

We may take $t \cong \dfrac{x_o}{\sqrt{2}\, v_A} = \dfrac{r_o^2}{2\, R\, v_A \sqrt{2}}$ (see previous derivations)

for velocities near v_A, where t = time for impinging drop of velocity v_A to reach a depth x_o.

$$\therefore \quad L = c\,t = \frac{r_o^2\, c}{2\, R\, v_A \sqrt{2}}$$, where L = unstrained molecular "chain" length

and c = speed of sound in the target material.

Strain $= \dfrac{\Delta L}{L} = \dfrac{x}{c\,t}$, and Strain Rate $= \xi = \dfrac{\Delta L}{L\,t}$

$$\therefore \quad \xi = \frac{x}{c\,t^2} = \frac{8\, R^2\, v_o^2\, x}{r_o^4\, c}$$

Since $$x_o \cong \frac{r_o^2}{2\,R} = \frac{R}{2}\left(\frac{r_o}{R}\right)^2 \cong \frac{R}{2}\left(\frac{6\, S_o}{Y}\right)$$

$$\frac{x_o}{R} \cong \frac{3\, S_o}{Y}$$

$$\xi = \frac{8}{c} \times v_o^2 \times \frac{x}{R^2}\left(\frac{R}{r_o}\right)^4$$

$$= \frac{8}{c} \times \frac{S_o}{\rho_\ell} \times \frac{3 S_o}{YR} \left(\frac{Y}{6 S_o} \right)^2$$

$$\xi = \frac{2 Y}{3 R c \rho_\ell}$$

For cold rolled steel, using 1.5 mm Hg drops, $Y = 30 \times 10^6$ psi, $c = 5.13 \times 10^5$ cm/sec, and $\rho_\ell = 13.546$

$$\xi = \frac{30.0 \times 10^6 \times 703.1 \times 10^{-1} \sqrt{2} \sqrt{2}}{3 \times 0.075 \times 5.13 \times 10^5 \times 13.546} = 2700 \text{ sec}^{-1}$$

In many cases, as seen on page 17, the dynamic yield strength is about equal to the tensile strength. A reasonable damage relation may be

$$E = k S_o V$$

rather than the form using S_t. The slope of the E vs V curve for mild C.R. steel (Figure 30) leads to:

$$k S_o = 190{,}300 \text{ psi}$$

For many other metals (which do not exhibit yield strength increases with strain rate), the value of $k \cong 2.7$ (reason unknown). Using this k value for steel also

$$S_o \cong 71{,}500 \text{ psi}$$

Since the static yield strength, S_o', of this material is 29,400 psi:

$$\frac{S_o}{S_o'} = \frac{71{,}500}{29{,}400} = 2.44$$

As may be seen in Figure 43, this ratio of yield strengths agrees exceptionally well, at the calculated strain rate, with values obtained by other investigators[3]. The validity of the above is further demonstrated by calculating the initial damage velocity:

$$v_A = 8.605 \sqrt{\frac{71{,}500}{13.546}} = \sqrt{\frac{S_o}{\rho_\ell}} = 625 \text{ ft/sec.}$$

A velocity of similar magnitude is obtained by extrapolation of the E vs V curve to zero volume. Even the γ vs impact velocity curve (Figure 41) indicates such a value at $\gamma \cong 1$.

A second example of apparent yield strength increase due to high strain rates is given by E vs V curve slopes for lead at low and high velocities. The average low velocity slope is 0.460×10^9 dynes/cm^2 (Brinell Ball data - Figures 14 and 15). The average high velocity slope is 1.30×10^9 dynes/cm^2 (mercury drop impacts - Figures 27 and 28). The ratio of these two values corresponds to the ratio of the dynamic and static yield strengths:

$$\frac{S_o'}{S_o} = \frac{1.30}{0.460} = 2.82$$

This ratio value agrees well with the results of Whiffin[13] and Taylor[11].

VI. MULTIPLE DROP RAIN DAMAGE STUDY

Extension of the theoretical work to a case of practical application - statistical rain drop damage on materials was desired. The theory as well as applications to all previous rain damaged samples is reported in WADC TR 58-427[6]. As seen in the derivation to follow the energy-volume equation may be extended to angle impacts by inserting the sine squared of the incidence angle. Because of the many variables involved, it has not been possible, heretofore, to compare damage observed on the different configurations of samples traveling through rains of different intensity at various speeds and at different exposures. From theoretical considerations it has been found that the product of the impact energy and the sine squared of the incidence angle is proportional to the volume of damaged material displaced. To apply this relation to a physical situation involving water drops of many sizes and materials of different tensile strengths, certain assumptions were necessary. First, to assume that the rainfall drop size distribution in each of the three artificial rain erosion ranges was constant and identical. We, naturally, have the conditions that the drop density (being water) is constant and that, in any practical rain erosion test, the sample is fired through a statistical number of rain drops. One may, therefore, consider that all of the rain damage caused in the Convair ranges is caused by drops of uniform size. Also assumed was that the tensile strength of any given sample or of several samples of similar composition may be constant or nearly so. Based on these assumptions, we may now derive the simple expression used to calculate the "correction factors" applied to the damage indices found in Tables II, III and IV of WADC TR 58-427.

(1) $$E \sin^2 \emptyset = k_1 V$$

where E = kinetic energy of impact, $\emptyset$ is the angle of incidence (equal to half the included angle of a cone or wedge), k_1 = constant of proportionality, and V = displaced volume.

(2) $$E = \frac{m v_o^2}{2}$$

where m = the drop mass and v_o = the impact velocity.

If the water drop sphere remains relatively rigid during impact, the volume displaced would be that of a spherical segment.

(3) $$V = \frac{\pi}{3} x^2 (3R - x)$$

where x = penetration depth and R = drop radius.

Because average water drop penetrations at 2240 feet per second are quite shallow compared to the drop radius,

$$3R >> x \qquad \text{and} \qquad (3R - x) \cong \text{Constant}$$

$$\therefore \qquad V = k_2 x^2$$

If the drop had been deformed to a hemisphere by the impact before any "damage" occurred,

$$V = k_3 x \qquad \text{instead.}$$

Substituting expressions for E and V into equation (1.):

$$\text{when} \quad V \propto x^2, \qquad v_o^2 \sin^2 \phi = K^2 x^2$$

$$(4) \quad \text{or} \quad v_o \sin \phi = Kx,$$

when $V \propto x$,

$$(5) \quad v_o^2 \sin^2 \phi = Kx.$$

The true equation governing this water erosion is probably a compromise of these two. Water drop impact marks in metals such as copper indicate some distortion from an original spherical shape although far from the hypothesized hemispherical shape.

Dividing equation (4) through by a standard conditions equation:

$$\frac{v_o}{2240} \frac{\sin \phi}{1.0000} = \frac{K x}{K x'}$$

$$\text{or} \quad x' = \frac{2240}{v_o \sin \phi} x$$

Of course the damage is directly proportional to the distance traveled through one inch per hour standard rainfall (equivalent exposure = T).

$$x' = \frac{2240 \cdot 1.0 \text{ nautical mile}}{v_o \sin \phi \; T \text{ (nautical miles)}} x$$

$$= \frac{2240 \cdot 6076.1}{v_o \sin \emptyset \, T \text{ (feet)}} \quad x$$

$$(6) \quad x' = \frac{13.61 \cdot 10^6}{v_o T \sin \emptyset} \quad x$$

In applying these factors to the various specimen shapes, the assumption was made that the tips of conical samples received approximately the damage that a flat plate specimen would have received under similar circumstances. Therefore, when calculating the tip "correction factors," the sine of 90° (= 1.0000) would be used.

For simplicity and because only negligible errors were introduced (compared to the approximated damage indices) equation 4 was used in WADC TR 58-427. To use this expression to correct actual penetrations to the equivalent penetration, this expression was "set up" under the arbitrary standard conditions of:

a) 1.0 nautical mile exposure,
b) 1 inch per hour rainfall intensity,
c) 2240 feet per second velocity, and
d) 90° incidence angle.

VII. SUMMARY

The single drop captured projectile method for theoretical damage studies has been extended to allow more accurate measurement of drop size and projectile velocity. For precision and accuracy in size measurements, each test drop is weighed individually on an analytical balance. Speeds up to Mach 5 are now attainable with nitrocellulose rifle powder.

A great number of single impact water and mercury drop tests have been done by the new method with a degree of precision not formerly possible. The data from these tests correlates very well with that of previous tests and in some cases provides a means for statistical correction of old data where there was some doubt as to values.

An equation which relates total energy of impact to the volume of metal displaced was derived and found adequate to explain damage in the velocity range from less than one foot per hour to greater than Mach 3. This equation together with results of incidence angle tests led to an overall damage equation which was successfully applied to the problem of multiple drop rain damage.

Reasonable preliminary equations were derived for the surface contours of certain impact marks.

The apparent increase in material yield strengths, due to the high strain rates present in ballistic impacts, was studied as an influencing parameter in the energy-volume damage equations. The ratio of dynamic to static yield strengths obtained for mercury drop impacts on steel was found to agree very well with ratios obtained by other investigators.

Though much of this work is unfinished, the way is open for complete correlation and unification of impact results. This unification would include a correct prediction of damage for impacts by single given drops or by a statistical number of these drops on any material of known physical properties.

BIBLIOGRAPHY

1. Aluminum Company of America. Alcoa Aluminum Handbook. Pittsburgh. 1956.

2. American Society for Metals. Metals Handbook. 1939.

3. Belsheim, R. O. "Delayed-Yield Time Effects in Mild Steel Under Oscillatory Axial Loads," Transactions of the ASME. Vol. 79, No. 7. Easton. October 1957.

4. Hurd, D. E., "High Density Liquid Erosion," A Study of Rain Erosion Testing Methods for Supersonic Speeds. WADC Tech. Report 53-173, Part IV. January 1957.

5. Hurd, D. E., "High Density Liquid Study," A Study of Rain Erosion Testing Methods for Supersonic Speeds. WADC Tech. Report 53-173, Part V. October 1957.

6. Hurd, D. E., et al. Summary Compilation of Supersonic Rain Erosion Results. WADC Tech. Report 58-427. June 1958.

7. Lange, Norbert A., Ph. D., Handbook of Chemistry. Handbook Publishers, Inc., Sandusky. 1946.

8. Marks, Lionel S., Mechanical Engineers' Handbook. McGraw-Hill Book Co., Inc., New York. 1950.

9. Nadai, A., Theory of Flow and Fracture of Solids. McGraw-Hill Book Co., Inc., New York. 1950.

10. Sneed, R. J. H. and Kornblum, H. N., The Pre-Yield Transient Behavior of Molybdenum. Convair, Pomona. May 1958. Tech. Memo 332-127.

11. Taylor, Geoffrey, Sir, F.R.S. "The Use of Flat-Ended Projectiles for Determining Dynamic Yield Stress," Proc. Roy. Soc. Vol. 194A. Pg. 306. 1948.

12. United States Steel Corporation. Fabrication. Aduco. 1957.

13. Whiffin, A. C., Proc. Roy. Soc. Vol. 194A. Pg. 300. 1948.

14. Engel, Olive G. Mechanism of Rain Erosion Part XII. Pits in Metals Caused by Collision with Liquid Drops. National Bureau of Standards. WADC Technical Report 53-192, Part XII. ASTIA Document No. 155756.

TABLE I

LOW VELOCITY DATA - STEEL BALL BRINELL TESTS ON LEAD

TEST NO.	TIME (sec)	DEPTH OF PENETRATION (cm X 10^2)	LOAD (dynes X 10^{-6})	LOADING RATE (dynes/sec X 10^{-6})	ENERGY (ergs X 10^{-6})	VOLUME DISPLACED (cm^3 X 10^3)
L5	6.00	1.143	16.043	2.6739	0.094	0.204
	11.00	2.184	29.413	2.6739	0.315	0.739
	15.90	3.073	42.515	2.6739	0.659	1.453
	21.00	4.089	56.152	2.6739	1.149	2.555
	25.90	5.105	69.254	2.6739	1.748	3.955
	31.00	6.096	82.891	2.6739	2.505	5.600
	36.00	7.137	96.260	2.6739	3.378	7.621
	41.20	8.103	110.160	2.6739	4.423	9.756
	48.00	8.915	123.000	2.6739	5.515	11.743
	51.00	10.058	136.370	2.6739	6.779	14.826
	56.10	11.074	150.010	2.6739	8.202	17.842
	67.40	13.437	177.940	0	12.368	25.819
	70.60	14.046	177.940	0	13.452	28.089
	76.10	14.503	177.940	0	14.266	29.847
	81.10	15.011	177.940	0	15.170	31.854
	86.10	15.265	177.940	0	15.622	32.879
	89.90	15.519	177.940	0	16.074	33.919
	96.20	15.773	177.940	0	16.525	34.972
	101.00	16.078	177.940	0	17.068	36.254
	106.40	16.357	177.940	0	17.565	37.447
	118.20	16.637	177.940	0	18.063	38.656
	138.20	17.043	177.940	0	18.785	40.444
	153.10	17.373	177.940	0	19.372	41.922
	183.20	17.754	177.940	0	20.050	43.655
	225.50	18.110	177.940	0	20.685	45.298

TABLE I (Continued)
LOW VELOCITY DATA - STEEL BALL BRINELL TESTS ON LEAD

TEST NO.	TIME (sec)	DEPTH OF PENETRATION (cm X 10^2)	LOAD (dynes X 10^{-6})	LOADING RATE (dynes/sec X 10^{-6})	ENERGY (ergs X 10^{-6})	VOLUME DISPLACED (cm^3 X 10^3)
L5	243.60	18.389	177.940	0	21.180	46.608
	267.90	18.694	177.940	0	21.723	48.055
	301.30	18.923	177.940	0	22.131	49.151
	312.30	19.075	177.940	0	22.401	49.888
L11	5.91	2.032	25.438	4.3042	0.253	0.640
	8.43	2.870	36.284	4.3042	0.509	1.269
	12.25	4.115	52.726	4.3042	1.086	2.587
	16.20	5.410	69.728	4.3042	1.899	4.432
	19.94	6.629	85.826	4.3042	2.876	6.598
	23.71	7.899	102.050	4.3042	4.067	9.286
	27.21	9.169	117.120	4.3042	5.357	12.333
	30.89	10.414	132.960	4.3042	6.903	15.853
	34.66	11.709	149.180	4.3042	8.690	19.856
	38.29	12.954	164.810	4.3042	10.607	24.083
	41.88	14.224	180.260	4.3042	12.722	28.767
	45.41	15.469	195.450	4.3042	14.917	33.710
	49.11	16.764	211.380	4.3042	17.448	39.211
	54.32	18.567	222.420	0	21.940	47.450
	57.31	19.329	222.420	0	23.634	51.126
	59.59	19.837	222.420	0	24.764	53.639
	62.94	20.345	222.420	0	25.894	56.202
	66.56	20.828	222.420	0	26.990	58.680
	71.33	21.361	222.420	0	28.154	61.469
	77.34	21.844	222.420	0	29.228	64.037

TABLE I (Continued)

LOW VELOCITY DATA - STEEL BALL BRINELL TESTS ON LEAD

TEST NO.	TIME (sec)	DEPTH OF PENETRATION (cm X 10^2)	LOAD (dynes X 10^{-6})	LOADING RATE (dynes/sec X 10^{-6})	ENERGY (ergs X 10^{-6})	VOLUME DISPLACED (cm^3 X 10^3)
L11	84.07	22.352	222.420	0	30.358	66.784
	93.13	22.860	222.420	0	31.488	69.577
	103.42	23.393	222.420	0	32.674	72.556
	116.86	23.901	222.420	0	33.804	75.437
	133.35	24.384	222.420	0	34.878	78.214
	148.93	24.892	222.420	0	36.007	81.177
	162.70	25.248	222.420	0	36.779	83.276
	178.22	25.629	222.420	0	37.647	85.546
	212.39	26.187	222.420	0	38.888	88.916
	227.62	26.441	222.420	0	39.453	90.463
	269.91	26.975	222.420	0	40.641	93.743
	303.82	27.457	222.420	0	41.712	96.746

TABLE II

LOW VELOCITY DATA - STEEL BALL BRINELL TESTS ON POLYETHYLENE

TEST NO.	TIME (sec)	DEPTH OF PENETRATION (cm X 10^2)	LOAD (dynes X 10^{-6})	LOADING RATE (dynes/sec X 10^{-6})	ENERGY (ergs X 10^{-6})	VOLUME DISPLACED (cm^3 X 10^3)
P3	4.23	2.87	15.13	3.577	0.218	0.502
	7.16	4.83	25.61	3.577	0.627	1.378
	9.59	6.43	35.30	3.577	1.120	2.378
	12.26	8.30	43.85	3.577	1.840	3.848
	13.94	9.40	49.86	3.577	2.380	4.832
	15.95	10.77	57.05	3.577	3.110	6.190
	17.85	12.22	63.85	3.577	3.900	7.760
	19.46	13.28	69.61	3.577	4.630	8.990
	21.76	14.99	77.84	3.577	5.790	11.090
	23.92	16.36	85.56	3.577	6.990	12.860
	25.65	17.60	91.75	3.577	8.050	14.510
	27.34	18.85	97.80	3.577	9.140	16.220
	28.64	20.12	102.45	3.577	10.030	17.990
	31.17	21.62	111.50	3.577	11.880	20.100
	32.82	22.68	117.39	3.577	13.170	21.610
	34.63	23.93	123.87	3.577	14.670	23.370
	37.26	25.70	133.50	0	16.980	25.840
	39.34	26.29	133.50	0	26.570	61.350
	40.62	26.47	133.50	0	26.810	62.320
	41.93	26.72	133.50	0	27.140	63.670
	44.62	26.97	133.50	0	27.480	65.040
	47.11	27.23	133.50	0	27.820	66.480
	49.82	27.41	133.50	0	28.060	67.490
	59.94	27.74	133.50	0	28.500	69.370
	65.46	27.99	133.50	0	28.840	70.820

TABLE II (Continued)

LOW VELOCITY DATA - STEEL BALL BRINELL TESTS ON POLYETHYLENE

TEST NO.	TIME (sec)	DEPTH OF PENETRATION (cm X 10^2)	LOAD (dynes X 10^{-6})	LOADING RATE (dynes/sec X 10^{-6})	ENERGY (ergs X 10^{-6})	VOLUME DISPLACED (cm^3 X 10^3)
	74.26	28.24	133.50	0	29.180	72.280
	86.92	28.50	133.50	0	29.520	73.820
	105.46	28.73	133.50	0	29.820	75.190
	140.01	28.96	133.50	0	30.130	76.590
	231.04	29.51	133.50	0	30.870	79.980
	258.76	29.64	133.50	0	31.040	80.800
	293.27	29.77	133.50	0	31.210	81.620

TABLE III

MODERATE VELOCITY DATA - STEEL INDENTER DROP TESTS ON 1100-0 ALUMINUM

SAMPLE MATERIAL	INDENTER RADIUS (cm)	DROP HEIGHT (cm)	INDENTER SHAPE	IMPACT VELOCITY (cm/sec X 10^{-2})	INDENTER MASS (g)	PENETRATION DEPTH (cm X 10^{2})	BASE AREA (cm^2 X 10^4)	ENERGY (ergs X 10^{-6})	VOLUME DISPLACED (cm^3 X 10^6)
1100-0	0.015	5.385	Cylinder	1.0273	447.1	5.1054	45.603	2.3593	232.82
AL		7.925	(Steel)	1.2463		7.4930		3.4724	341.70
		10.465		1.4322		9.2710		4.5852	422.78
		13.005		1.5965		10.1350		5.6983	462.19
		15.545		1.7455		10.4390		6.8111	476.05
		18.085		1.8827		12.7250		7.9242	580.30
1100-0		5.3848	Cylinder	1.0273	447.1	2.0066	126.68	2.3590	254.20
AL	0.025	5.4864	(Steel)	1.0370		1.8796		2.4038	238.11
		7.925		1.2462		2.7432		3.4720	347.51
		8.0264		1.2543		2.8956		3.5169	366.81
		10.465		1.4322		3.8862		4.5850	492.30
		10.566		1.4391		3.5306		4.6295	447.26
		10.566		1.4391		3.8608		4.6295	489.09
		13.005		1.5965		4.7752		5.6980	604.92
		13.106		1.6027		4.3942		5.7425	556.66
		13.106		1.6027		4.7244		5.7425	598.49
		13.106		1.6027		5.1308		5.7425	649.97
		15.545		1.7455		5.4610		6.8110	691.80
		15.545		1.7455		5.6134		6.8110	711.10
		15.646		1.7512		5.7658		6.8554	730.41
		18.085		1.8827		6.3246		7.9240	801.20
		18.186		1.8880		6.8072		7.9680	862.34
		20.625		2.0106		7.0358		9.0370	891.30
		20.726		2.0155		7.0870		9.0813	897.73
		20.726		2.0155		7.3152		9.0813	926.69
		20.726		2.0155		7.4168		9.0813	939.56
		23.165		2.1308		7.8740		10.1500	997.48
		23.266		2.1354		8.1280		10.1940	1029.60
		23.266		2.1354		8.9660		10.1940	1135.80
		25.705		2.2446		8.6360		11.263	1094.00
		28.245		2.3529		8.8140		12.376	1116.50
		28.346		2.3571		8.8390		12.420	1119.70
		28.346		2.3571		8.9410		12.420	1132.60
		28.346		2.3571		10.1850		12.420	1290.20
		29.616		2.4093		9.4230		12.976	1193.80

TABLE III (Continued)

MODERATE VELOCITY DATA - STEEL INDENTER DROP TESTS ON 1100-0 ALUMINUM

SAMPLE MATERIAL	INDENTER RADIUS (cm)	DROP HEIGHT (cm)	INDENTER SHAPE	IMPACT VELOCITY (cm/sec X 10^{-2})	INDENTER MASS (g)	PENETRATION DEPTH (cm X 10^{2})	BASE AREA (cm^2 X 10^{4})	ENERGY (ergs X 10^{-6})	VOLUME DISPLACED (cm^3 X 10^{6})
1100-0	0.075	7.9248	Cylinder	1.2463	447.1	0.2540	1140.1	3.4724	2895.80
AL		13.0050	(Steel)	1.5965		0.5080		5.6983	5791.70
		15.545		1.7455		0.4064		6.6811	4633.40
		18.085		1.8827		0.6604		7.9242	7529.20
		20.625		2.0106		0.5580		9.0370	6370.90
		23.165		2.1308		0.7620		10.1498	8687.60
		25.705		2.2446		0.7620		11.2630	8687.60
		28.245		2.3529		0.8128		12.3757	9266.70
		28.245		2.3529		1.0414		12.3760	11873.00
		29.515		2.4052		1.1176		12.9320	12742.00
1100-0	0.18675	7.8233	Sphere	1.2383	450.3	1.3208		3.4520	261.97
AL		12.9030	(Steel)	1.5903		1.7272		5.6940	439.14
		17.9830		1.8774		2.0574		7.9359	621.64
		23.0630		2.1261		2.2098		10.1770	716.38
		28.1430		2.3486		2.5908		12.4190	982.02
1100-0	0.18675	8.0518	Sphere	1.2562	1126.8	1.4478		8.8910	309.16
AL		13.1320	(Steel)	1.6043		2.0066		14.5010	591.52
		18.2120		1.8893		2.4892		20.1100	907.17
		23.2920		2.1366		2.7940		25.7200	1140.48
		28.3720		2.3581		2.9210		31.3300	1245.29
1100-0	90° incl.	8.1788	Cone	1.2661	448.8	5.8166		3.5971	206.08
AL	Angle	13.2590	(Steel)	1.6121		6.6040		5.8317	301.62
		18.3390		1.8959		7.9502		8.0658	526.22
		23.4190		2.1424		9.3472		10.3000	855.21
		28.4990		2.3634		8.8900		12.5340	735.75
1100-0	90° incl.	8.8646	Cone	1.3181	1127.2	7.4930		9.7925	440.55
AL	Angle	13.9450	(Steel)	1.6532		8.8646		15.4040	729.47
		19.0250		1.9310		10.0840		21.0160	1073.80
		24.1050		2.1736		11.0490		26.6280	1412.50
		29.1850		2.3917		11.8360		32.2400	1736.30

TABLE III (Continued)
MODERATE VELOCITY DATA - STEEL INDENTER DROP TESTS ON 1100-0 ALUMINUM

SAMPLE MATERIAL	INDENTER RADIUS (cm)	DROP HEIGHT (cm)	INDENTER SHAPE	IMPACT VELOCITY (cm/sec X 10^{-2})	INDENTER MASS (g)	PENETRATION DEPTH (cm X 10^{2})	BASE AREA (cm^2 X 10^4)	ENERGY (ergs X 10^{-6})	VOLUME DISPLACED (cm^3 X 10^6)
1100-0	0.0375	5.563	Cylinder	1.0442	447.1	0.9398	277.47	2.4374	260.77
AL		8.103	(Steel)	1.2602		1.3970		3.5502	387.62
		10.643		1.4443		2.0066		4.6632	556.77
		13.183		1.6074		2.2352		5.7763	620.20
		15.723		1.7555		2.9718		6.8891	824.58
		18.263		1.8919		3.3528		8.0020	930.30
		20.803		2.0192		3.6068		9.1150	1000.80
		23.343		2.1390		4.0894		10.2280	1134.70
		25.883		2.225		4.8006		11.3410	1332.00
		28.423		2.3601		4.9784		12.4520	1381.40
		29.693		2.4124		5.2578		13.0100	1458.90
1100-0	0.0375	8.7376	Cylinder	1.3087	1125.0	2.6416	277.47	9.6334	732.96
AL		13.818	(Steel)	1.6457		4.3688		15.2340	1212.20
		18.898		1.9246		6.2738		20.8350	1740.80
		23.978		2.1679		7.0866		26.4360	1966.30
		29.058		2.3865		8.1280		32.0370	2255.30
		29.058		2.3865		8.8900		32.0370	2466.70
1100-0	0.050	5.486	Cylinder	1.0370	447.1	0.3810	506.71	2.4038	195.06
AL		5.486	(Steel)	1.0370		0.4826		2.4038	244.54
		10.566		1.4391		0.9652		4.6295	489.08
		13.106		1.6027		1.4732		5.7425	746.48
		13.106		1.6027		1.6002		5.7425	810.84
		15.646		1.7512		1.8288		6.8554	926.67
		18.186		1.8880		1.8542		7.9682	939.54
		18.186		1.8880		2.2098		7.9682	1119.70
		20.726		2.0155		2.3368		9.0813	1184.10
		23.266		2.1354		2.2606		10.1940	1145.50
		23.266		2.1354		2.4638		10.1940	1248.40
		23.266		2.1354		2.5400		10.1940	1287.00
		25.806		2.2490		2.7686		11.3070	1402.90
		28.346		2.3571		3.1242		12.420	1583.10

TABLE IV
HIGH VELOCITY IMPACT DATA - MERCURY DROPS

SAMPLE MATERIAL	DROP DIAMETER (mm)	DROP SHAPE	IMPACT VELOCITY (cm/sec X 10^{-4})	DROP MASS (g)	DEPTH OF PENETRATION (cm X 10^3)	DAMAGE RADIUS (cm X 10^3)	ENERGY (ergs X 10^{-6})	VOLUME DISPLACED (cm^3 X 10^3)	γ	MEASURED ACCURACY INDEX
AL 1100-0	1.0	Sphere (Hg)	1.058	0.0071	2.79	20.57	0.397	0.0013	1.424	2
			1.402		2.54	26.28	0.697	0.0011	2.361	3
			1.414		4.32	22.86	0.709	0.0032	1.203	2
			1.622		2.54	26.28	0.932	0.0011	2.191	3
			1.631		7.62	33.15	0.943	0.0087	1.438	3
			2.091		16.51	59.05	1.550	0.056	2.273	3
			2.094		15.24	50.67	1.555	0.047	1.814	3
			2.134		22.60	63.50	1.614	0.111	2.145	2
			2.444		24.13	68.58	2.119	0.127	2.399	3
			2.758		35.05	59.69	2.698	0.273	2.126	2
			2.780		30.48	70.87	2.740	0.350	2.341	3
			3.657		60.96	57.15	4.744	0.495	1.492	3
			4.572		83.82	62.23	7.413	0.889	1.926	3
			4.785		90.67	60.96	8.121	9.277	1.811	2
			5.394		98.81	60.96	10.322	1.023	1.801	2
			5.791		121.92	59.69	11.894	1.234	1.700	3
			5.913		104.14	57.15	12.400	0.938	1.492	3
			6.096		124.46	59.69	13.179	1.262	1.700	3
			6.431		135.38	74.93	14.668	2.257	3.363	2
			7.132		154.94	68.58	18.040	2.158	2.578	3
			8.047		160.0	76.20	22.962	2.788	3.537	2
AL 1100-0	1.5	Sphere (Hg)	1.051	0.0239	3.81	34.29	1.323	0.0039	1.844	3
			1.390		6.35	38.10	2.312	0.012	1.454	2
			1.402		10.92	57.15	2.353	0.040	1.898	2
			1.631		10.16	59.43	3.183	0.034	1.962	3
			1.631		11.43	54.86	3.183	0.043	1.870	3
			2.088		44.45	89.15	5.218	0.547	1.726	3
			2.103		26.67	101.85	5.294	0.320	2.810	3
			2.444		45.72	113.03	7.152	1.393	3.423	2
			2.780		55.88	109.73	9.248	1.672	3.131	3
			3.124		88.90	94.86	11.682	2.072	2.024	3
			3.124		91.44	92.58	11.682	2.020	1.881	3
			4.374		121.92	93.72	22.897	2.923	1.951	3
			4.755		147.32	105.02	27.060	4.664	2.726	3

TABLE IV (Continued)
HIGH VELOCITY IMPACT DATA - MERCURY DROPS

SAMPLE MATERIAL	DROP DIAMETER (mm)	DROP SHAPE	IMPACT VELOCITY (cm/sec X 10^{-4})	DROP MASS (g)	DEPTH OF PENETRATION (cm X 10^3)	DAMAGE RADIUS (cm X 10^3)	ENERGY (ergs X 10^{-6})	VOLUME DISPLACED (cm^3 X 10^3)	γ	MEASURED ACCURACY INDEX
AL	1.5	Sphere	4.998	0.0239	137.16	102.87	29.907	4.118	2.580	3
1100-0		(Hg)	5.182		189.23	102.87	32.135	5.849	2.580	3
			5.303		213.36	104.01	33.665	6.810	2.667	3
			6.248		220.98	107.44	46.729	7.572	2.940	3
			6.248		223.52	102.87	46.729	6.989	2.580	3
			6.827		226.06	101.85	55.793	7.074	2.504	3
			6.827		226.06	102.87	55.793	6.926	2.580	3
			7.925		292.10	114.30	75.167	11.547	3.539	3
AL	1.612	Sphere	3.139	0.0297	80.77	110.49	14.641	2.550	2.577	1
1100-0	1.571	(Hg)	3.536	0.0275	95.76	108.20	17.156	3.016	2.824	1
	1.630		4.816	0.0307	167.13	112.40	35.619	6.066	2.623	1
	1.588		5.639	0.0284	191.52	119.38	45.155	8.050	3.399	1
	1.584		5.730	0.0282	196.85	121.67	46.280	8.634	3.624	1
	1.548		5.730	0.0263	213.61	119.13	43.195	9.038	3.648	1
	1.671		6.462	0.0331	249.43	135.26	68.965	13.725	4.241	1
	1.571		6.949	0.0275	264.67	126.75	66.279	13.440	4.202	1
	1.567		6.949	0.0273	287.53	127.76	65.774	14.242	4.334	1
	1.630		7.437	0.0307	436.88	125.73	84.948	21.180	3.671	1
	1.626		7.620	0.0305	335.03	132.08	88.522	17.798	4.286	1
	1.630		7.620	0.0307	347.98	139.06	89.177	20.575	4.967	1
AL	1.95	Sphere	1.060	0.0526	2.54	44.58	2.958	0.0020	2.949	3
1100-0		(Hg)	1.390		11.43	59.44	5.080	0.038	1.483	3
			1.390		12.70	54.86	5.080	0.0505	1.265	3
AL	1.97	Sphere	1.622	0.542	12.70	70.87	7.129	0.0711	1.890	3
1100-0		(Hg)	2.091		30.48	111.88	11.854	0.554	2.174	3
			2.444		43.18	141.86	16.202	1.253	2.900	3
			2.780		55.88	135.00	20.951	2.199	2.460	3
AL	2.0	Sphere	3.429	0.0567	132.1	112.14	33.358	4.171	1.415	3
1100-0		(Hg)	3.917		152.40	110.99	43.522	4.852	1.368	3
			4.176		165.1	110.99	49.470	5.343	1.368	3
			4.176		173.99	118.87	49.470	6.677	1.680	3

TABLE IV (Continued)
HIGH VELOCITY IMPACT DATA - MERCURY DROPS

SAMPLE MATERIAL	DROP DIAMETER (mm)	DROP SHAPE	IMPACT VELOCITY (cm/sec X 10^{-4})	DROP MASS (g)	DEPTH OF PENETRATION (cm X 10^3)	DAMAGE RADIUS (cm X 10^3)	ENERGY (ergs X 10^{-6})	VOLUME DISPLACED (cm^3 X 10^3)	γ	MEASURED ACCURACY INDEX
AL 1100-0	2.0	Sphere (Hg)	4.343	0.0567	177.8	112.14	53.522	5.977	1.415	3
			4.724		205.74	114.30	63.323	7.397	1.493	3
			5.517		283.2	118.87	86.349	11.525	1.680	3
			7.071		373.3	123.32	141.865	16.791	1.881	3
AL 1100-0	2.5	Sphere (Hg)	0.698	0.1108	2.54	41.14	2.700	0.0027	2.114	3
			1.039		7.62	48.26	5.986	0.022	1.271	2
			1.390		17.78	68.58	10.704	0.189	1.388	3
			1.390		22.86	59.44	10.704	0.341	1.0	3
			1.670		33.02	91.44	15.456	0.821	1.151	3
			2.091		60.19	160.02	24.226	1.195	2.204	2
			2.780		99.06	173.9	42.817	7.376	5.747	3
AL 1100-0	2.85	Sphere (Hg)	0.701	0.1642	3.81	38.10	4.035	0.064	1.270	2
			1.055		6.60	44.45	9.130	0.192	1.088	2
			1.390		20.06	86.36	15.859	1.718	1.314	2
			1.640		39.88	105.41	22.075	6.455	1.108	2
			2.081		76.20	173.99	35.578	5.488	1.908	3
			2.444		99.06	219.7	49.056	11.992	6.472	3
			2.780		114.30	191.77	63.436	10.175	2.438	3
			2.780		123.19	194.3	63.436	11.581	2.536	3
AL 2024	1.032	Sphere (Hg)	1.966	0.0078	80.01	40.00	1.506	0.021	1.738	1
	0.956		2.454	0.0062	20.07	57.15	1.865	0.084	2.242	1
	0.940		2.816	0.0059	23.36	66.04	2.336	0.116	3.104	1
	1.032		2.890	0.0078	25.62	71.12	3.254	0.157	3.123	1
	0.976		3.413	0.0066	35.31	72.39	3.842	0.460	3.264	1
	0.996		3.627	0.0070	44.69	71.12	5.119	0.773	2.913	1
	1.037		3.797	0.0079	49.02	76.20	5.688	0.749	3.174	1
	0.996		3.822	0.0070	46.10	73.66	4.610	0.565	3.236	1
	1.037		4.322	0.0079	61.47	74.93	7.366	0.939	3.018	1
	1.009		4.669	0.0073	67.56	71.76	7.920	0.959	2.877	1
	0.946		4.745	0.0060	59.44	67.31	6.762	0.735	2.882	1
	1.041		4.995	0.0080	76.71	71.12	9.957	1.072	2.555	1
	1.000		5.145	0.0071	77.22	71.12	9.388	1.118	2.878	1

TABLE IV (Continued)
HIGH VELOCITY IMPACT DATA - MERCURY DROPS

SAMPLE MATERIAL	DROP DIAMETER (mm)	DROP SHAPE	IMPACT VELOCITY (cm/sec X 10^{-4})	DROP MASS (g)	DEPTH OF PENETRATION (cm X 10^3)	DAMAGE RADIUS (cm X 10^3)	ENERGY (ergs X 10^{-6})	VOLUME DISPLACED (cm^3 X 10^3)	γ	MEASURED ACCURACY INDEX
AL	1.058	Sphere	5.517	0.0084	93.73	76.20	12.783	1.555	2.988	1
2024	1.014	(Hg)	5.752	0.0074	95.50	69.85	12.231	1.327	2.615	1
	0.971		6.004	0.0065	99.06	74.93	11.670	1.628	3.676	1
	0.961		6.066	0.0063	96.77	73.66	11.543	1.534	3.603	1
	1.032		6.251	0.0076	112.52	74.93	15.233	1.841	3.062	1
	1.028		6.736	0.0074	130.80	73.66	17.481	2.088	2.943	1
	0.971		7.047	0.0065	124.08	72.39	16.073	2.125	3.314	1
	0.971		7.047	0.0065	149.86	74.93	16.073	2.031	3.676	1
	1.032		7.525	0.0078	13.33	81.28	22.074	2.624	3.908	1
	1.028		8.019	0.0077	146.56	79.37	24.776	2.759	3.683	1
	1.037		8.071	0.0079	159.77	85.09	26.391	3.489	4.421	1
	1.014		8.074	0.0074	148.84	82.55	24.104	3.050	4.316	1
	1.023		8.525	0.0076	166.50	86.36	27.514	3.887	4.813	1
	1.045		8.772	0.0081	176.27	90.81	31.052	4.417	5.249	1
	0.946		9.195	0.0060	162.81	86.36	25.388	3.704	6.086	1
	0.966		9.229	0.064	163.57	82.55	27.230	3.384	4.992	1
	1.019		9.623	0.0075	182.88	86.99	34.642	4.210	4.978	1
	0.956		10.058	0.0062	162.56	82.55	31.348	3.366	5.151	1
AL	1.5	Sphere	1.335	0.0239	7.24	39.37	2.133	0.014	1.390	3
2024		(Hg)	2.243		22.86	84.45	6.023	0.215	2.160	3
			2.999		26.16	106.7	10.766	0.230	2.878	2
			3.459		58.42	95.25	14.324	1.223	2.048	2
			3.475		58.42	104.1	14.451	1.549	2.677	3
			3.536		60.96	100.3	14.962	1.486	2.394	2
			3.962		81.28	93.98	18.792	1.820	1.967	3
			4.694		120.65	113.03	26.371	4.401	3.423	3
AL	1.9514	Sphere	1.7586	0.0527	12.44	71.12	8.133	0.058	1.872	1
2024	1.9175	(Hg)	2.316	0.0499	27.18	106.68	13.427	0.323	2.208	1
	1.998		2.554	0.0566	38.35	116.84	18.454	0.738	2.032	1
	2.0122		2.682	0.0578	48.39	128.27	20.781	1.242	2.184	1
	1.969		2.789	0.0543	49.02	135.89	21.024	1.248	2.569	1
	1.984		3.048	0.0554	55.88	144.78	25.730	2.658	2.162	1
	2.017		3.200	0.0582	71.12	165.10	29.762	5.018	5.123	1
	1.9672		3.377	0.0540	85.60	151.13	30.735	5.147	3.627	1

TABLE IV (Continued)
HIGH VELOCITY IMPACT DATA - MERCURY DROPS

SAMPLE MATERIAL	DROP DIAMETER (mm)	DROP SHAPE	IMPACT VELOCITY (cm/sec X 10^{-4})	DROP MASS (g)	DEPTH OF PENETRATION (cm X 10^{3})	DAMAGE RADIUS (cm X 10^{3})	ENERGY (ergs X 10^{-6})	VOLUME DISPLACED (cm^3 X 10^3)	γ	MEASURED ACCURACY INDEX
AL	2.0330	Sphere	3.596	0.0596	94.36	142.88	38.490	4.961	2.777	1
2024	2.047	(Hg)	4.008	0.0608	264.16	132.08	48.795	4.642	2.149	1
	2.031		4.084	0.0594	109.47	143.51	49.489	5.988	2.822	1
	2.010		4.517	0.0576	259.08	129.54	58.762	6.703	2.141	1
	2.0572		5.489	0.0671	241.55	143.50	92.876	14.491	2.716	1
	2.000		5.727	0.0567	206.50	146.05	93.058	12.671	3.075	1
	1.982		6.834	0.0067	264.67	201.93	128.942	32.885	8.763	1
AL	1.5	Sphere	3.627	0.0239	29.72	120.65	15.746	0.917	4.162	2
7075-T4		(Hg)	3.779		30.48	127.0	17.097	1.103	4.855	3
			3.978		38.35	127.00	18.937	1.502	4.855	2
			4.526		47.50	104.14	24.521	1.176	2.678	2
			4.907		66.04	105.41	28.823	1.863	2.776	3
			5.364		76.20	93.98	34.444	1.672	1.967	3
			5.502		86.11	116.84	36.227	3.521	3.780	2
			6.541		127.76	127.00	51.208	6.032	4.855	2
			6.706		140.72	111.76	53.818	5.080	3.308	2
			6.858		125.98	107.95	56.292	4.170	2.982	2,
			7.284		166.12	114.30	63.515	6.372	3.539	2
			7.620		157.48	106.68	69.496	4.924	2.677	2
COPPER	1.0	Sphere	1.631	0.0071	3.81	31.75	0.943	0.0023	2.339	3
		(Hg)	1.875		7.62	35.56	1.246	0.0090	1.623	3
			2.115		10.16	40.64	1.587	0.0159	1.643	3
			2.444		16.51	45.72	2.119	0.0414	1.430	3
			2.658		20.32	49.53	2.505	0.0619	1.308	3
			2.896		25.40	54.61	2.973	0.0948	1.519	3
			2.987		25.40	53.34	3.164	0.217	1.213	2
			3.566		38.10	68.58	4.510	0.432	2.578	2
			4.267		48.26	73.66	6.458	0.692	3.195	2
			5.060		63.50	82.55	9.079	1.228	4.497	2
			5.486		71.12	81.28	10.675	1.345	4.292	2
			6.066		78.74	86.36	13.047	1.714	5.149	2
			6.523		81.28	86.36	15.088	1.774	5.149	3

TABLE IV (Continued)
HIGH VELOCITY IMPACT DATA - MERCURY DROPS

SAMPLE MATERIAL	DROP DIAMETER (mm)	DROP SHAPE	IMPACT VELOCITY (cm/sec X 10^{-4})	DROP MASS (g)	DEPTH OF PENETRATION (cm x 10^3)	DAMAGE RADIUS (cm X 10^3)	ENERGY (ergs X 10^{-6})	VOLUME DISPLACED (cm^3 X 10^3)	γ	MEASURED ACCURACY INDEX
COPPER	1.0	Sphere	7.620	0.0071	99.06	93.98	20.592	2.618	6.635	2
		(Hg)	7.864		104.14	96.52	21.930	2.917	7.188	2
COPPER	0.946	Sphere	1.965	0.0060	9.39	37.46	1.160	0.020	1.598	1
	0.913	(Hg)	1.965	0.0054	10.16	40.00	1.040	0.024	1.753	1
	1.005		1.965	0.0072	13.97	30.48	1.387	0.056	1.000	1
	0.966		1.965	0.0064	16.25	42.54	1.236	0.076	1.322	1
	1.041		1.978	0.0077	16.256	42.54	1.561	0.083	1.218	1
	0.976		2.432	0.0066	21.59	52.07	1.951	0.178	1.562	1
	1.037		2.829	0.0079	29.46	64.77	3.155	0.378	1.980	1
	1.054		3.246	0.0079	39.11	77.47	4.376	0.584	3.177	1
	1.102		3.706	0.0095	44.45	87.63	6.520	0.897	4.022	1
	0.981		3.761	0.0067	43.68	72.39	4.722	0.596	3.214	1
	1.070		3.944	0.0081	51.31	80.01	6.758	0.871	3.345	1
	1.045		4.401	0.0081	58.67	80.65	7.817	1.050	3.677	1
	0.991		4.724	0.0069	61.47	83.18	7.680	1.209	4.731	1
	0.951		5.038	0.0061	59.94	78.10	7.718	1.037	14.413	1
	0.890		5.371	0.0050	64.52	78.70	7.211	1.164	5.540	1
	0.956		5.779	0.0062	74.16	83.19	10.348	1.498	5.270	1
	1.045		6.126	0.0081	83.56	100.33	15.146	2.494	7.080	1
	0.951		6.486	0.0061	84.58	92.71	15.620	2.172	7.412	1
	1.041		6.772	0.0080	97.28	101.60	18.298	3.007	7.348	1
	0.991		7.0896	0.0069	92.96	101.60	17.296	2.889	8.621	1
	1.010		7.388	0.0073	93.22	104.14	19.945	3.041	8.769	1
	0.991		7.5255	0.0697	97.03	111.76	19.488	3.680	11.474	1
	0.935		8.074	0.0060	97.03	97.79	18.837	2.808	9.153	1
	1.065		8.409	0.0086	116.84	115.57	30.209	4.745	10.224	1
	1.019		8.708	0.0075	113.79	111.76	28.371	4.327	10.554	1
	1.028		9.832	0.0077	138.94	124.5	37.249	6.619	14.187	1
	1.036		10.500	0.0079	130.30	135.9	43.478	7.414	18.053	1
COPPER	1.5	Sphere	1.390	0.0239	6.35	39.37	2.312	0.0109	1.536	3
		(Hg)	1.631		7.62	45.72	3.183	0.0161	1.710	3
			1.874		13.97	54.61	4.206	0.0604	1.450	3
			2.118		16.51	62.23	5.371	0.0876	1.584	3

TABLE IV (Continued)
HIGH VELOCITY IMPACT DATA - MERCURY DROPS

SAMPLE MATERIAL	DROP DIAMETER (mm)	DROP SHAPE	IMPACT VELOCITY (cm/sec X 10^{-4})	DROP MASS (g)	DEPTH OF PENETRATION (cm X 10^3)	DAMAGE RADIUS (cm X 10^3)	ENERGY (ergs X 10^{-6})	VOLUME DISPLACED (cm^3 X 10^3)	γ	MEASURED ACCURACY INDEX
COPPER	1.5	Sphere (Hg)	2.444	0.0239	25.40	69.85	7.152	0.230	1.435	3
			2.780		33.02	77.47	9.248	0.414	1.465	3
			2.926		38.10	86.36	10.248	0.567	1.700	3
			3.200		43.18	88.90	12.260	0.739	1.720	3
			3.657		55.88	100.33	16.012	1.325	2.394	3
			4.145		66.04	102.87	20.566	1.754	2.581	3
			5.090		93.98	115.57	31.011	3.502	3.659	3
			6.492		137.16	130.81	50.448	6.931	5.306	3
			7.452		142.24	134.62	66.472	7.656	5.784	3
COPPER	1.62	Sphere (Hg)	2.804	0.0301	35.56	96.52	11.856	0.648	2.571	3
			3.535	0.0301	76.20	116.84	18.848	2.712	3.780	3
			4.633	0.0301	88.90	119.38	32.362	3.424	4.032	3
			5.121	0.0301	109.22	120.65	39.534	4.438	4.162	3
			5.486	0.0301	109.22	132.08	45.384	5.429	5.461	3
			6.156	0.0301	111.76	139.70	57.155	6.296	6.462	3
			6.568	0.0301	132.08	146.05	65.050	8.924	7.384	3
COPPER	2.027	Sphere (Hg)	1.773	0.0059	29.16	67.3	9.281	0.389	1.042	1
	2.002		2.402	0.0569	47.75	96.52	16.416	1.748	1.183	1
	2.064		2.542	0.0624	66.04	120.63	20.149	3.517	1.279	1
	1.989		2.7157	0.0588	59.69	127.64	20.550	2.747	2.111	1
	1.953		2.779	0.0528	58.67	123.19	20.382	2.579	2.393	1
	2.030		2.8407	0.0593	64.01	125.73	23.940	3.234	1.795	1
	2.113		2.850	0.0669	74.67	130.81	27.134	2.781	1.899	1
	2.012		2.865	0.0578	65.53	142.24	23.711	2.234	2.827	1
	2.012		2.865	0.0578	67.82	124.46	23.711	3.099	1.824	1
	2.004		2.890	0.0571	65.02	133.35	23.830	2.579	2.357	1
	1.991		2.984	0.0560	76.96	172.72	24.885	6.181	7.76	1
	2.032		3.2247	0.0595	82.29	153.67	30.942	4.906	3.209	1
	1.889		3.310	0.0478	76.71	138.43	26.150	3.737	3.149	1
	1.951		3.313	0.0527	76.58	140.97	28.865	3.818	2.967	1
	2.006		3.438	0.0573	73.66	148.59	33.839	4.053	3.281	1
	1.972		3.575	0.0544	94.74	158.75	34.764	6.497	4.174	1
	2.032		3.663	0.0595	131.82	233.68	39.938	21.516	13.604	1

TABLE IV (Continued)
HIGH VELOCITY IMPACT DATA - MERCURY DROPS

SAMPLE MATERIAL	DROP DIAMETER (mm)	DROP SHAPE	IMPACT VELOCITY (cm/sec X 10^{-4})	DROP MASS (g)	DEPTH OF PENETRATION (cm X 10^3)	DAMAGE RADIUS (cm X 10^3)	ENERGY (ergs X 10^{-6})	VOLUME DISPLACED (cm^3 X 10^3)	γ	MEASURED ACCURACY INDEX
COPPER	1.997	Sphere	3.697	0.0565	83.57	167.64	38.549	6.337	4.721	1
	2.011	(Hg)	3.986	0.0577	123.19	198.12	45.773	14.128	7.650	1
	2.006		4.084	0.0573	107.31	168.91	47.754	8.551	4.819	1
	2.004		4.096	0.0571	110.74	156.2	47.896	7.436	3.818	1
	2.048		4.322	0.0609	122.68	165.10	56.905	9.381	4.191	1
	2.003		4.401	0.0570	123.19	153.67	55.123	8.089	3.612	1
	2.025		4.450	0.0588	123.44	161.29	58.230	9.003	4.042	1
	1.990		4.8615	0.0559	135.4	165.10	66.053	10.562	4.709	1
	2.099		5.919	0.0669	191.38	182.24	114.743	18.774	5.225	1
	2.046		6.069	0.0607	179.19	214.63	111.858	24.831	9.235	1
	2.018		6.315	0.0583	177.54	177.80	116.239	16.557	5.472	1
	1.995		6.410	0.0563	169.92	201.9	115.522	19.103	8.312	1
	1.990		6.461	0.0589	199.90	208.28	116.692	26.211	9.172	1
LEAD	1.0	Sphere	1.027	0.0071	8.89	40.01	0.374	0.0230	1.725	3
		(Hg)	1.036		15.24	45.72	0.381	0.0864	1.497	3
			1.432		20.57	64.77	0.728	0.161	2.399	2
			1.432		24.13	65.15	0.728	0.254	2.173	3
			1.618		21.59	73.15	0.929	0.198	3.147	3
			2.057		17.15	69.72	1.501	4.122	2.726	3
			2.082		40.64	86.87	1.537	0.832	5.244	3
			2.444		50.31	82.55	2.119	0.968	4.500	2
			2.780		58.42	94.74	2.740	1.516	6.803	3
			2.789		23.24	80.01	2.758	1.044	4.098	3
			3.658		30.48	91.44	4.744	1.937	6.117	3
			4.754		39.62	10.52	8.018	3.557	9.303	3
LEAD	1.5	Sphere	0.695	0.0239	7.87	35.56	0.578	0.023	1.101	2
		(Hg)	1.058		20.07	76.20	1.339	0.226	1.953	2
			1.396		38.61	107.95	2.332	0.972	3.015	2
			1.622		30.48	116.58	3.147	0.658	3.767	3
			1.859		65.02	123.19	4.138	2.658	4.431	2
			2.081		66.54	128.27	5.187	2.998	5.002	2
			2.451		84.83	140.97	7.188	4.855	6.640	2
			2.780		106.68	146.43	9.248	6.744	7.461	3

TABLE IV (Continued)
HIGH VELOCITY IMPACT DATA - MERCURY DROPS

SAMPLE MATERIAL	DROP DIAMETER (mm)	DROP SHAPE	IMPACT VELOCITY (cm/sec X 10^{-4})	DROP MASS (g)	DEPTH OF PENETRATION (cm X 10^3)	DAMAGE RADIUS (cm X 10^3)	ENERGY (ergs X 10^{-6})	VOLUME DISPLACED (cm^3 X 10^3)	γ	MEASURED ACCURACY INDEX
LEAD	1.5	Sphere (Hg)	2.987	0.0239	134.62	146.43	10.679	8.611	7.422	3
			3.368		146.05	160.02	13.577	11.307	9.712	2
LEAD	1.95	Sphere (Hg)	0.694	0.0526	12.70	54.86	1.270	0.081	1.233	3
			1.061		25.40	89.15	2.958	0.436	2.660	3
			1.061		25.40	100.58	2.958	0.436	2.038	3
			1.133		43.18	128.27	3.381	1.557	2.277	3
			1.390		34.29	102.87	5.080	0.906	1.174	3
			1.390		38.10	137.16	5.080	1.165	2.784	3
			1.390		45.72	134.87	5.080	1.780	2.662	3
LEAD	1.98	Sphere (Hg)	1.390	0.0551	35.56	118.87	5.318	0.911	2.030	3
			1.622		83.82	146.30	7.238	4.620	3.132	3
			2.091		81.28	155.57	12.035	5.164	3.775	3
			2.441		100.33	167.01	16.408	7.775	4.668	3
			2.780		119.38	169.29	21.271	9.732	4.863	3
			2.780		126.42	161.29	21.271	9.322	4.196	2
LEAD	2.0	Sphere (Hg)	3.155	0.0567	149.86	164.46	28.234	11.687	4.438	3
			3.810		190.50	189.60	41.183	20.469	6.831	3
			4.191		215.90	195.58	49.832	24.898	7.481	3
			5.014		254.0	214.63	71.323	35.712	9.887	3
LEAD	2.5	Sphere (Hg)	0.695	0.1108	7.62	64.01	2.676	0.0288	1.928	3
			1.061		32.51	125.73	6.234	0.885	1.946	2
			1.390		66.04	164.46	10.704	4.450	2.281	3
			1.646		78.48	189.20	15.011	6.784	3.469	2
			2.097		121.92	219.70	24.367	16.444	5.430	3
			2.451		178.31	227.30	33.278	26.904	6.015	2
LEAD	2.85	Sphere (Hg)	0.695	0.1642	16.00	66.04	3.965	0.168	1.010	2
			1.061		45.72	138.43	9.236	2.065	1.608	2
			1.622		111.25	219.0	21.586	13.744	3.640	2
			2.115		158.49	237.49	36.734	25.054	4.629	2
			2.444		182.88	252.73	49.056	33.667	5.507	2
			2.780		226.06	251.46	63.436	41.876	5.495	3

TABLE IV (Continued)
HIGH VELOCITY IMPACT DATA - MERCURY DROPS

SAMPLE MATERIAL	DROP DIAMETER (mm)	DROP SHAPE	IMPACT VELOCITY (cm/sec X 10^{-4})	DROP MASS (g)	DEPTH OF PENETRATION (cm X 10^3)	DAMAGE RADIUS (cm X 10^3)	ENERGY (ergs X 10^{-6})	VOLUME DISPLACED (cm^3 X 10^3)	γ	MEASURED ACCURACY INDEX
COLD	1.5	Sphere	4.846	0.0239	21.08	110.49	28.111	0.347	3.797	2
ROLLED		(Hg)	5.730		38.10	123.19	39.301	1.375	3.905	3
STEEL			5.425		30.48	115.57	35.231	0.836	4.218	3
(ANNEALED)			5.776		33.02	123.19	39.903	1.132	3.905	3
			6.431		40.64	130.80	49.505	1.743	5.305	3
			6.523		45.72	132.08	50.923	2.065	5.461	3
			7.406		58.42	135.89	65.659	2.947	5.948	3
			7.544		66.04	137.16	68.114	3.461	6.116	3
			7.742		68.58	137.16	71.738	3.611	6.116	3
			7.894		67.56	143.5	74.590	3.930	7.005	2
321	1.440	Sphere	2.840	0.0212	6.096	50.80	8.545	0.014	2.390	1
Stainless	1.440	(Hg)	3.234	0.0212	10.160	63.50	11.075	0.049	2.531	1
Steel	1.438		3.331	0.0211	8.890	63.50	11.704	0.035	2.751	1
	1.417		3.773	0.0202	13.208	76.20	14.336	0.093	2.884	1
	1.503		4.782	0.0241	38.10	104.77	27.483	1.287	3.260	1
	1.471		6.157	0.0226	51.82	123.19	42.704	2.055	4.699	1
	1.467		6.449	0.0224		121.92			4.592	1
	1.440		6.928	0.0212	53.84	127.00	50.827	2.338	5.488	1
	1.445		7.254	0.0214	54.86	133.35	56.191	2.671	6.287	1
	1.429		7.299	0.0207	57.658	135.89	55.031	2.964	6.880	1
	1.422		8.239	0.0204	74.17	135.89	72.177	3.910	6.982	1
	1.461		8.525	0.0221	81.03	140.97	80.215	4.651	7.186	1
	1.476		8.839	0.0228	87.12	140.97	89.097	5.018	6.970	1
	1.532		10.229	0.0255	88.90	141.605	133.423	5.130	6.317	1
	1.508		10.564	0.0243	107.18	147.32	135.728	6.859	7.459	1
	1.489		11.235	0.0234	111.25	148.59	147.479	7.286	7.958	1
	1.538		12.607	0.0258	135.89	160.02	205.04	10.455	9.010	1
	1.431		14.868	0.0208	124.96	154.31	229.246	8.965	10.031	1

TABLE V

HIGH VELOCITY IMPACT DATA - STEEL BALLS AND WATER DROPS

SAMPLE MATERIAL	DROP DIAMETER (mm)	DROP SHAPE	IMPACT VELOCITY (cm/sec X 10^{-4})	DROP MASS (g)	DEPTH OF PENETRATION (cm X 10^3)	DAMAGE RADIUS (cm X 10^3)	ENERGY (ergs X 10^{-6})	VOLUME DISPLACED (cm^3 X 10^3)	γ	MEASURED ACCURACY INDEX
AL 1100-0	1.0	Sphere (Steel Ball)	3.484	0.0071	56.13	50.80	2.478	0.324	1.048	1
			4.654		86.87	55.24	4.424	0.702	1.395	1
			4.654		89.28	58.42	4.424	0.828	1.594	1
			6.797		149.86	63.50	9.434	1.767	2.047	1
			9.449		125.09	67.31	18.231	3.430	2.438	1
AL 2024	2.0	Sphere (H_2O)	4.581	0.00419	2.29	49.02	43.95	0.0016	3.555	2
			4.581		2.54	57.15	43.95	0.0020	4.141	2
			4.852		5.33	46.99	49.32	0.0088	1.782	2
			5.456		4.57	62.23	62.34	0.0065	3.062	2
			6.370		10.67	143.51	84.99	0.0345	6.378	2
			6.584		11.68	78.74	90.78	0.0412	2.268	2
			7.224		14.73	99.06	109.29	0.0648	2.773	2
			7.498		20.57	116.84	117.75	0.1239	2.934	2
COPPER	2.0	Sphere (H_2O)	4.593	0.00419	3.05	109.98	47.96	0.0029	8.289	2
			4.983		5.08	137.92	52.01	0.0080	9.864	2
			5.297		9.40	110.19	58.77	0.0269	4.512	2
			5.486		3.56	50.80	63.04	0.0039	3.025	2
			6.111		10.41	104.14	78.22	0.0329	3.982	2
			6.584		9.91	93.47	90.78	0.0298	3.323	2
			6.660		6.10	80.77	92.89	0.0114	3.774	2
			7.041		12.95	108.46	103.83	0.0504	3.592	2
			7.041		19.30	128.27	103.83	0.1095	3.592	2
			8.839		17.02	127.00	163.64	0.0858	3.823	2
LEAD	2.0	Sphere (H_2O)	2.560	0.00419	5.08	91.44	13.73	0.0080	5.171	3
			3.322		6.35	95.25	23.12	0.0124	4.720	3
			3.490		5.08	91.44	13.73	0.0080	5.171	3
			3.673		7.62	109.22	28.25	0.0179	5.267	3
			5.060		12.70	128.27	53.62	0.0485	4.600	3
			6.462		20.32	137.16	87.451	0.1209	3.930	3
			6.492		22.09	116.84	88.28	0.1421	4.691	3
			6.706		22.86	142.24	94.17	0.1517	3.909	3
			7.041		33.02	172.72	103.83	0.3048	5.017	2
			7.925		38.10	144.78	131.53	0.3981	3.174	3

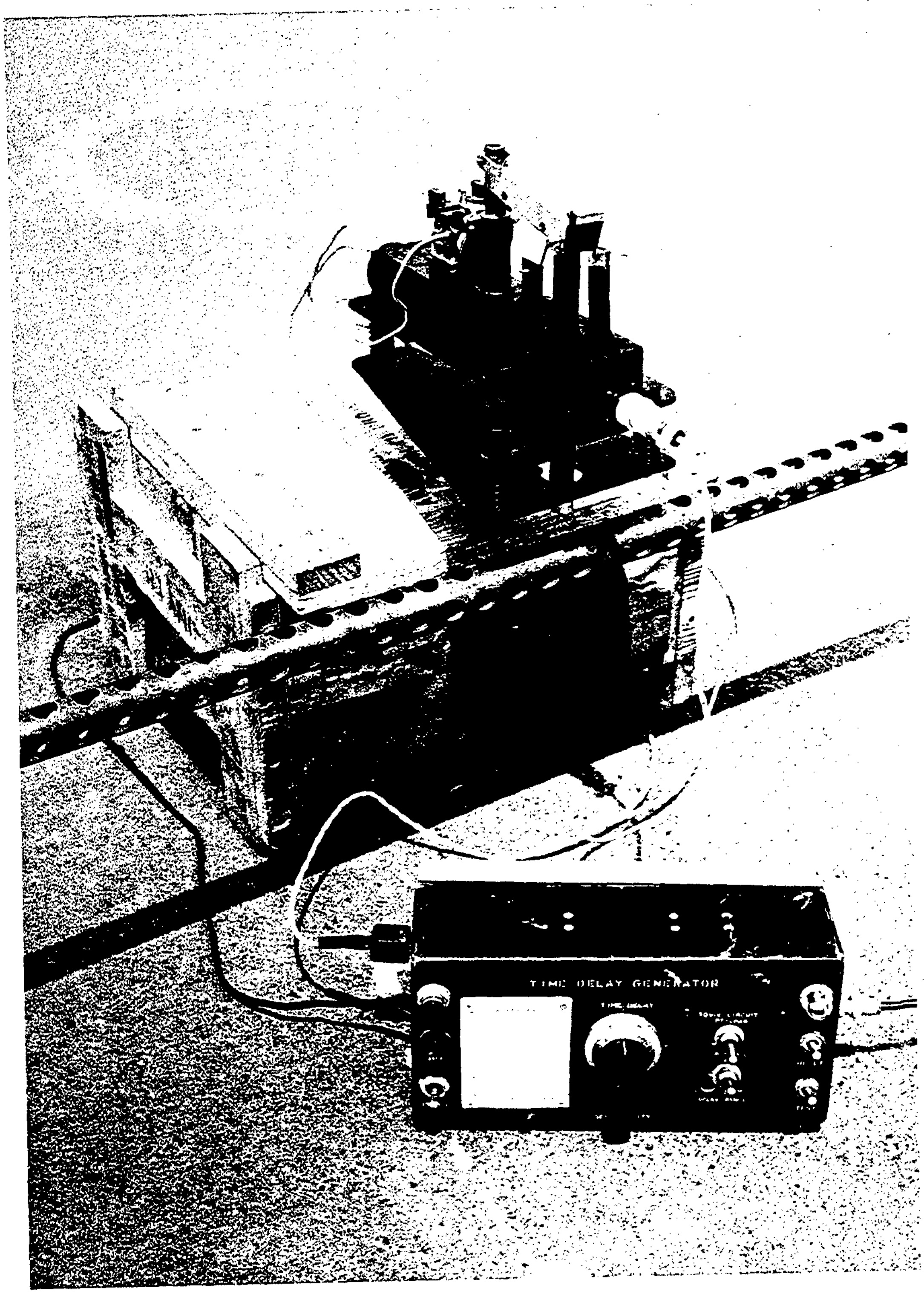

Figure 1. Time Delay Generator and Drop Release System

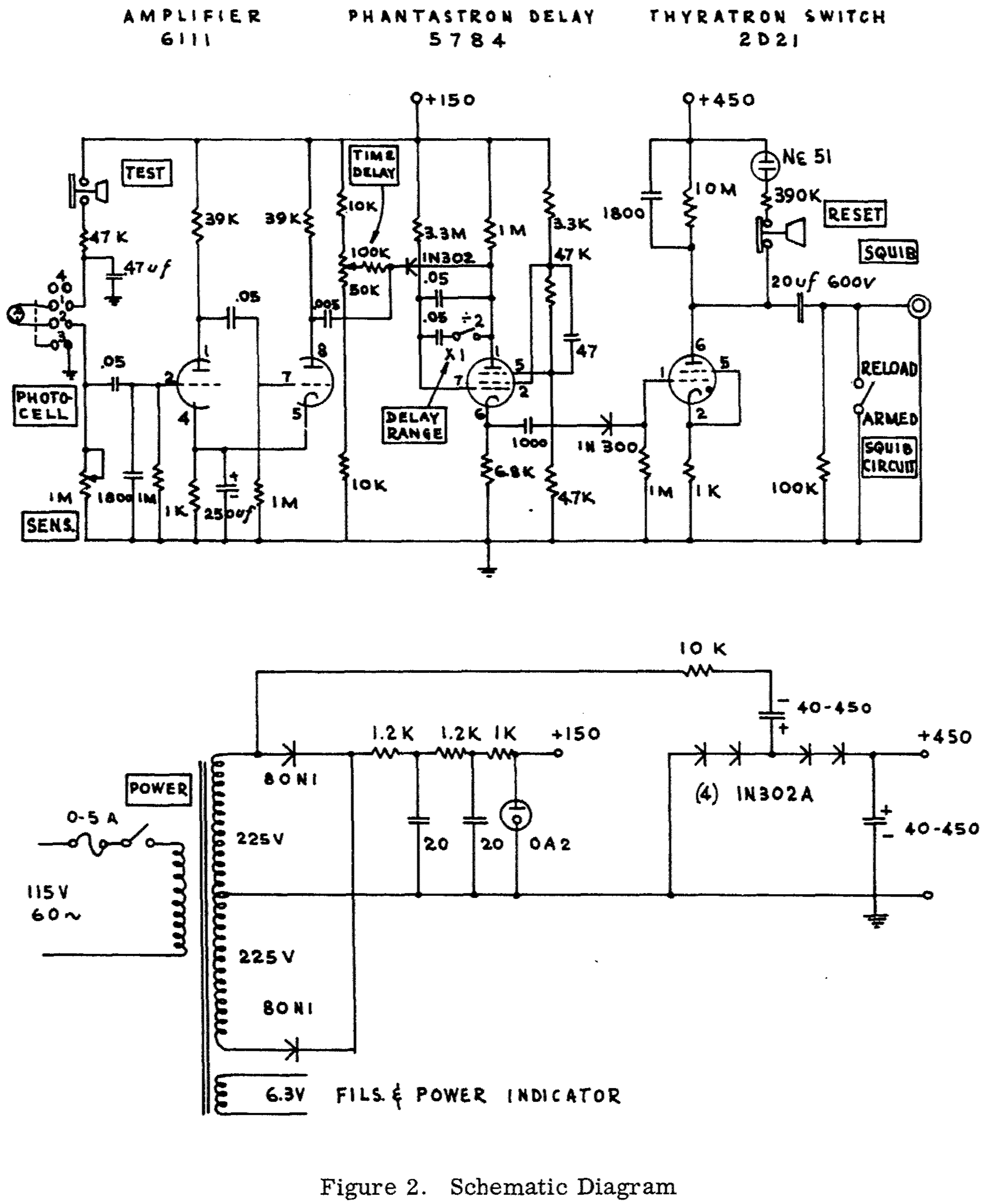

Figure 2. Schematic Diagram

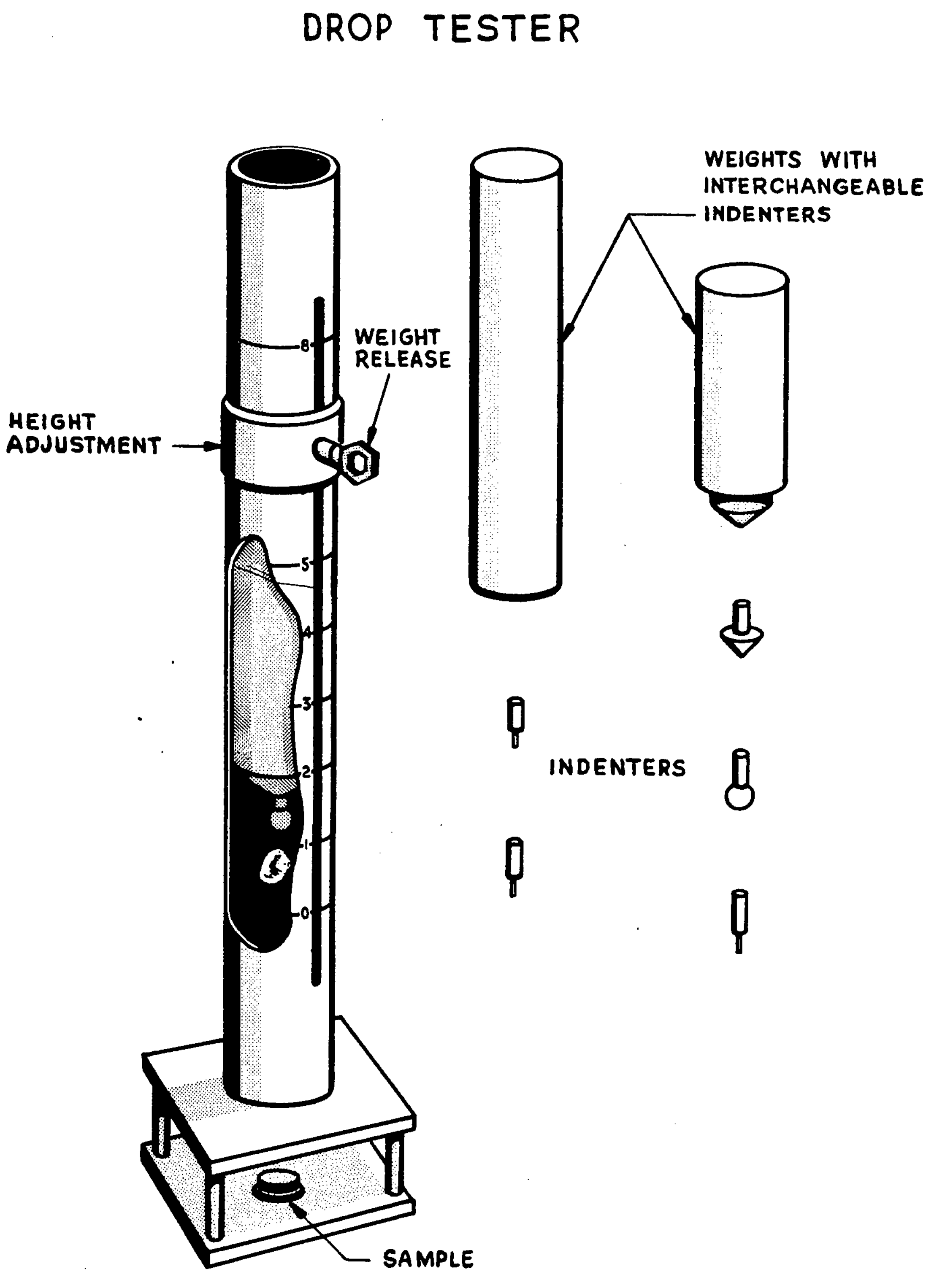

Figure 3. Drop Tester

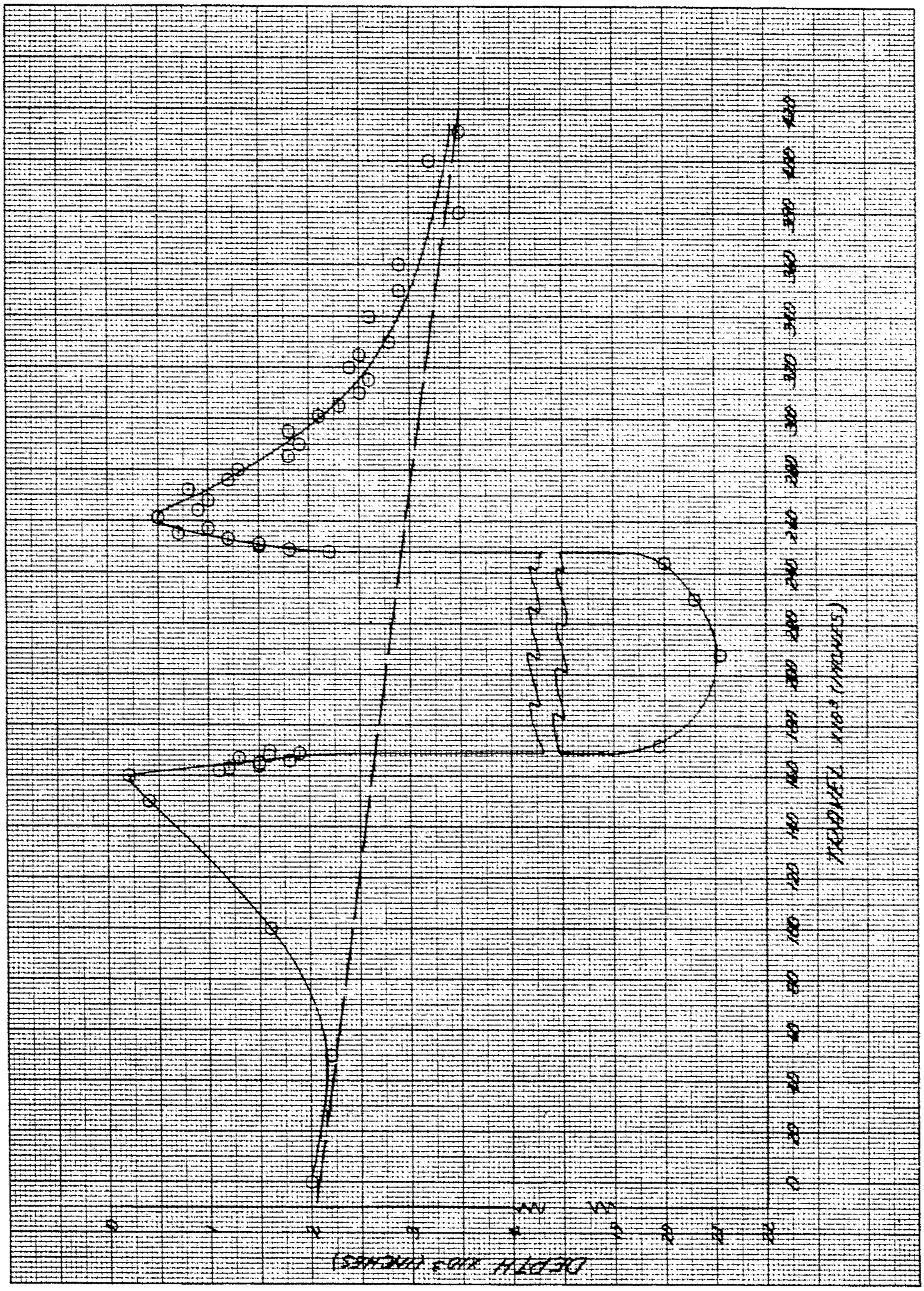

Figure 4. Damage Mark Contour - Cylindrical Indenter

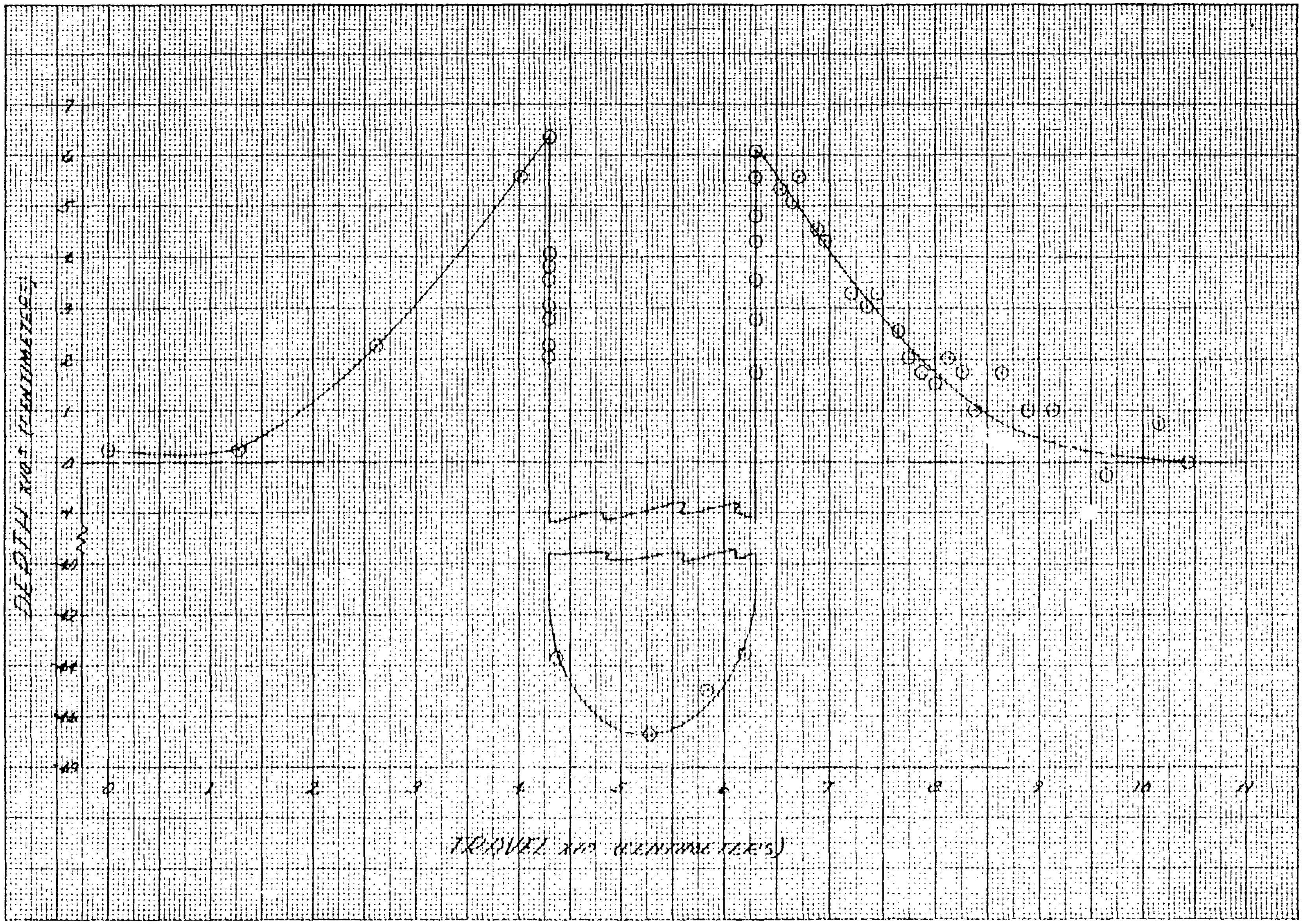

Figure 5. Normalized Damage Mark Contour - Cylindrical Indenter

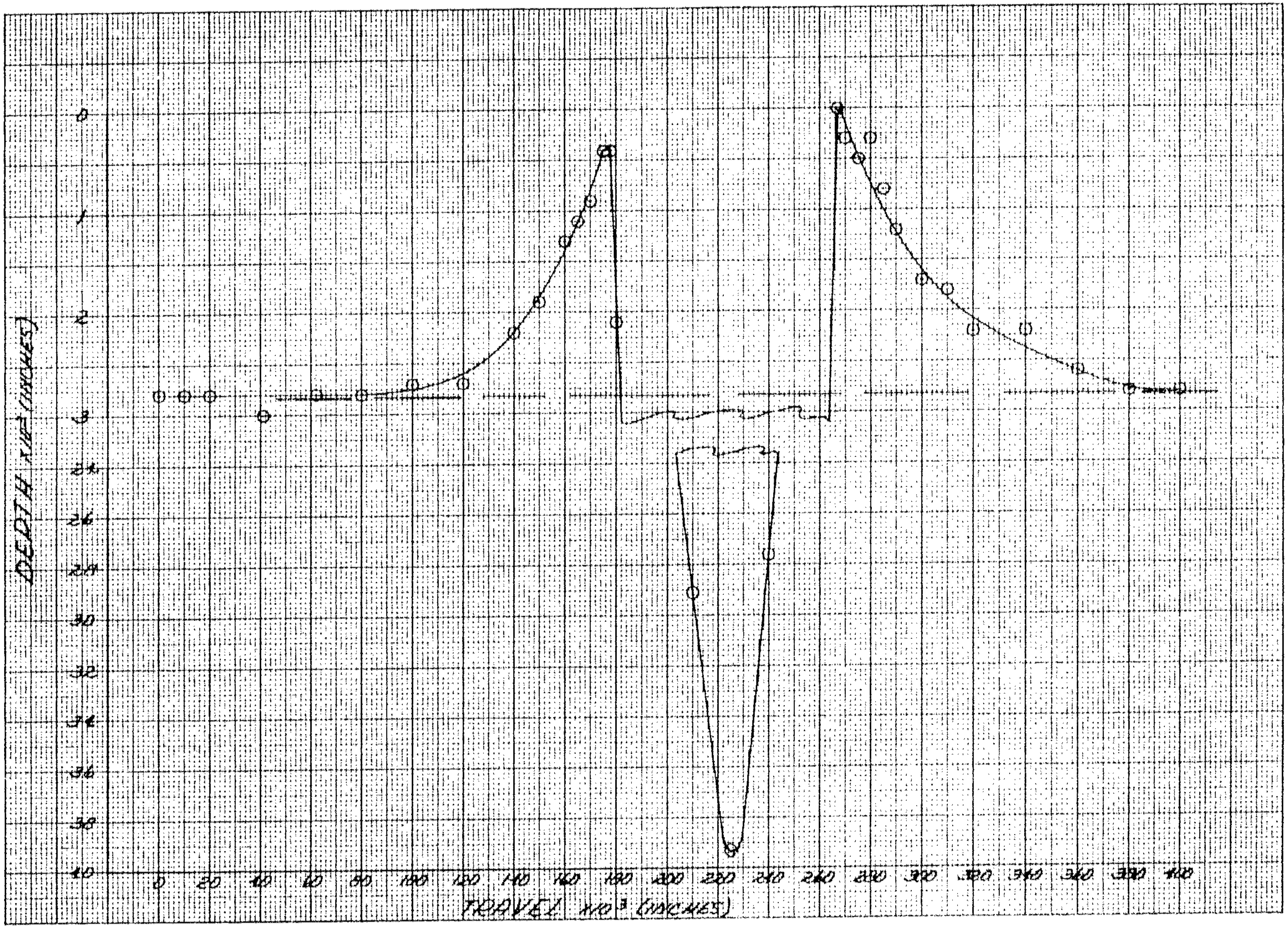

Figure 6. Normalized Damage Mark Contour - Conical Indenter - 90° Included Angle

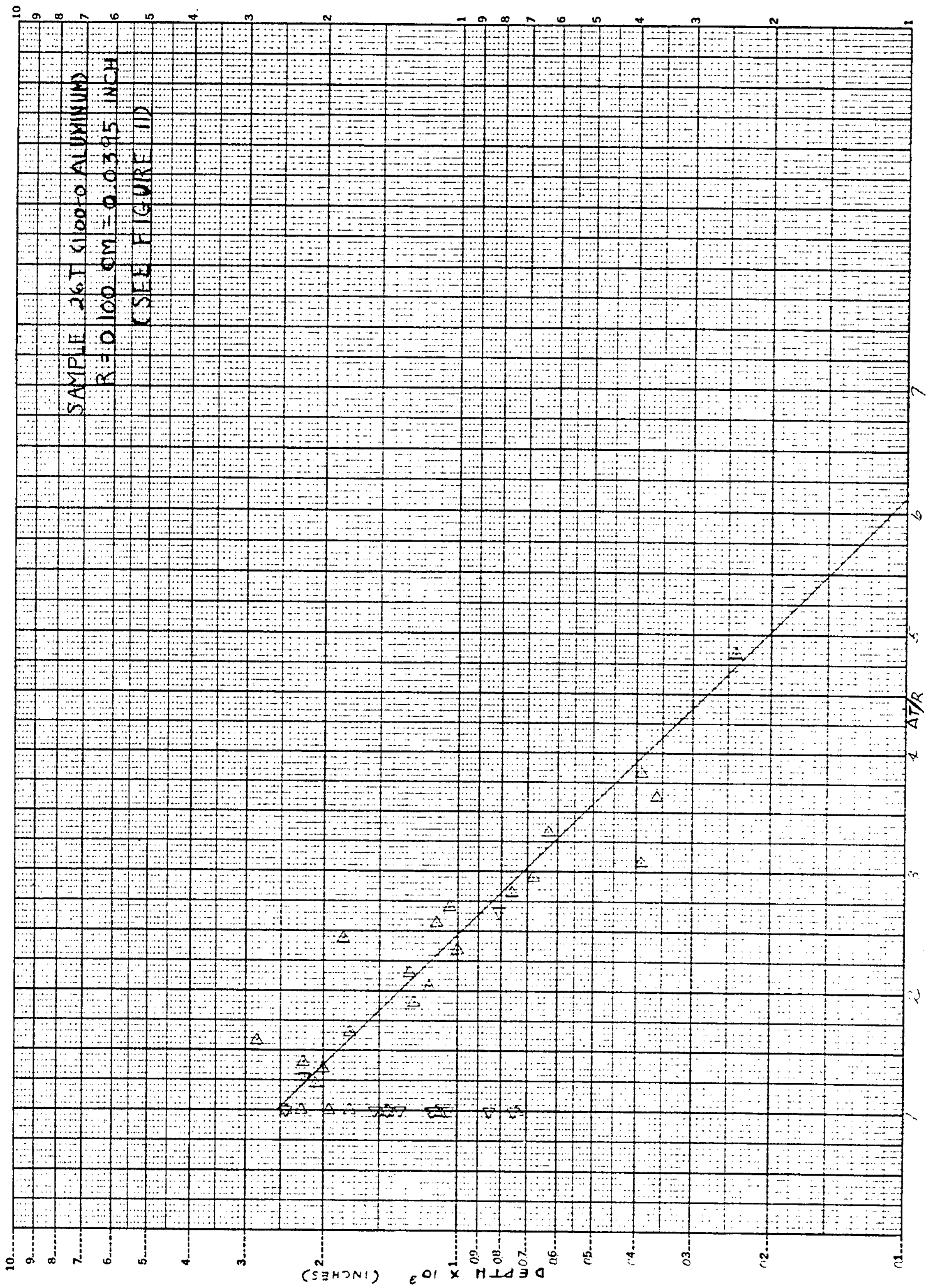

Figure 7. Depth vs $\frac{\text{Travel}}{\text{Cylinder Radius}}$

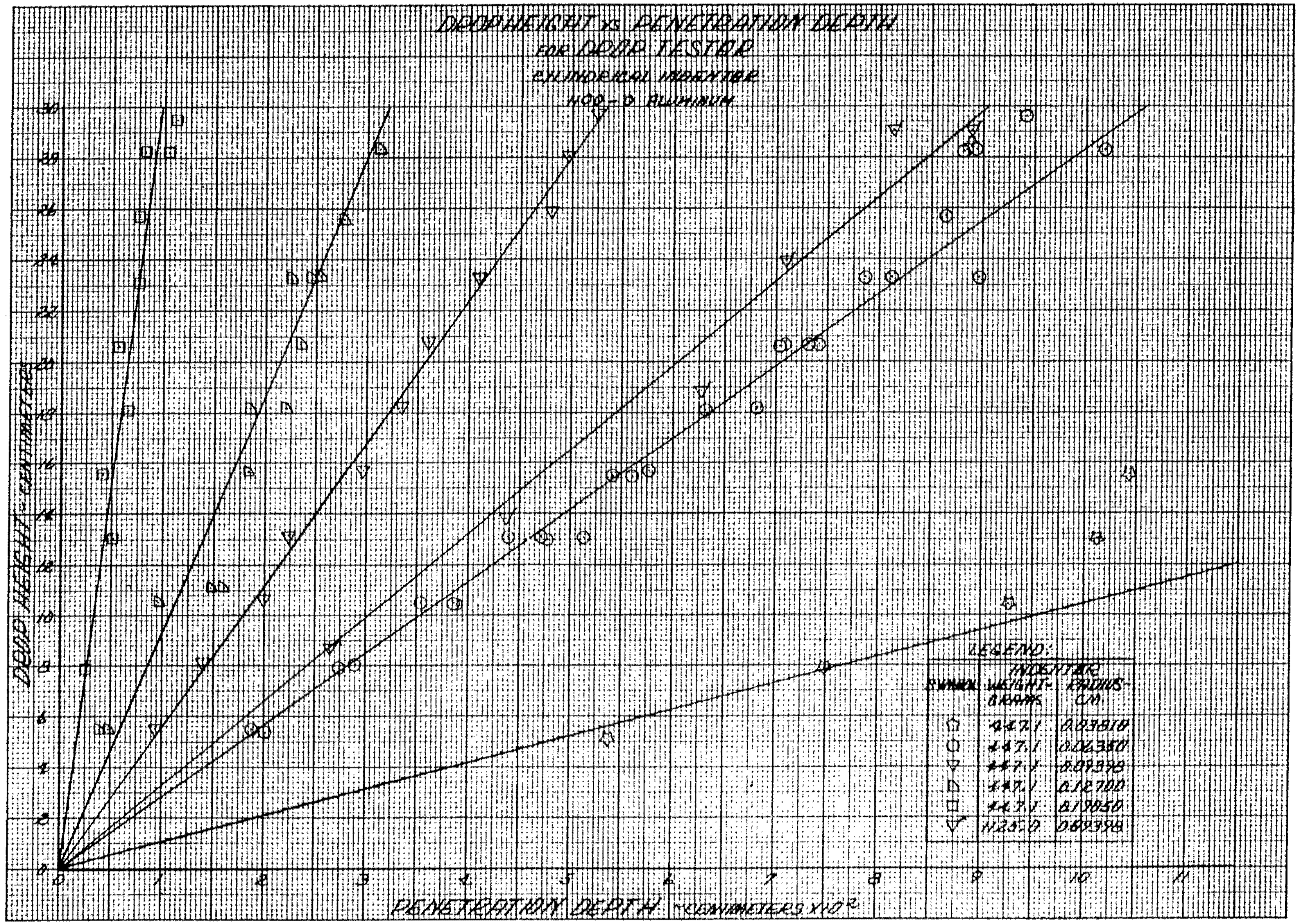

Figure 8. Drop Height vs Penetration Depth for Drop Tester - Cylindrical Indenter

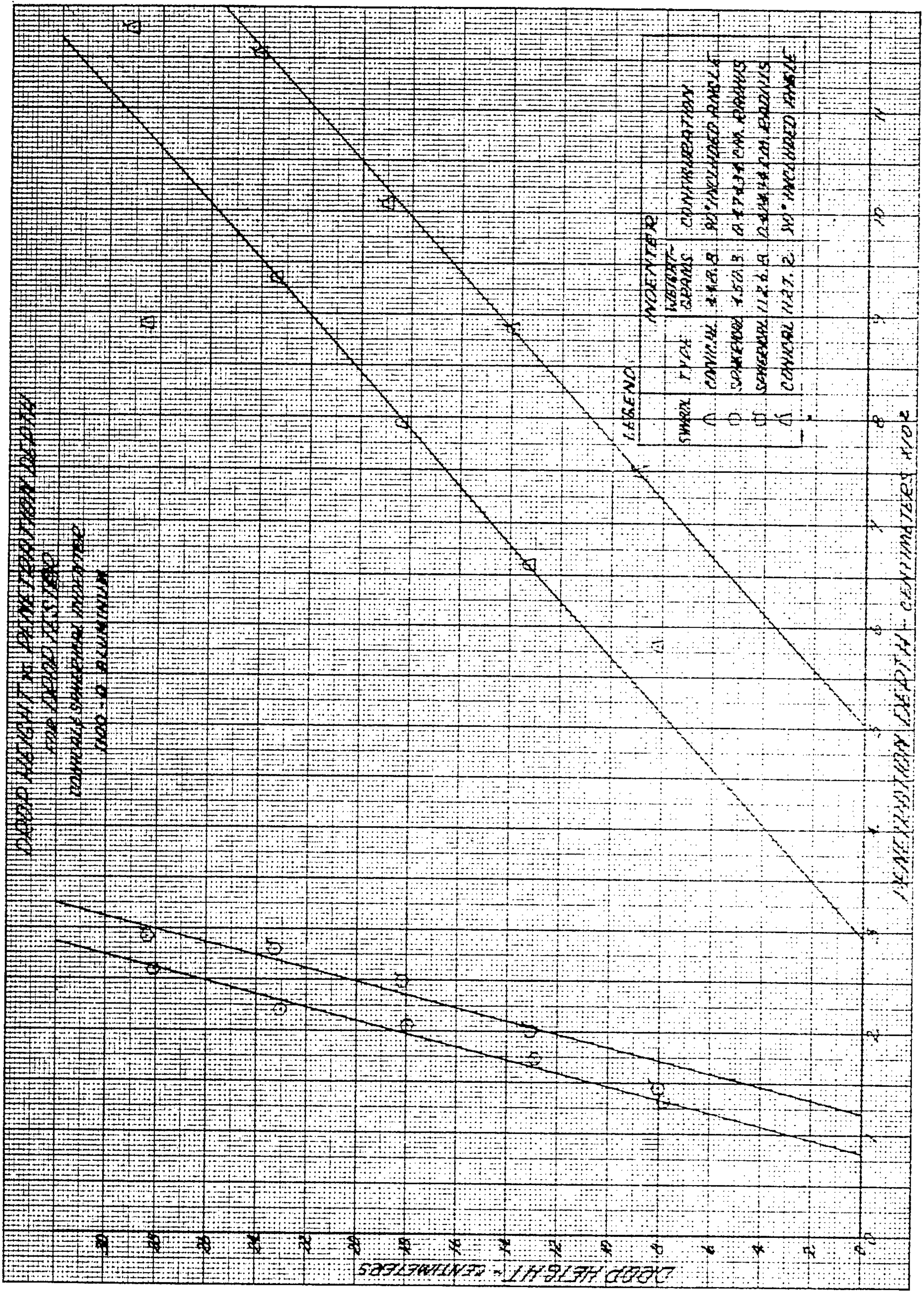

Figure 9. Drop Height vs Penetration Depth for Drop Tester - Conical and Spherical Indenters

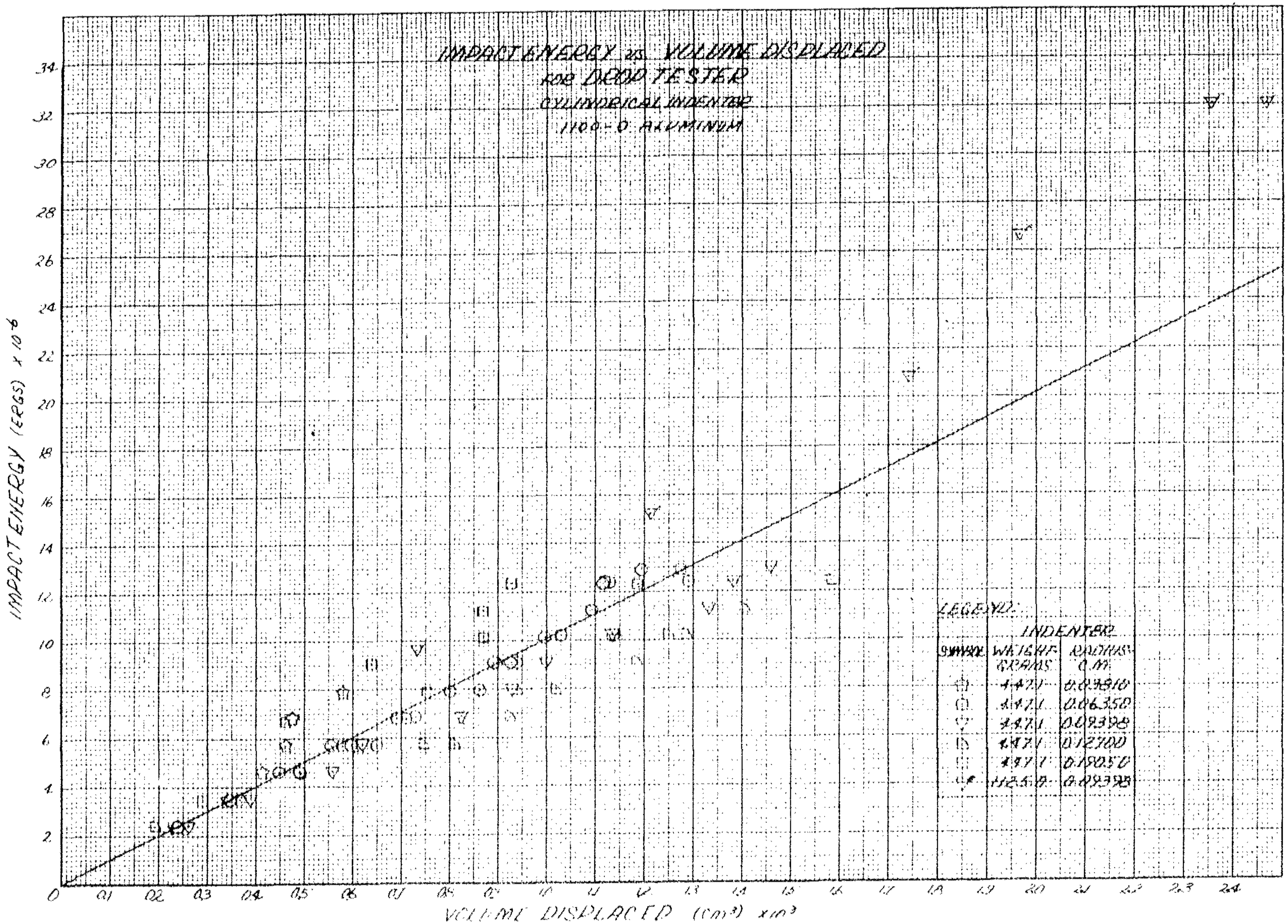

Figure 10. Impact Energy vs Volume Displaced for Drop Tester - Cylindrical Indenter

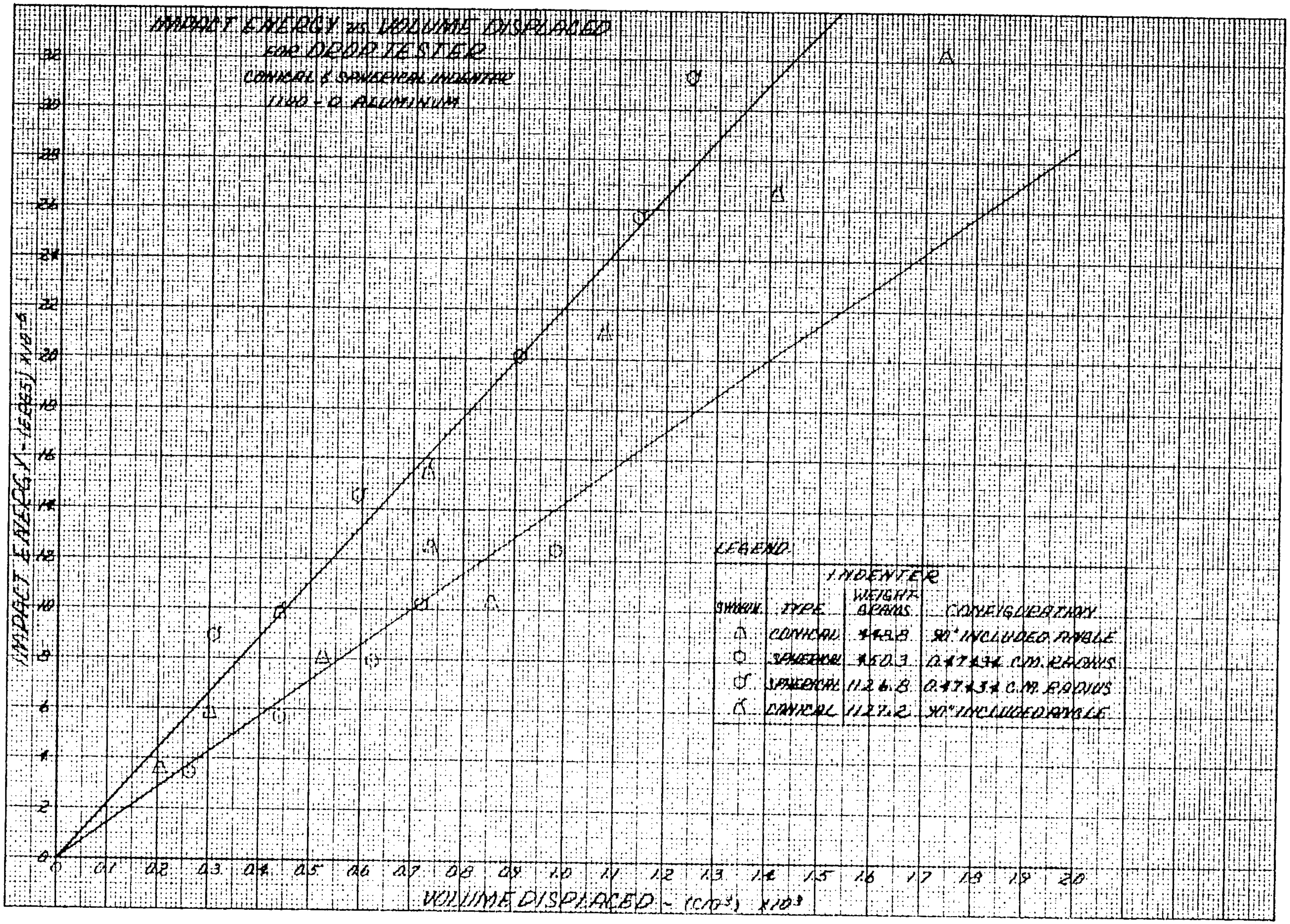

Figure 11. Impact Energy vs Volume Displaced for Drop Tester - Conical and Spherical Indenters

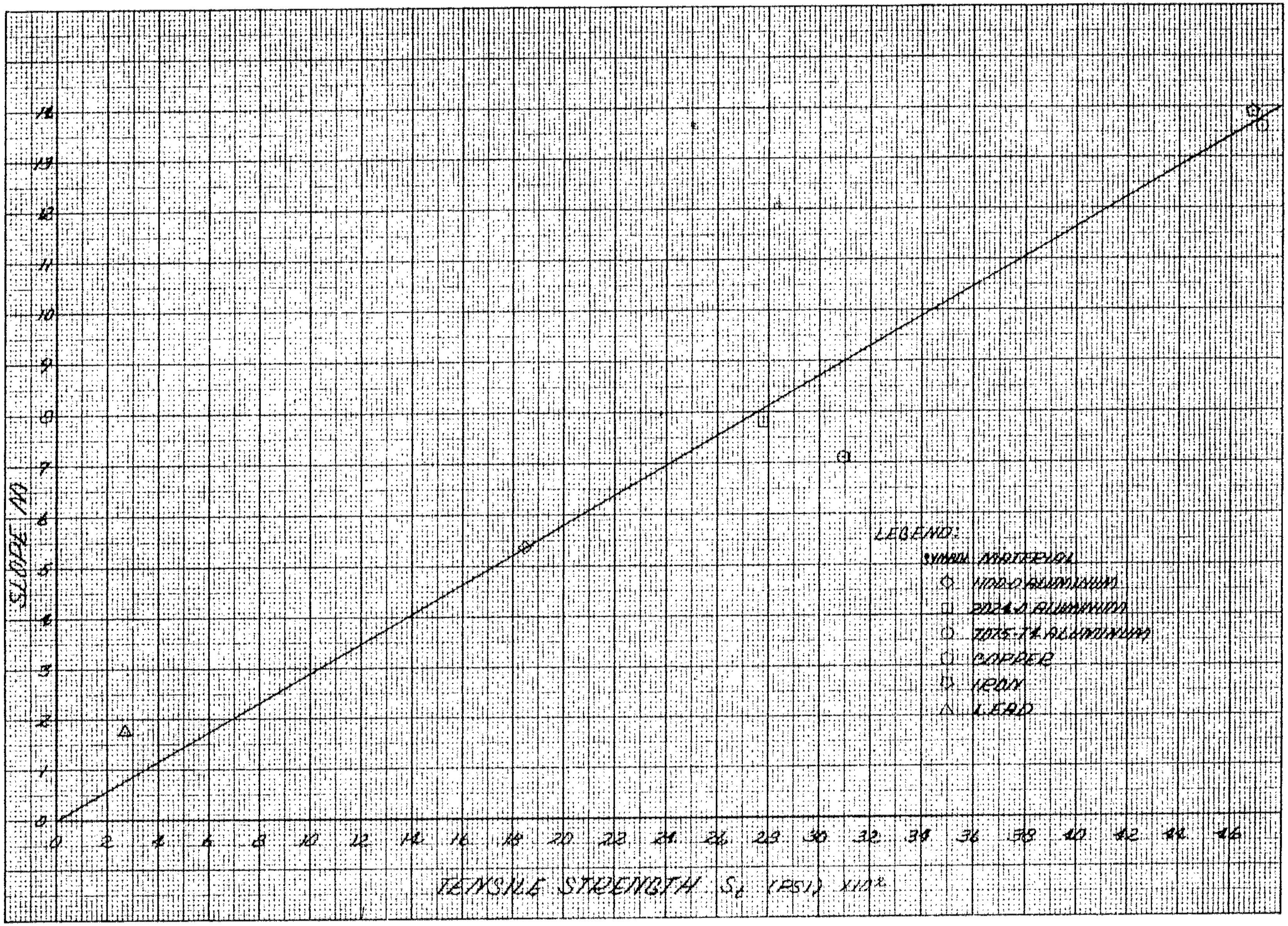

Figure 12. Slope M of "Energy vs Displaced Volume Curve" vs Target Tensile Strength

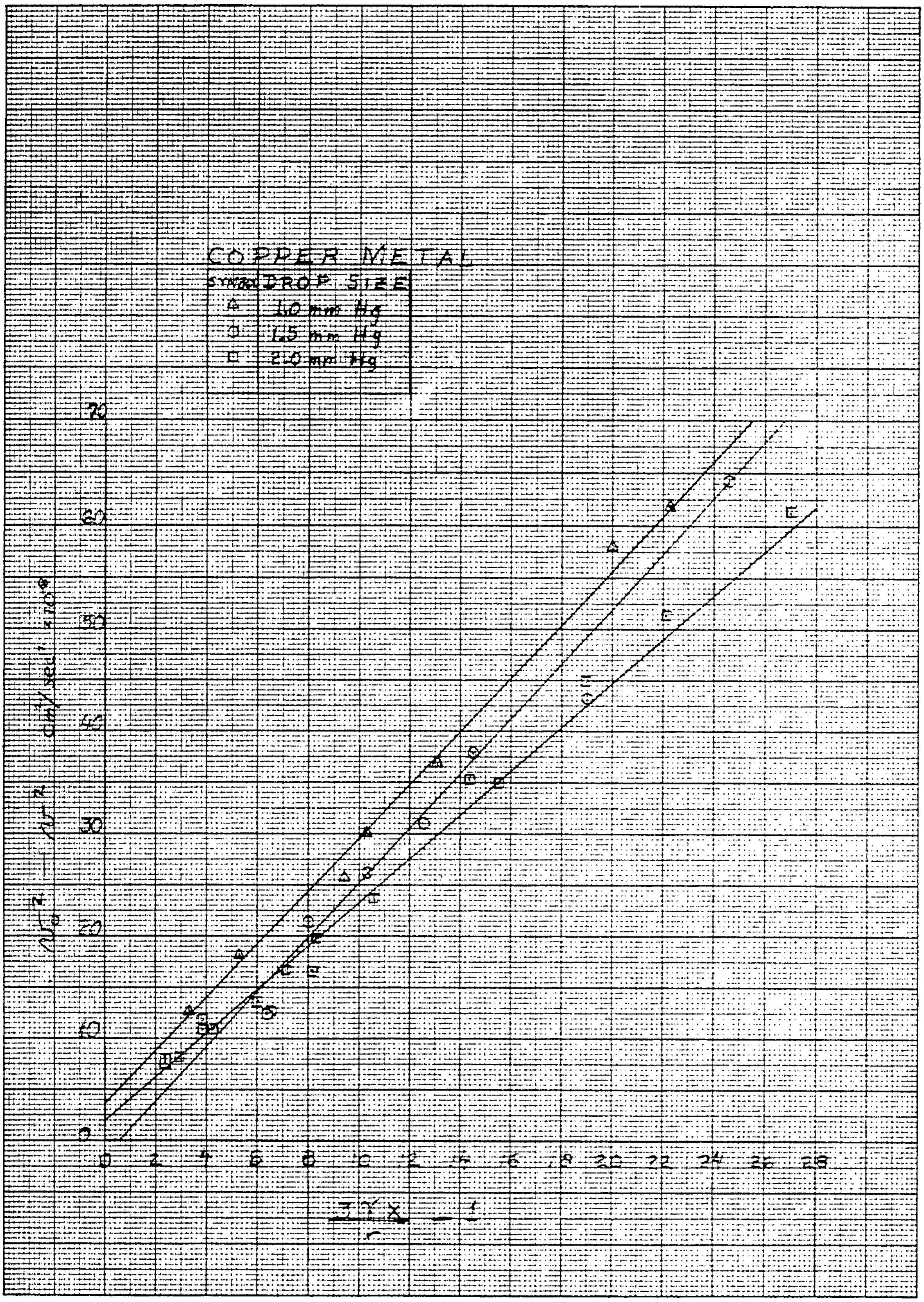

Figure 13. $v_o^2 - v^2$ vs An Expression Containing Gamma

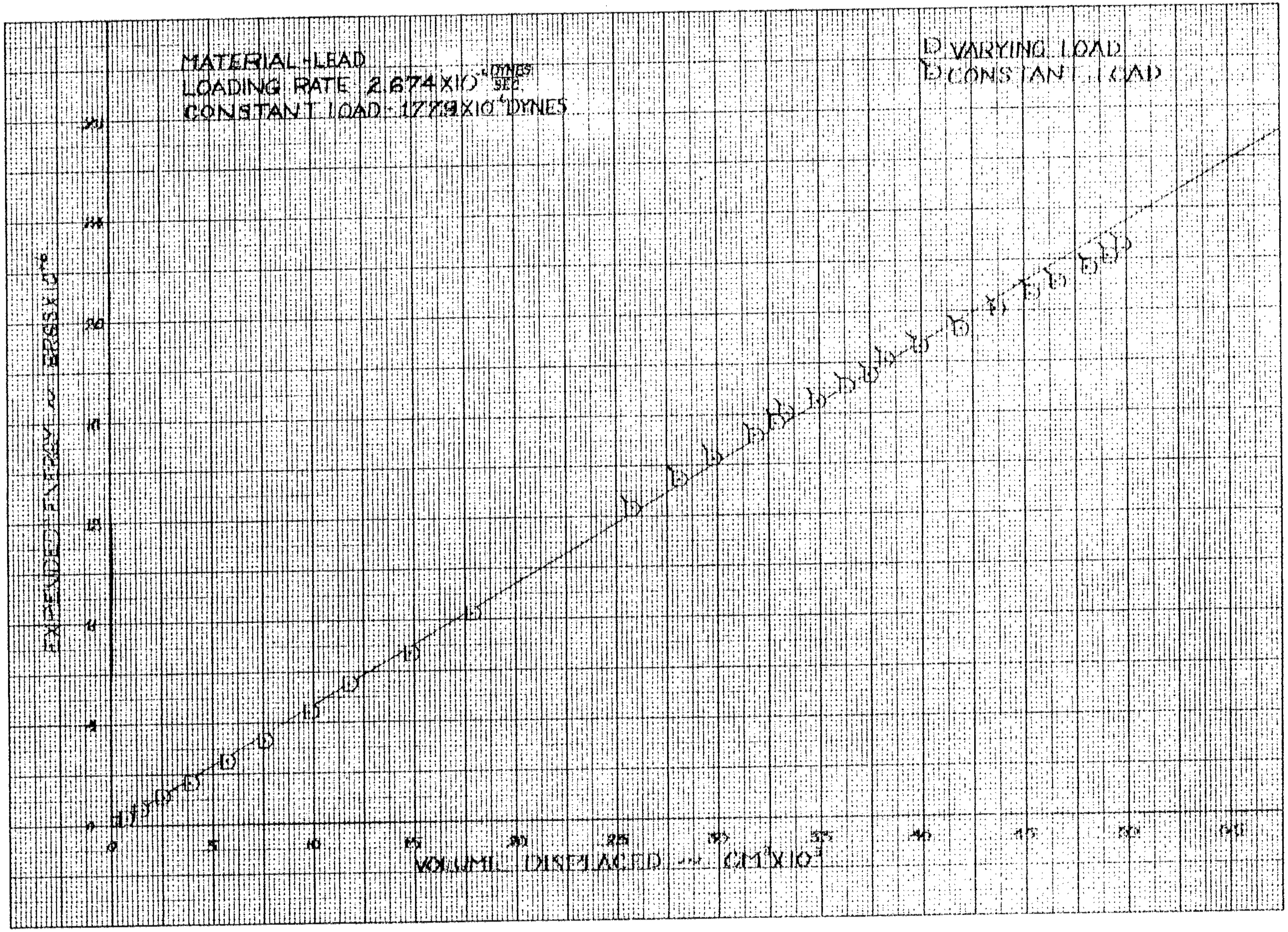

Figure 14. Energy vs Volume - Low Velocity - Lead No. 1

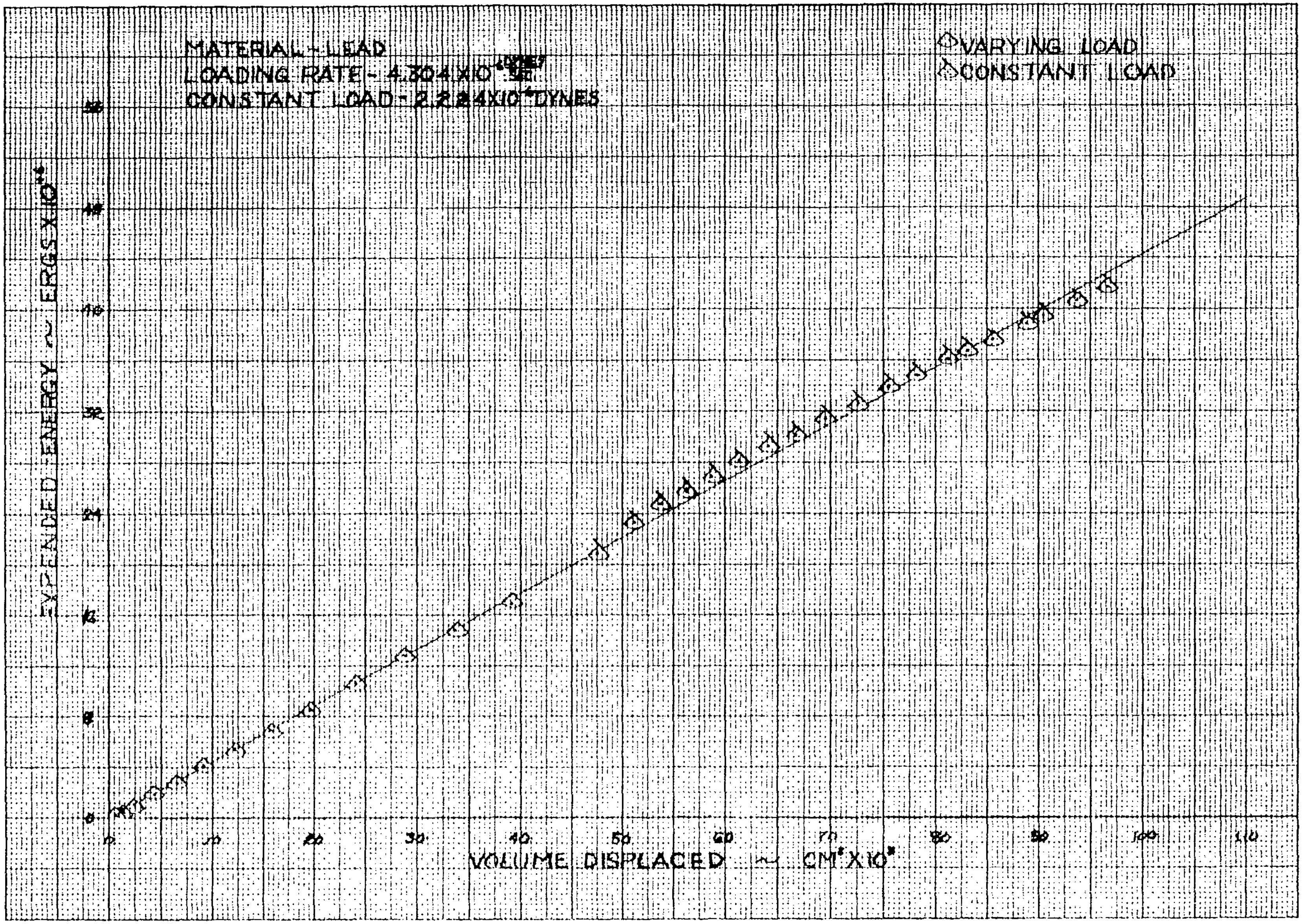

Figure 15. Energy vs Volume - Low Velocity - Lead No. 2

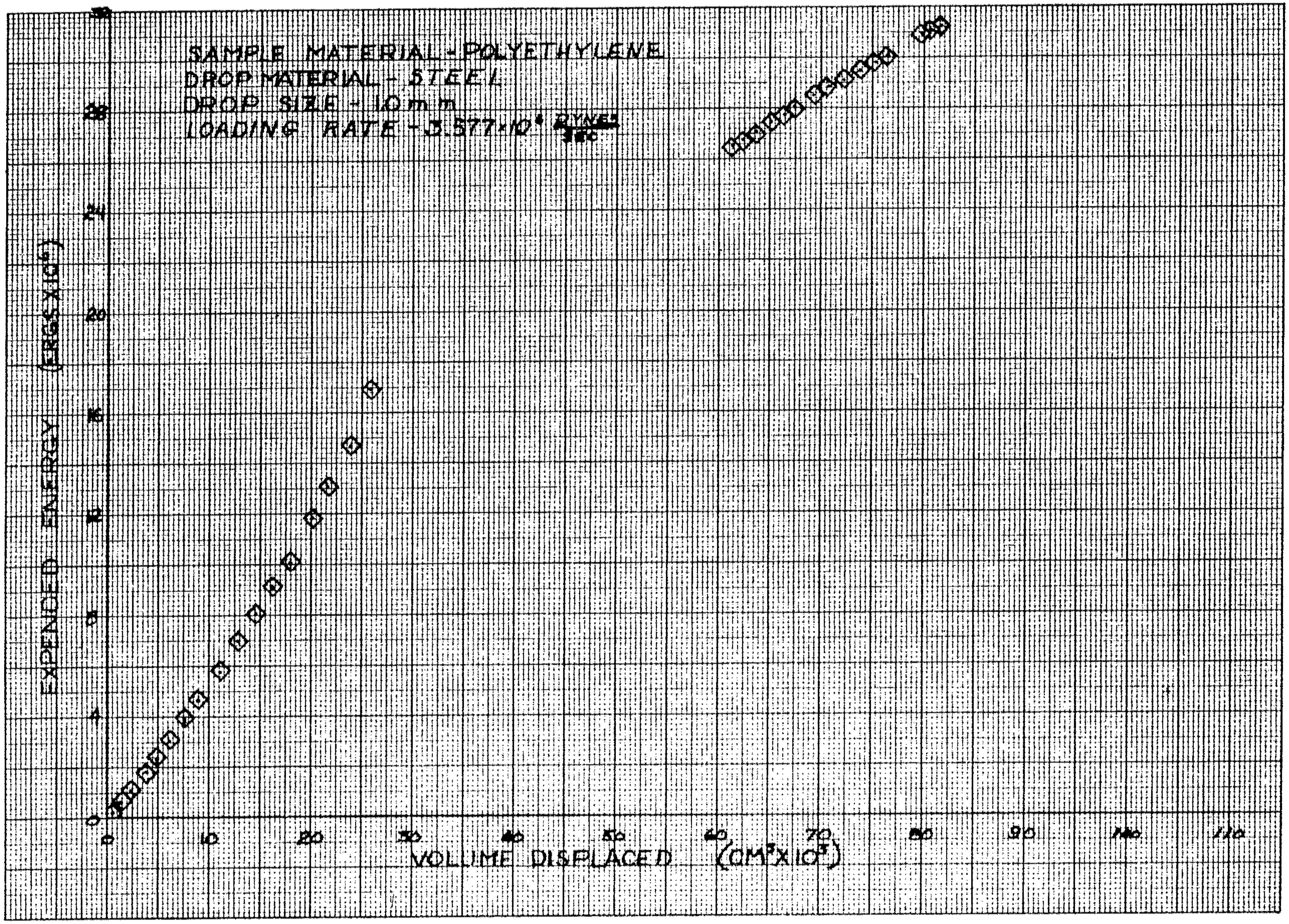

Figure 16. Energy vs Volume - Low Velocity - Polyethylene

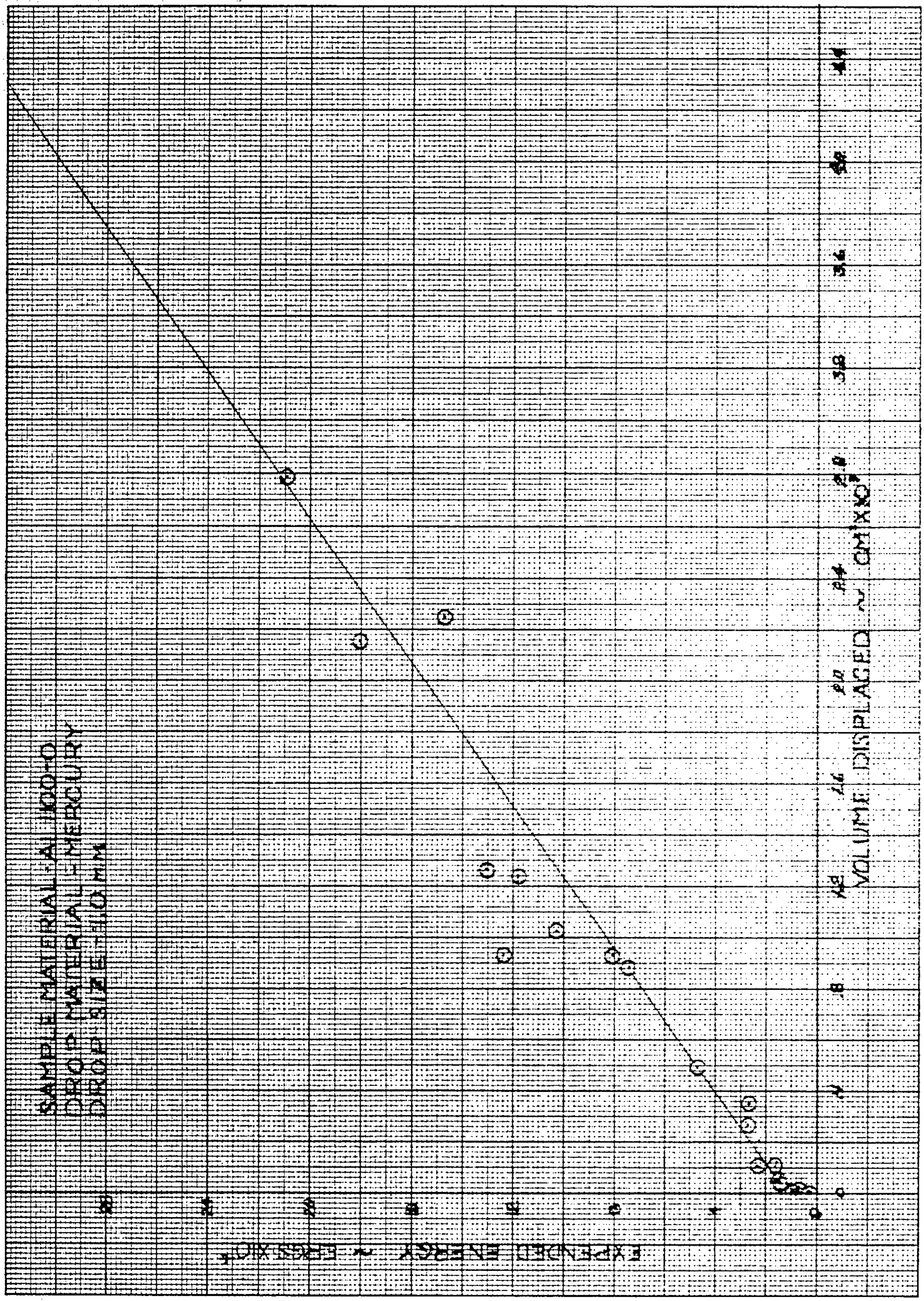

Figure 17. Energy vs Volume - 1100-0 Aluminum - 1.0 mm Mercury

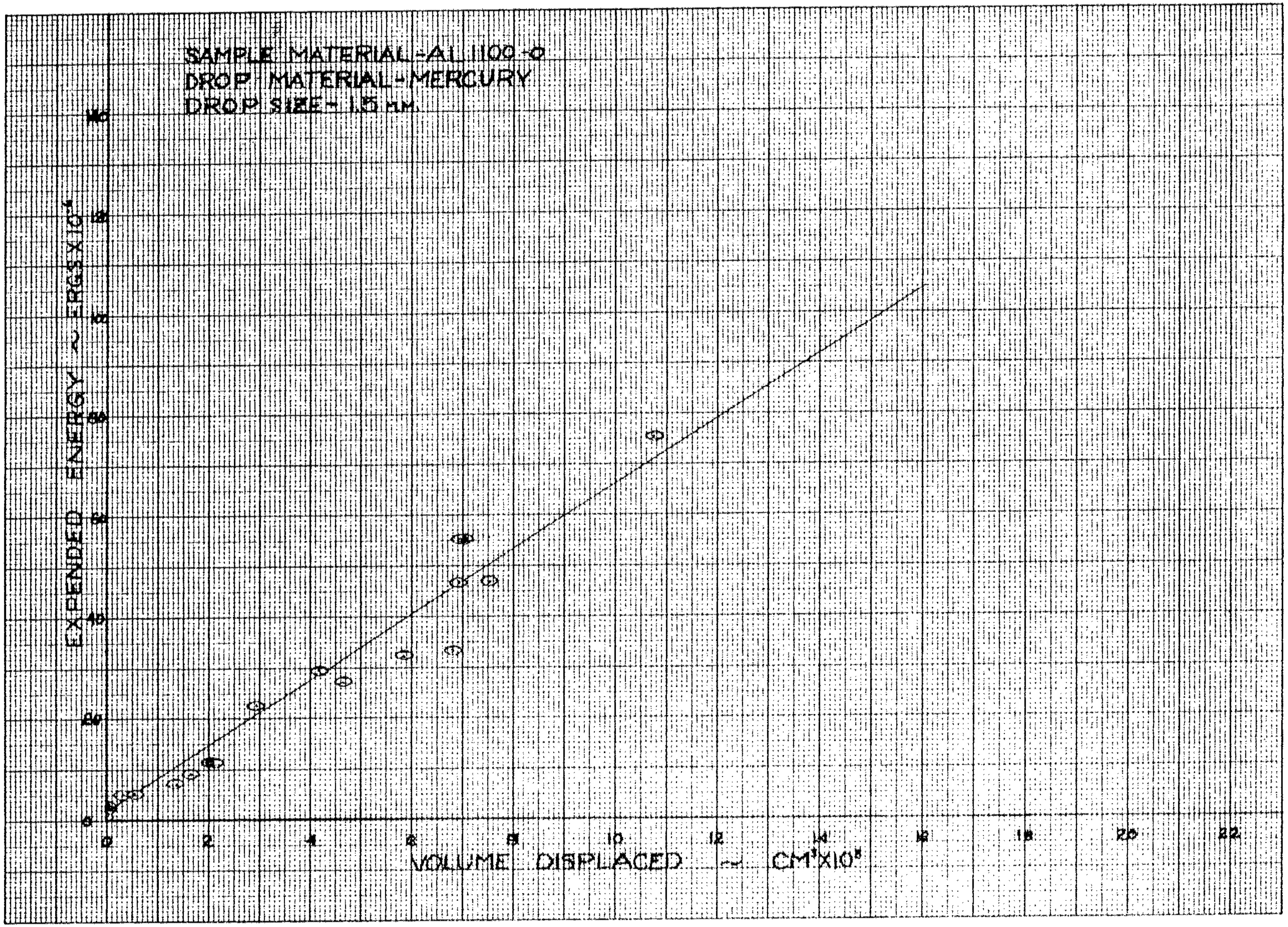

Figure 18. Energy vs Volume - 1100-0 Aluminum - 1.5 mm Mercury

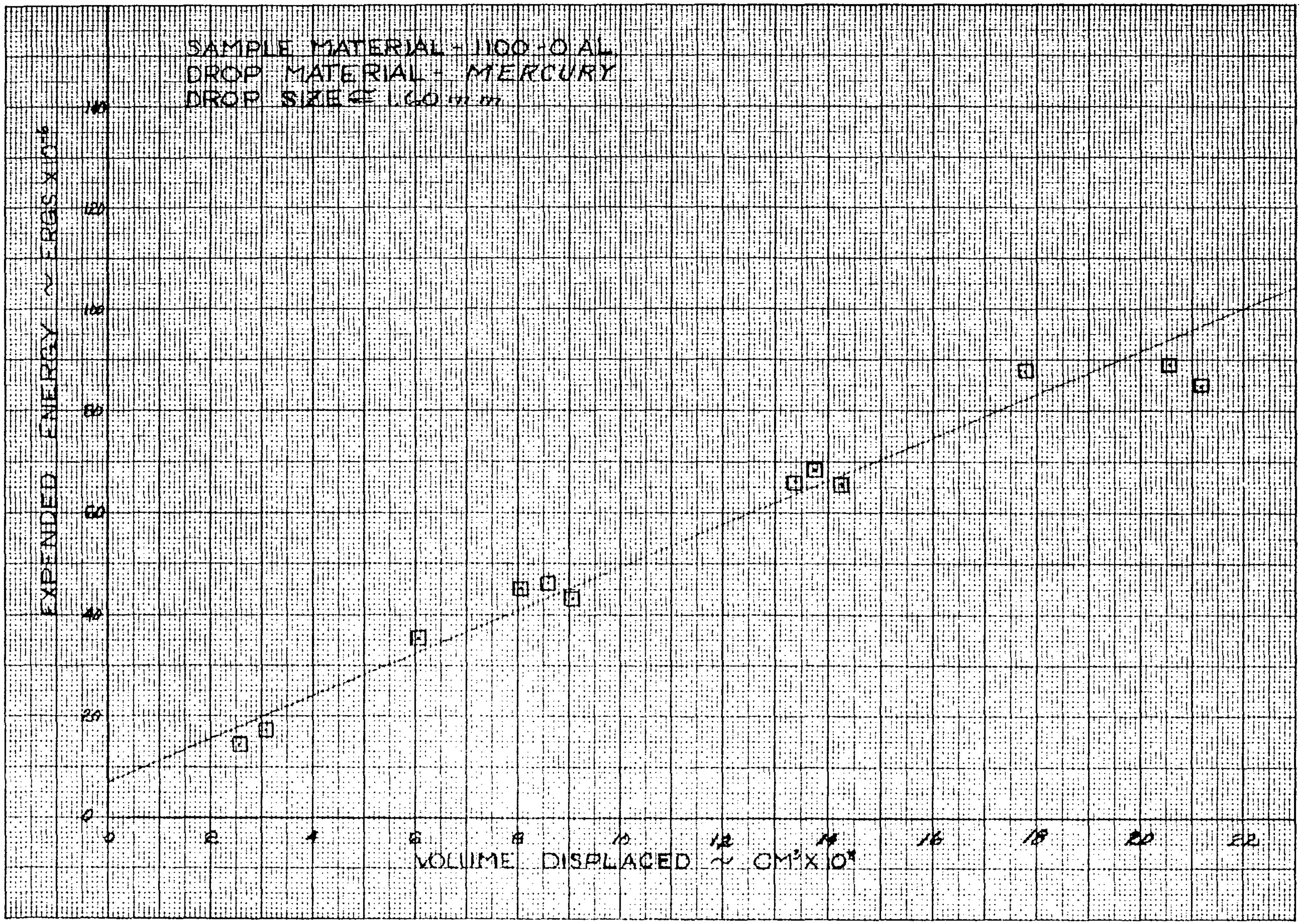

Figure 19. Energy vs. Volume - 1100-0 Aluminum - 1.6 mm Mercury

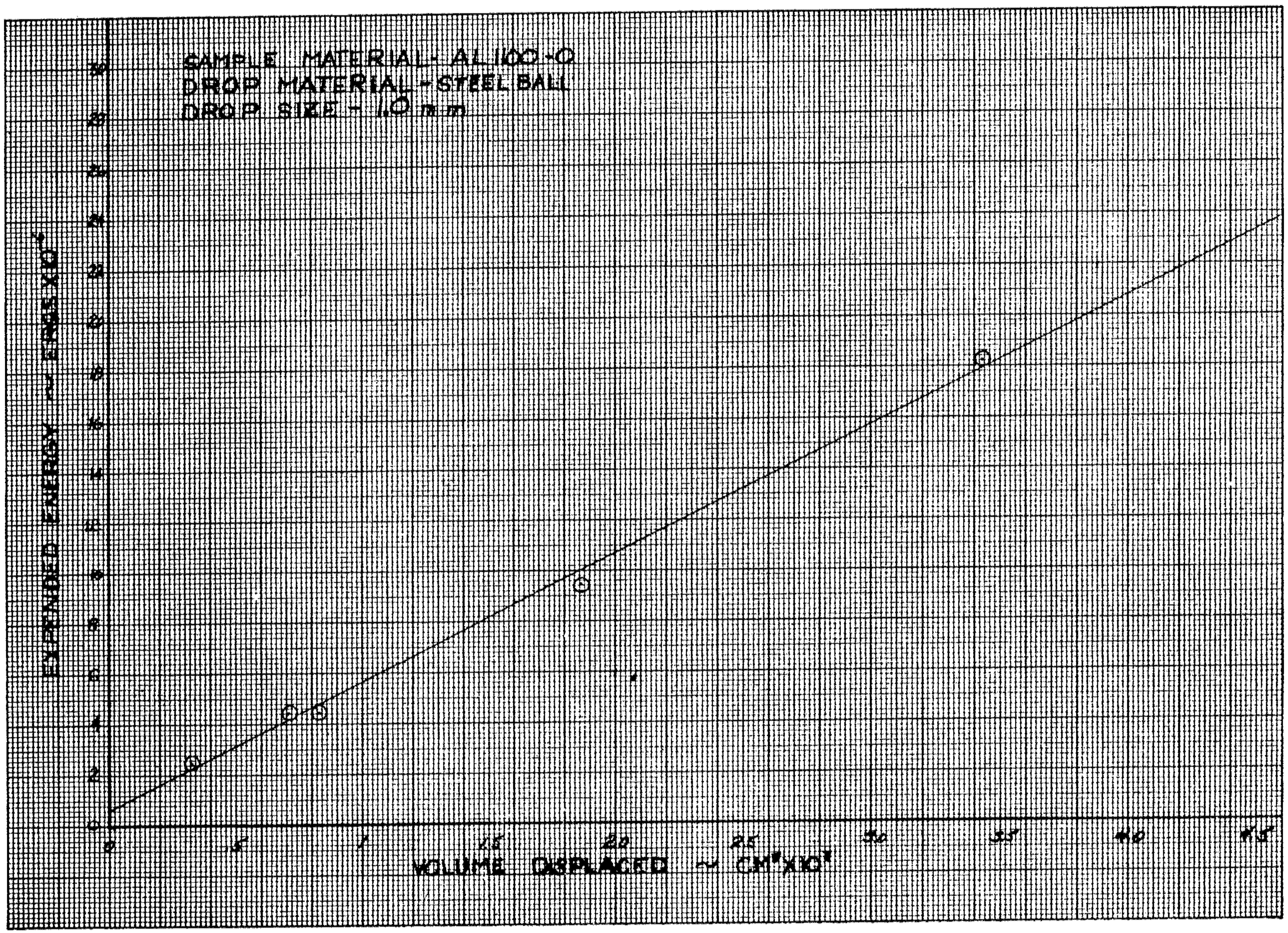

Figure 20. Energy vs Volume - 1100-0 Aluminum - 1.0 mm Steel Ball

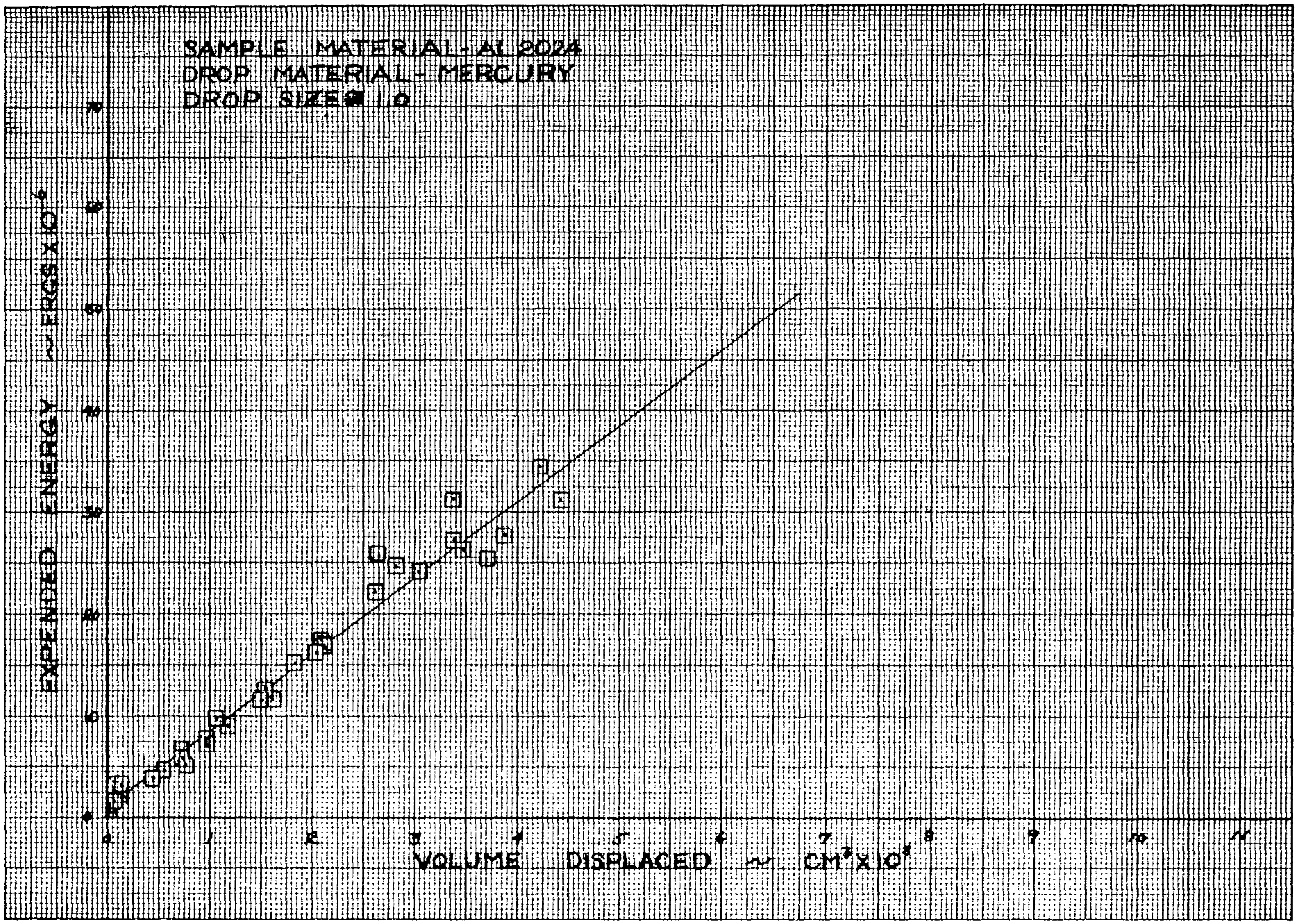

Figure 21. Energy vs Volume - 2024 Aluminum - 1.0 mm Mercury

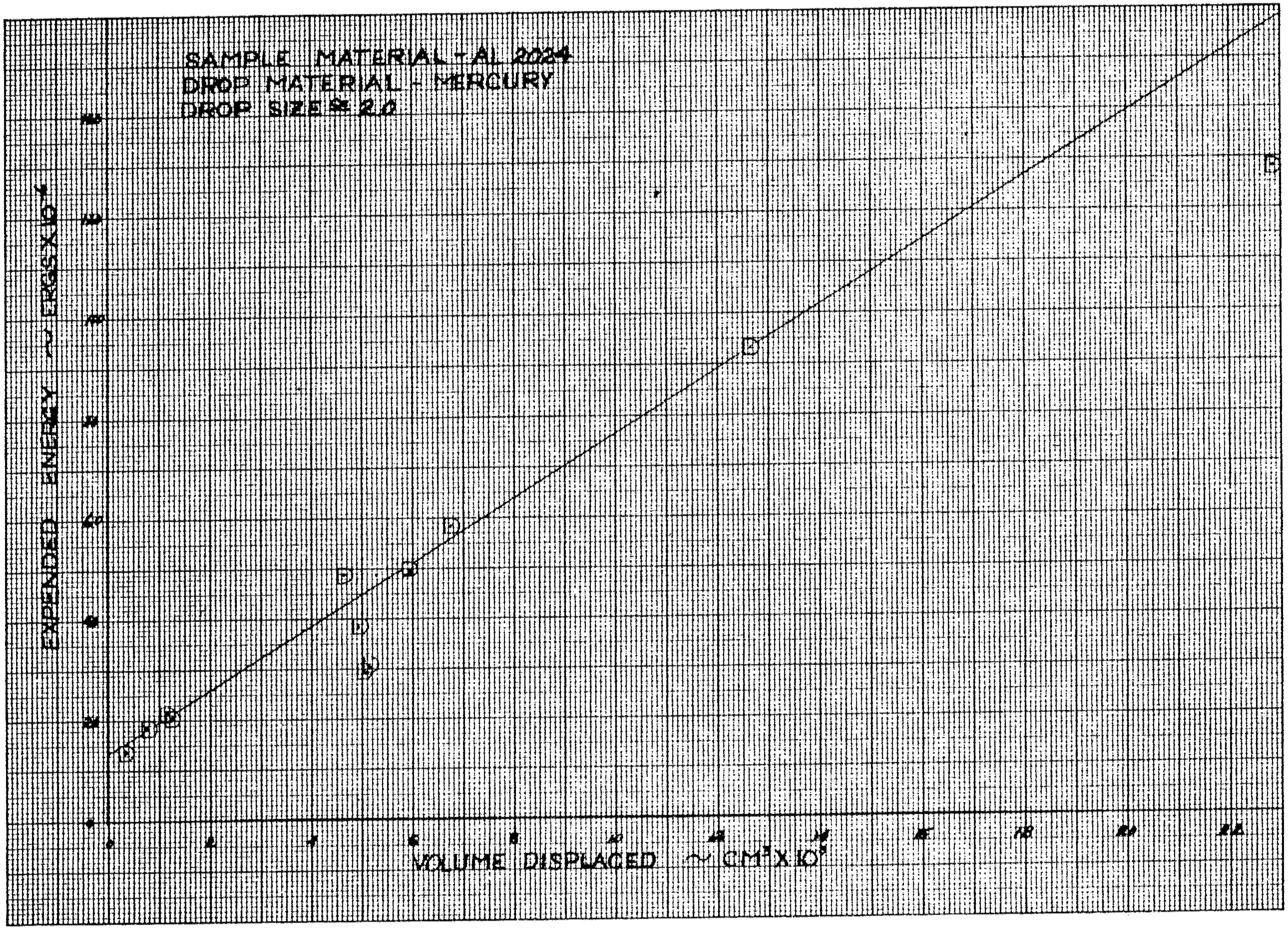

Figure 22. Energy vs Volume - 2024 Aluminum - 2.0 mm Mercury

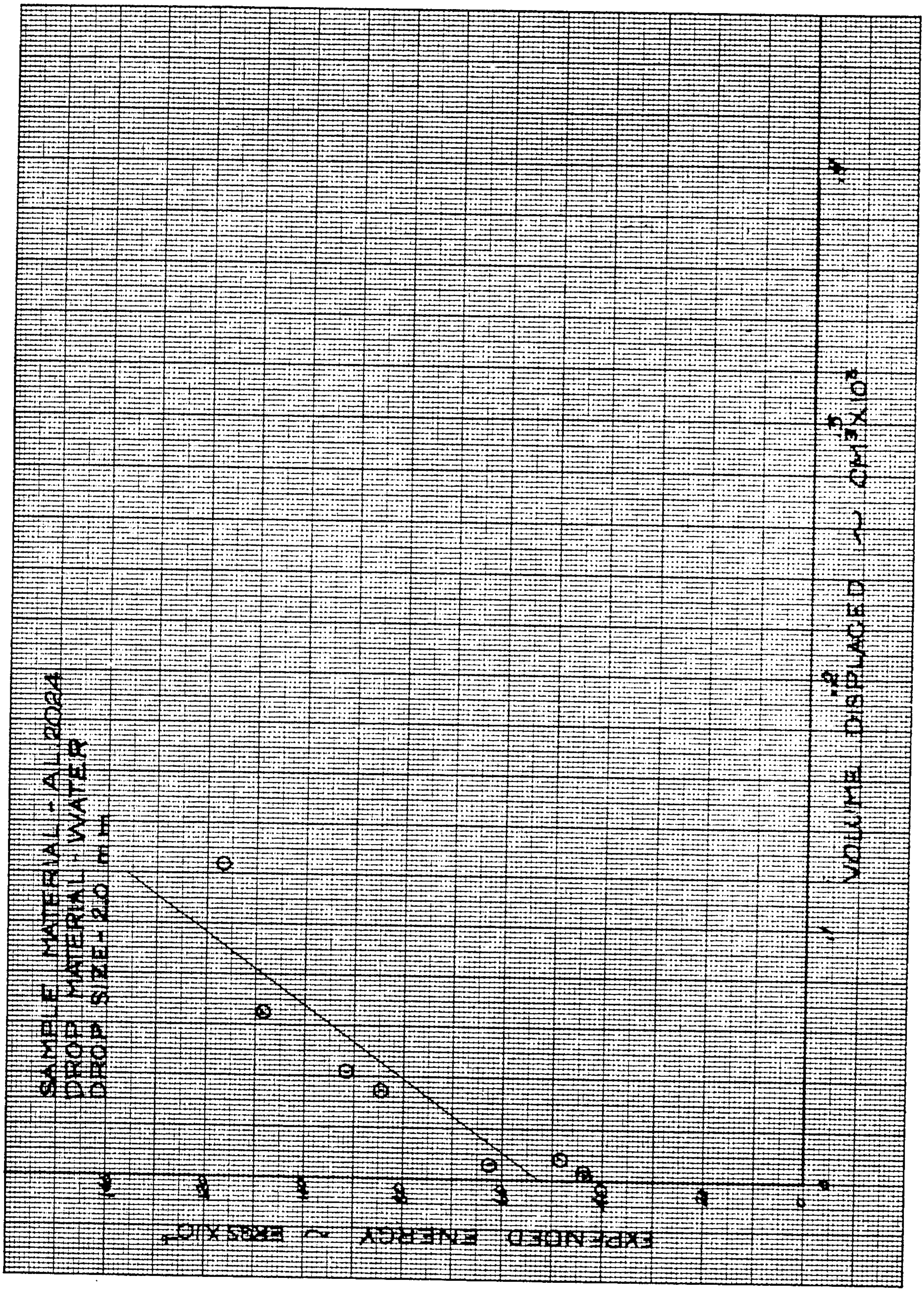

Figure 23. Energy vs Volume - 2024 Aluminum - 2.0 mm Water

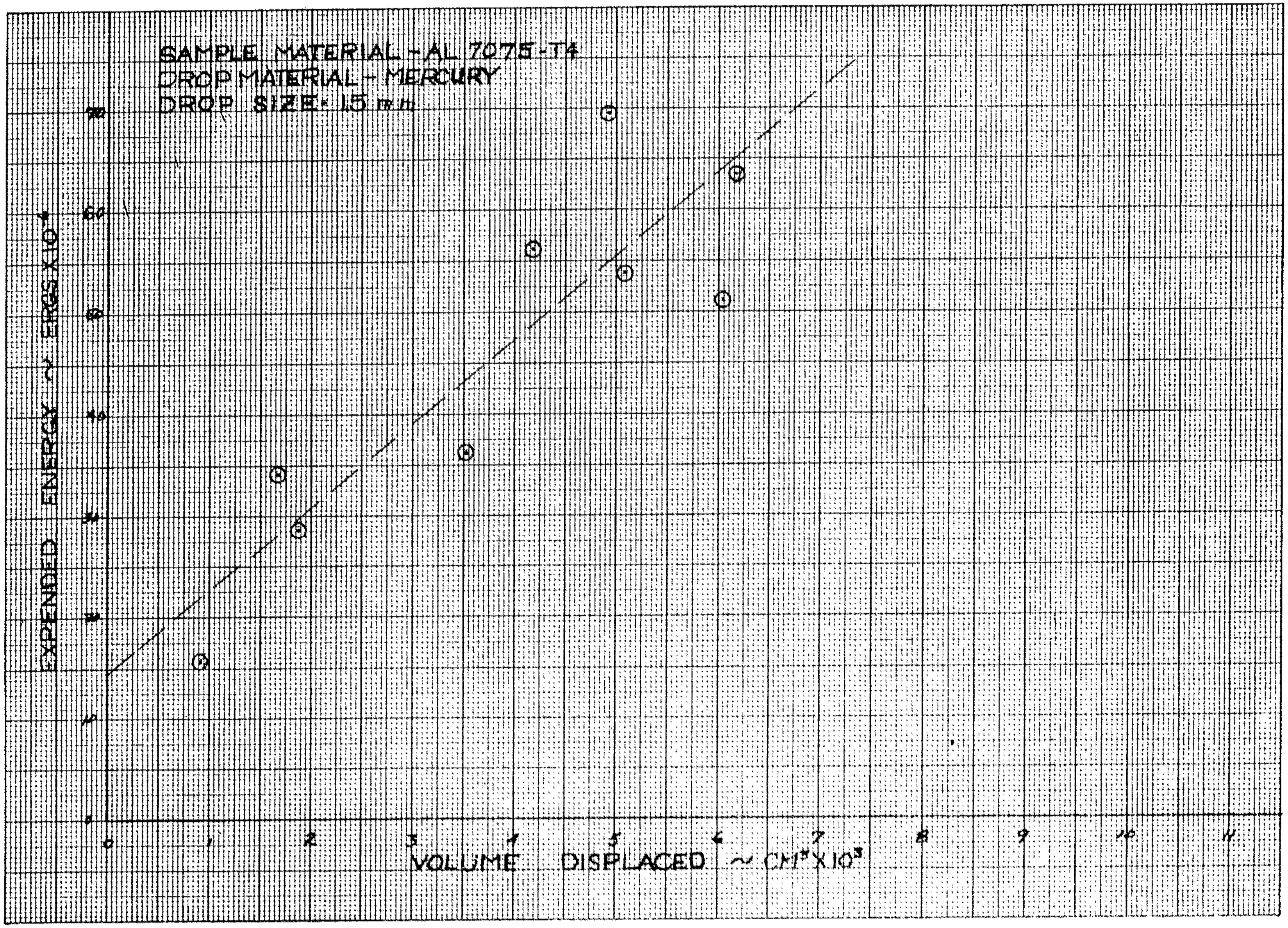

Figure 24. Energy vs Volume - 7075-T4 Aluminum - 1.5 mm Mercury

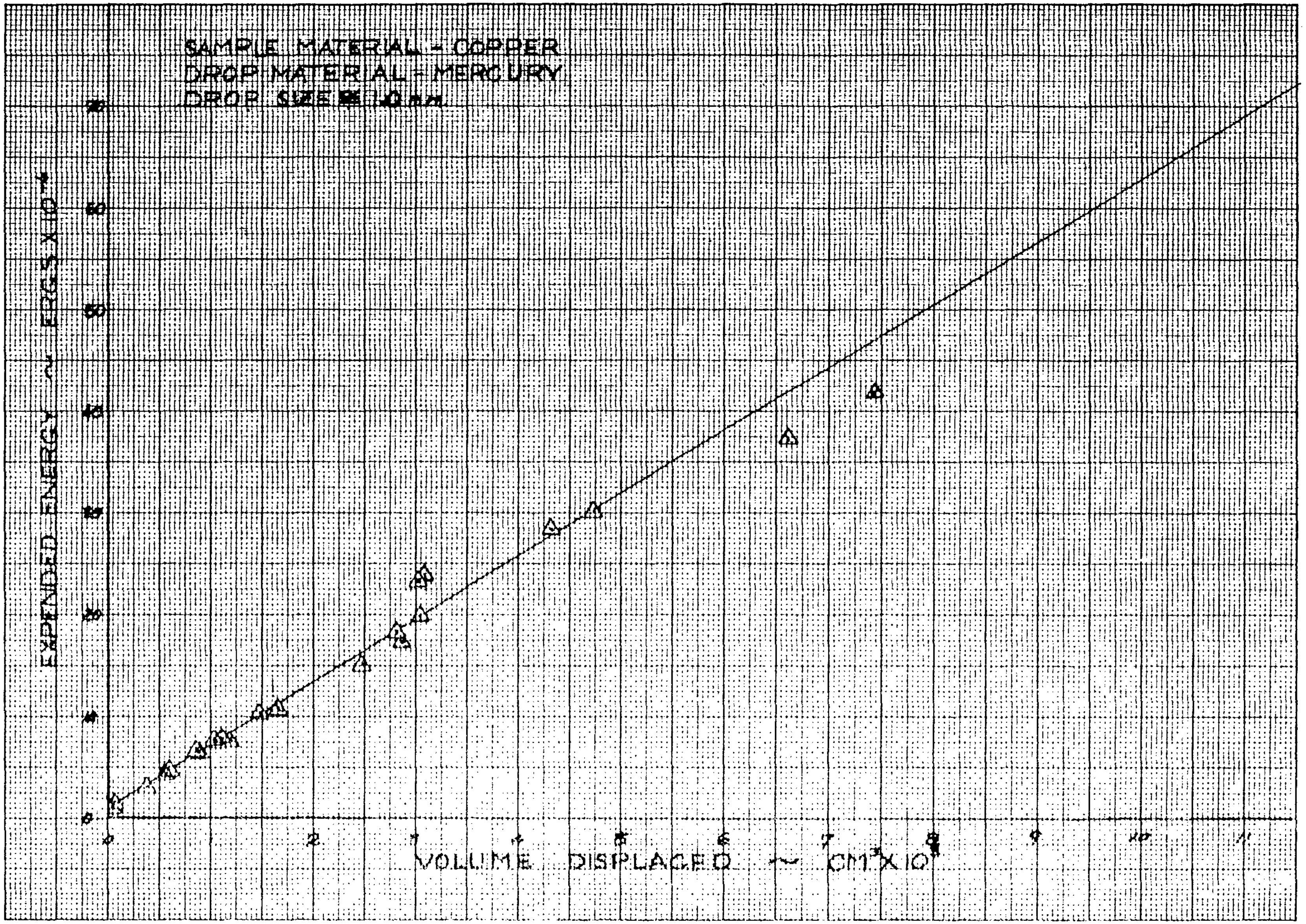

Figure 25. Energy vs Volume - Copper - 1.0 mm Mercury

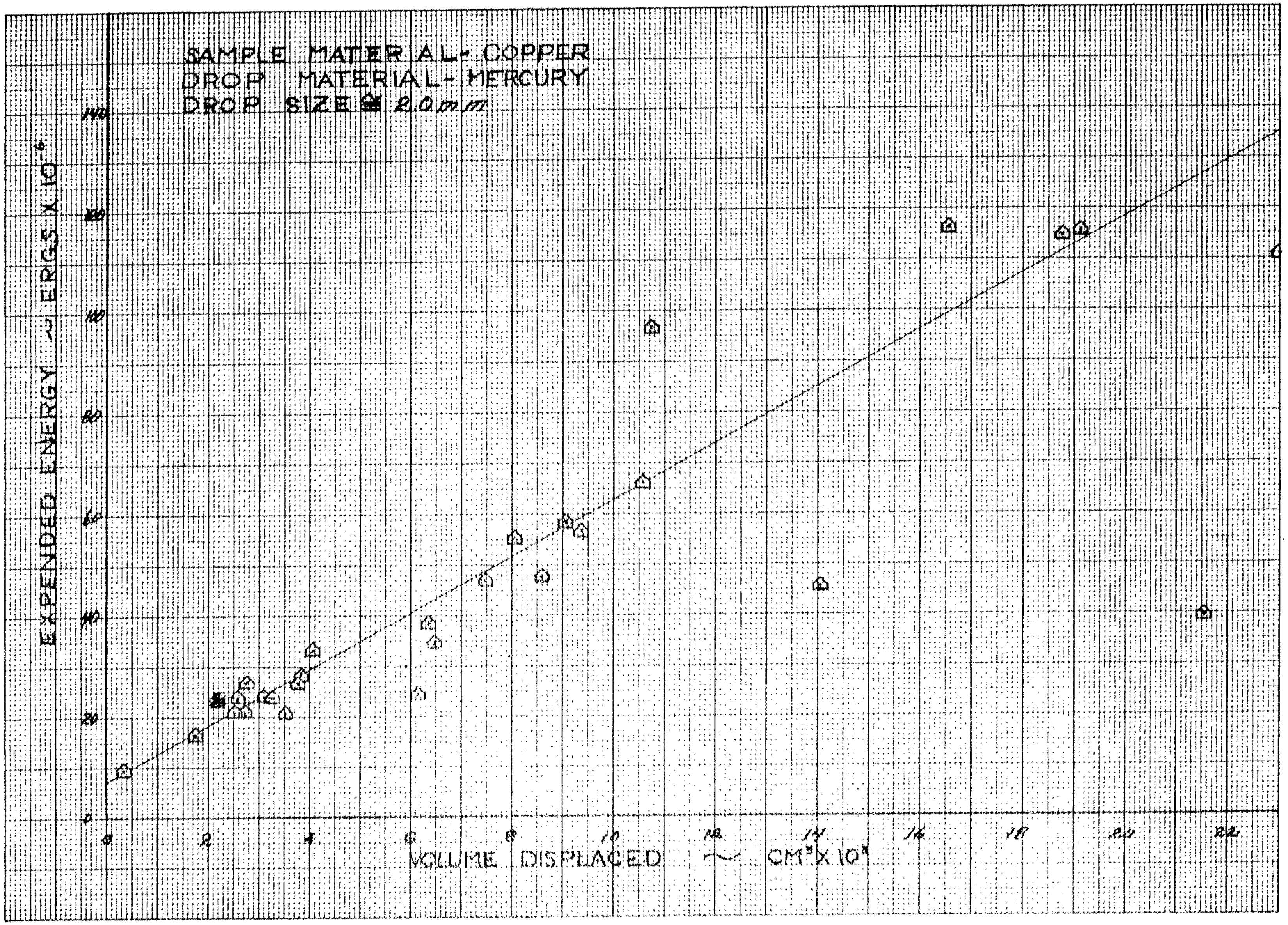

Figure 26. Energy vs Volume - Copper - 2.0 mm Mercury

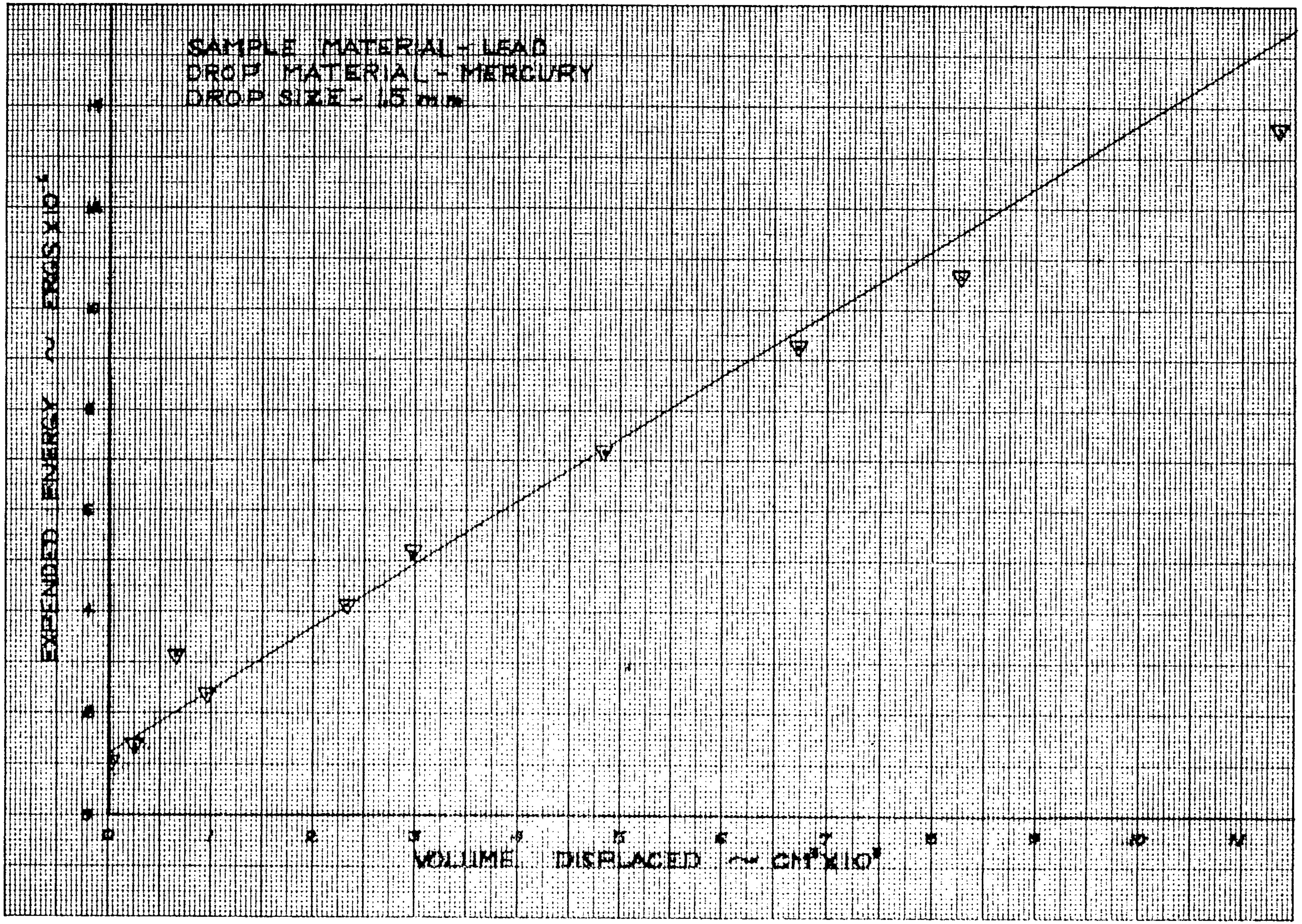

Figure 27. Energy vs Volume - Lead - 1.5 mm Mercury

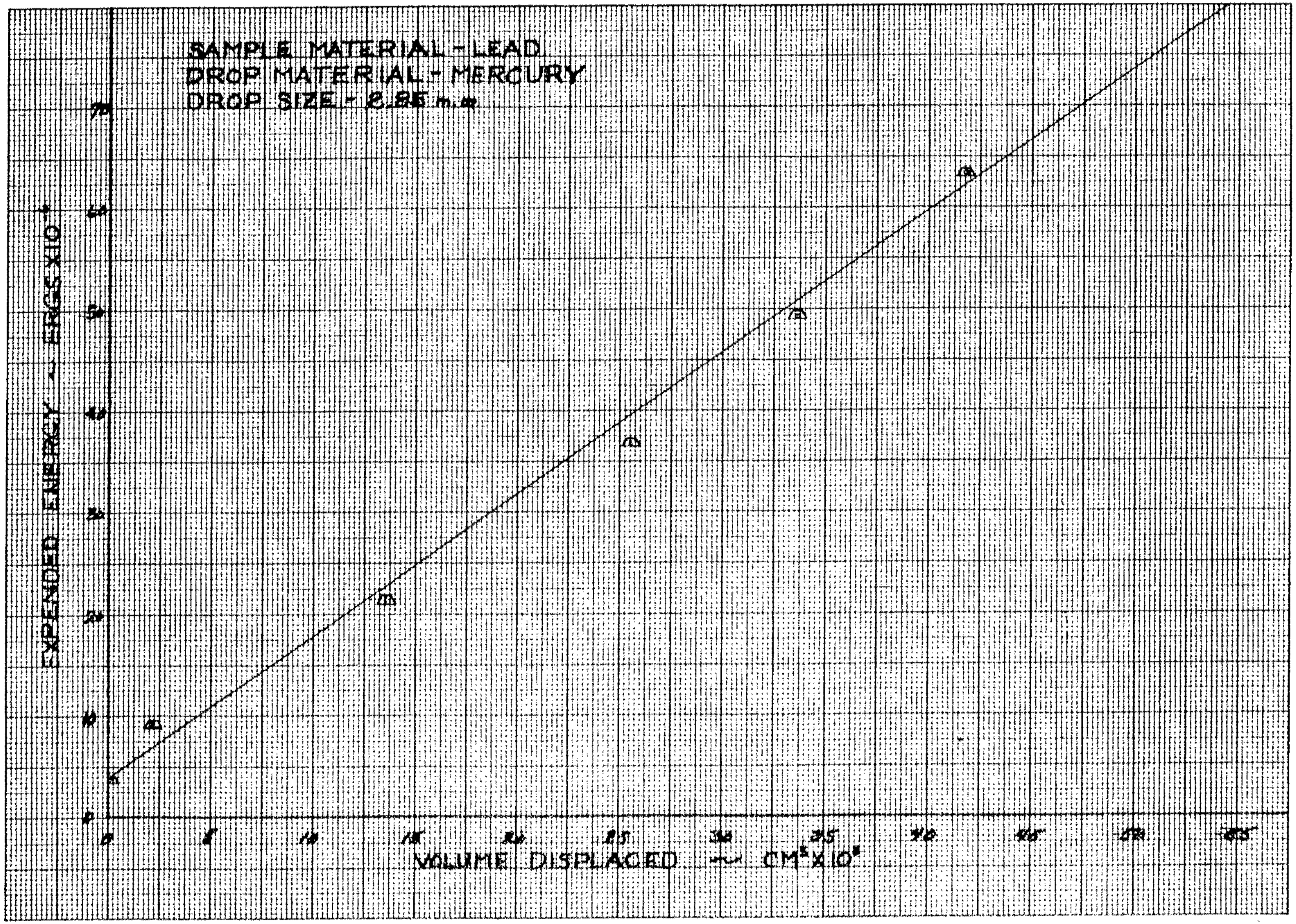

Figure 28. Energy vs Volume - Lead - 2.85 mm Mercury

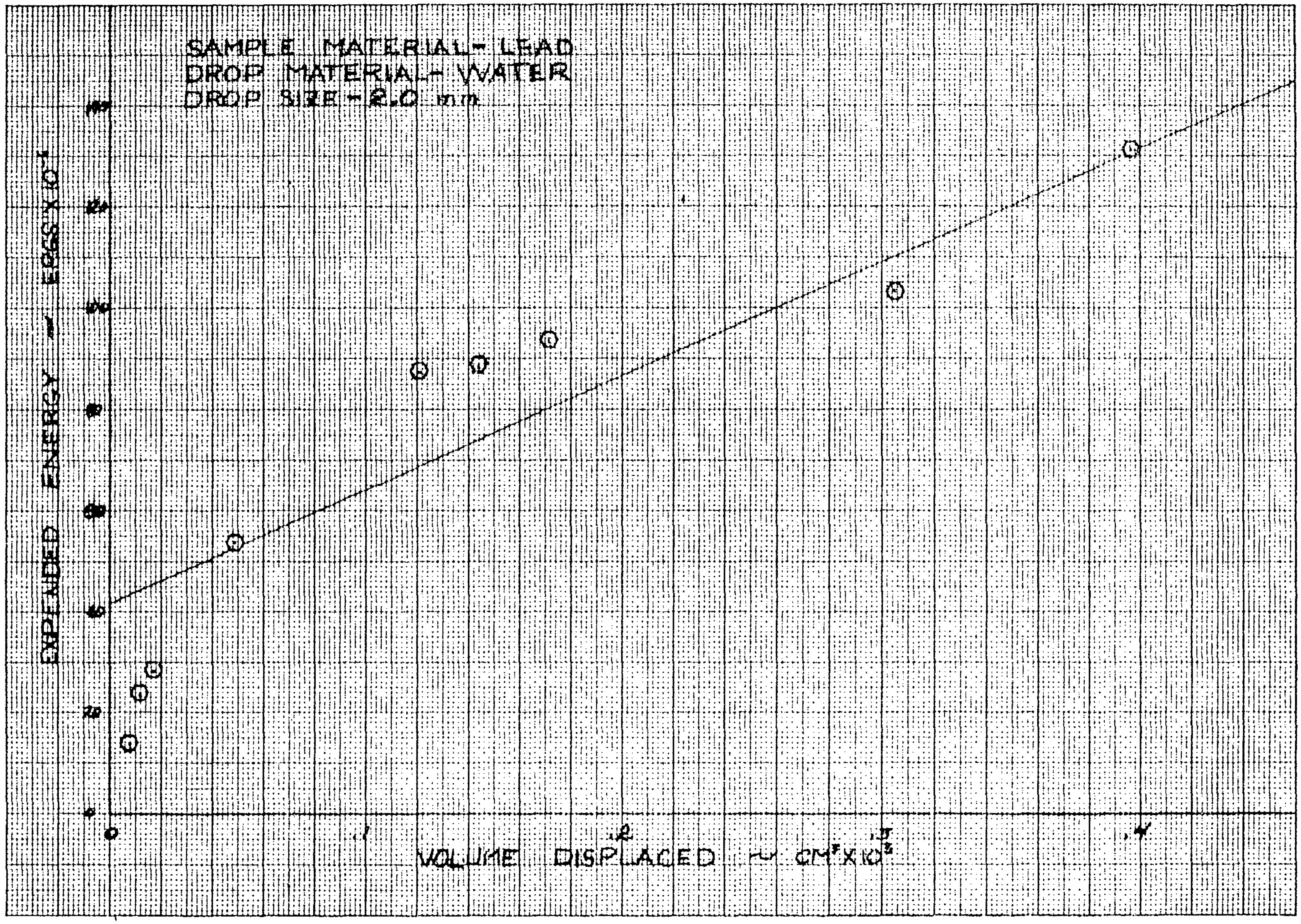

Figure 29. Energy vs Volume - Lead - 2.0 mm Water

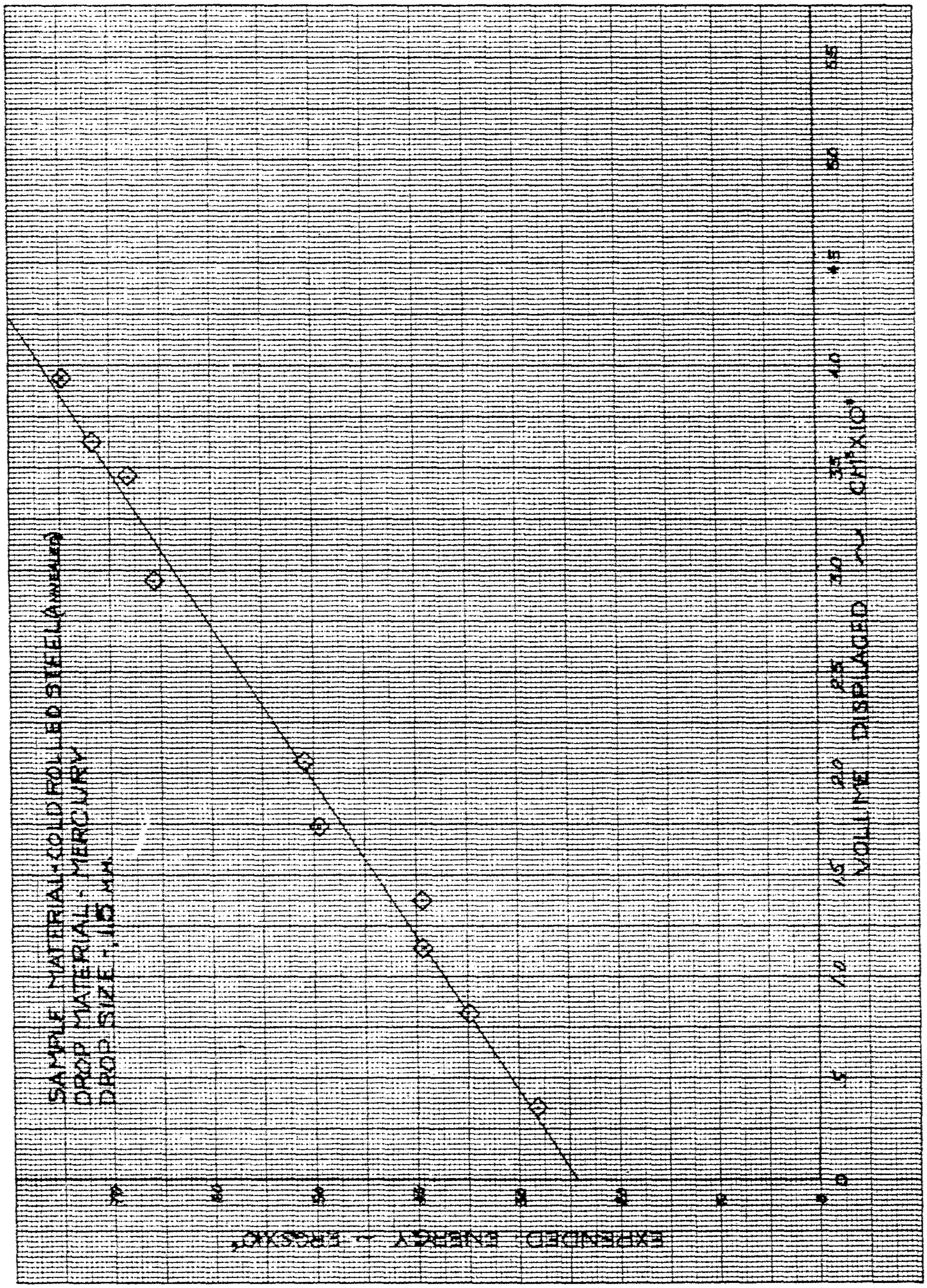

Figure 30. Energy vs Volume - Cold Rolled Steel (Annealed) - 1.5 mm Mercury

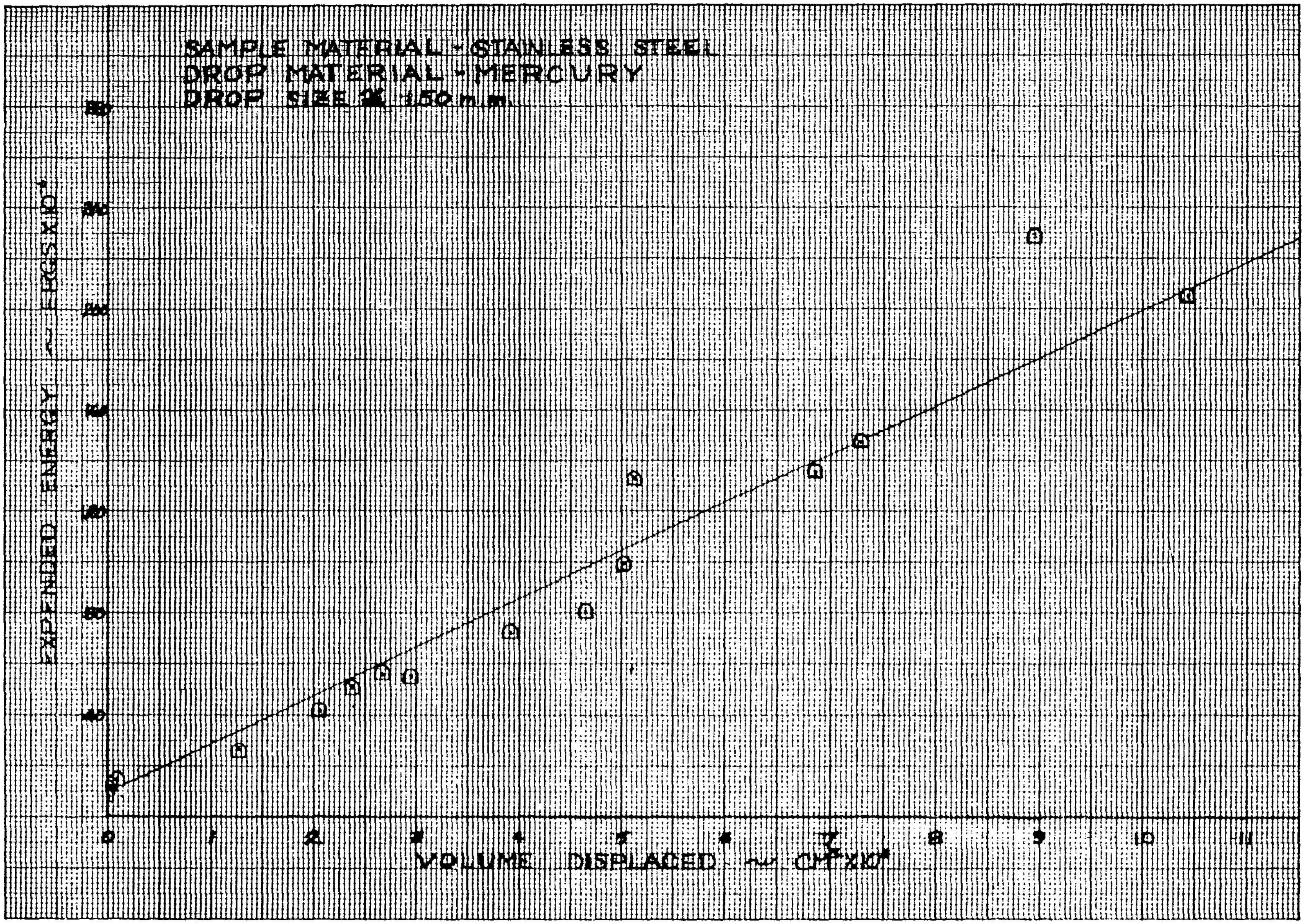

Figure 31. Energy vs Volume - Stainless Steel - 1.50 mm Mercury

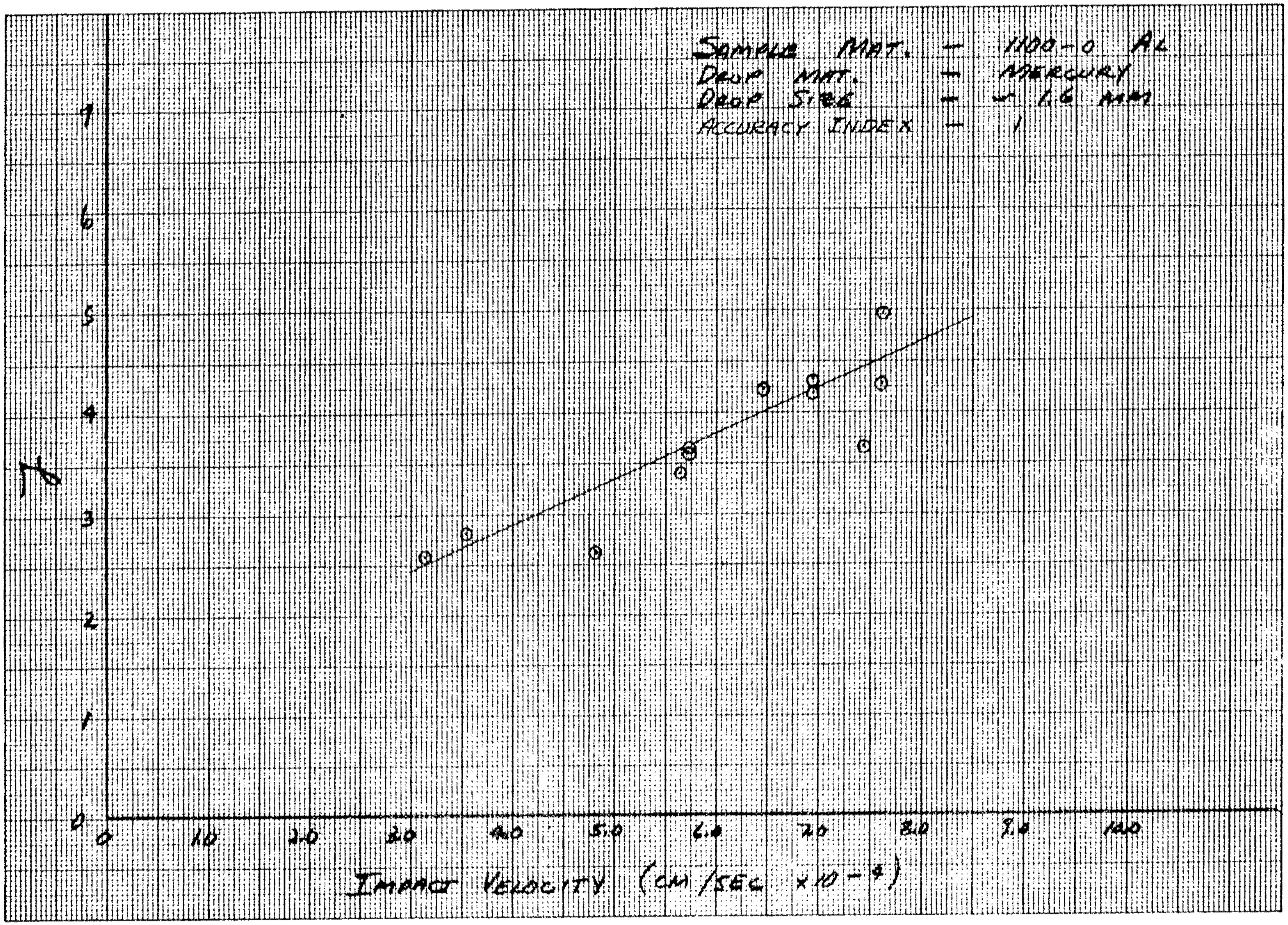

Figure 32. Gamma vs Impact Velocity - 1100-0 Aluminum - 1.6 mm Mercury

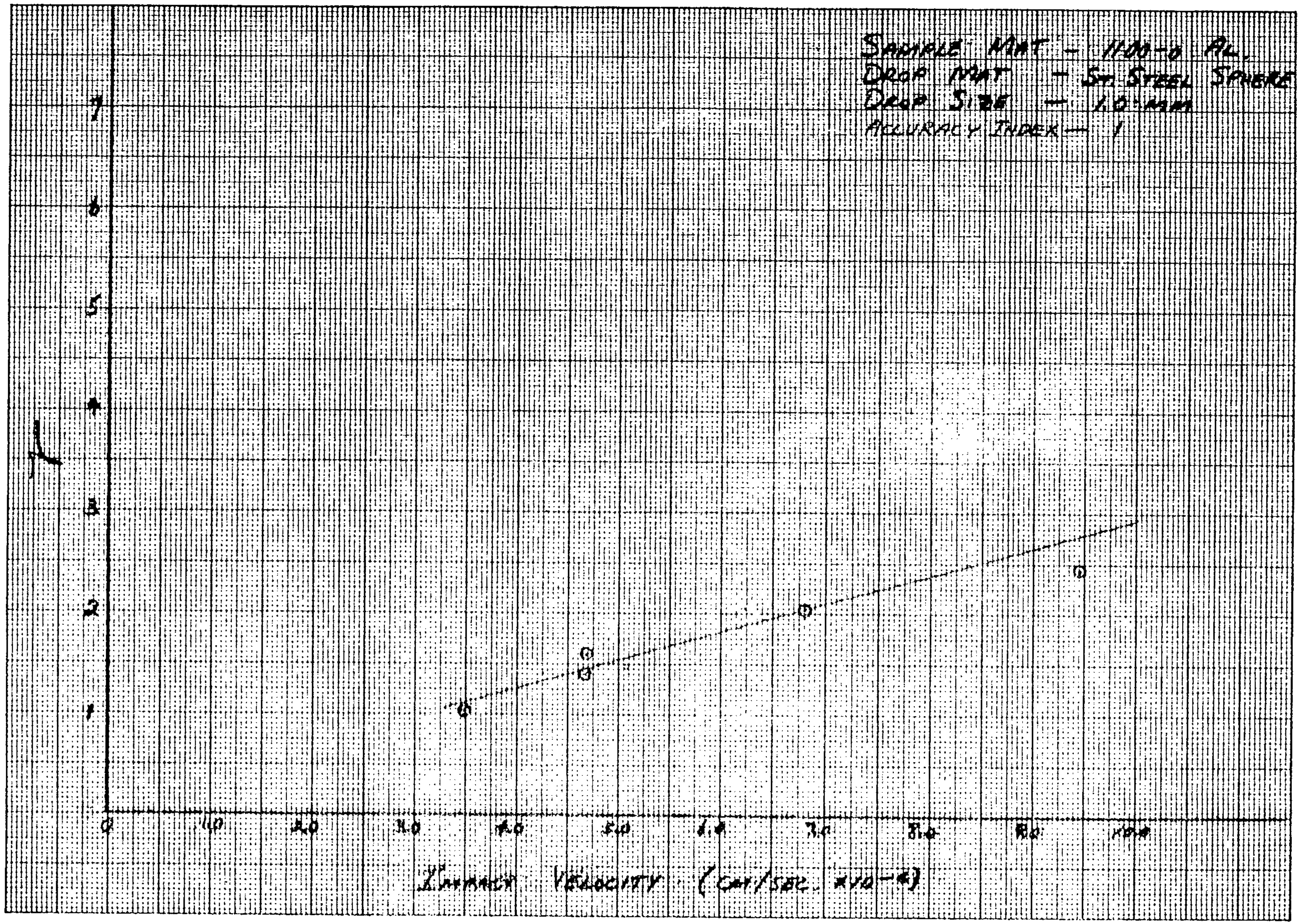

Figure 33. Gamma vs Impact Velocity - 1100-0 Aluminum - 1.0 mm Stainless Steel Sphere

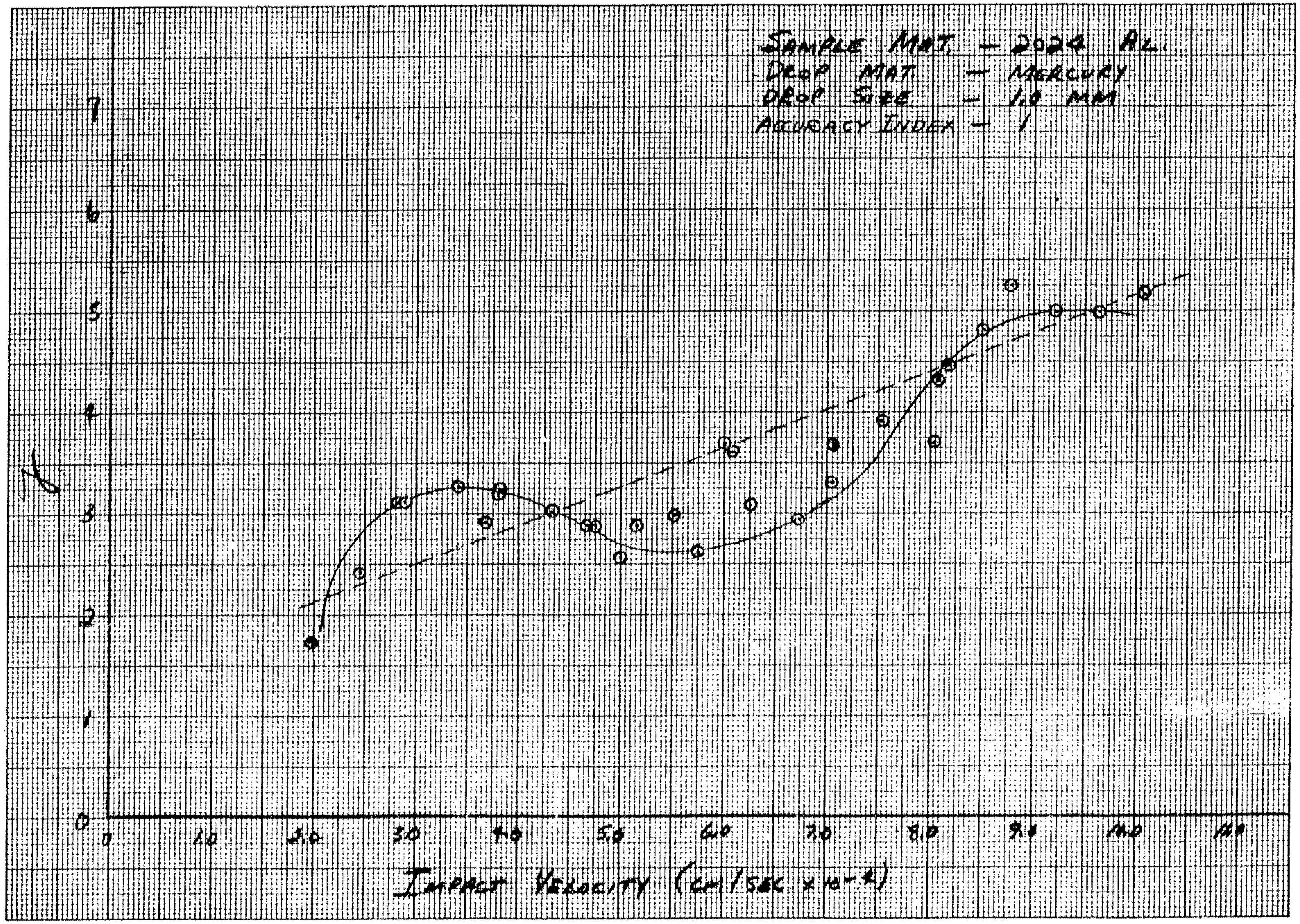

Figure 34. Gamma vs Impact Velocity - 2024 Aluminum - 1.0 mm Mercury

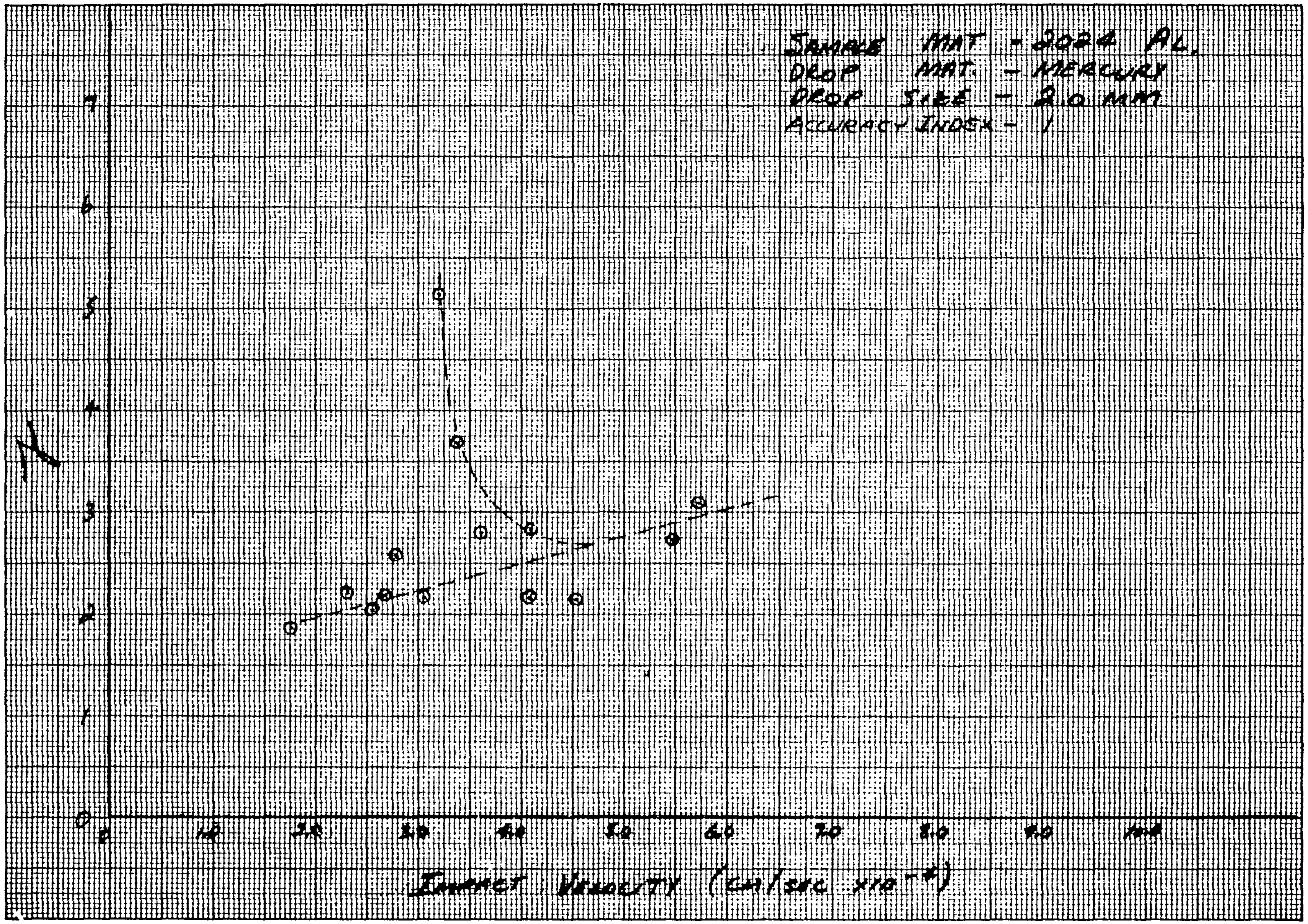

Figure 35. Gamma vs Impact Velocity - 2024 Aluminum - 2.0 mm Mercury

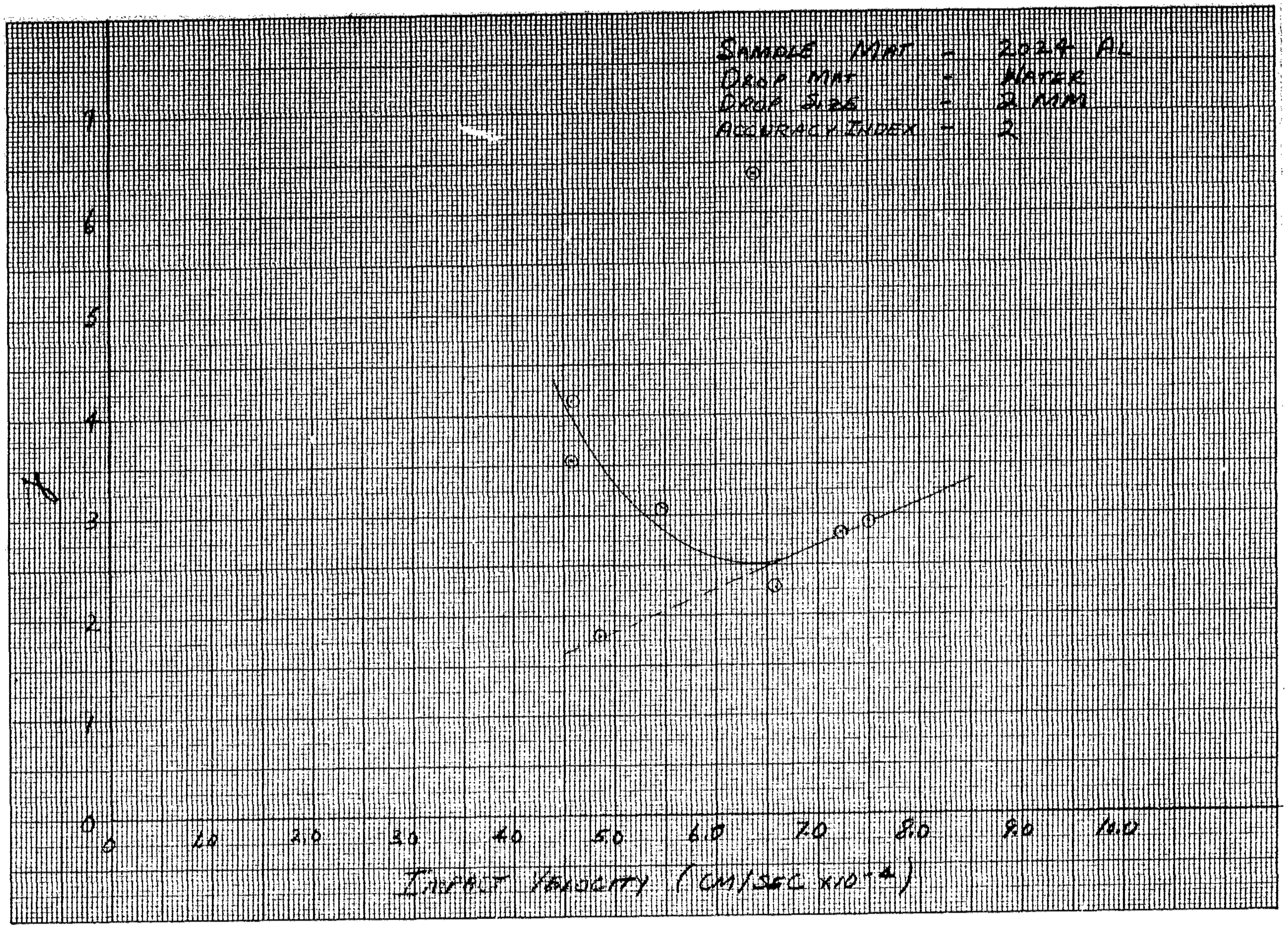

Figure 36. Gamma vs Impact Velocity - 2024 Aluminum - 2.0 mm Water

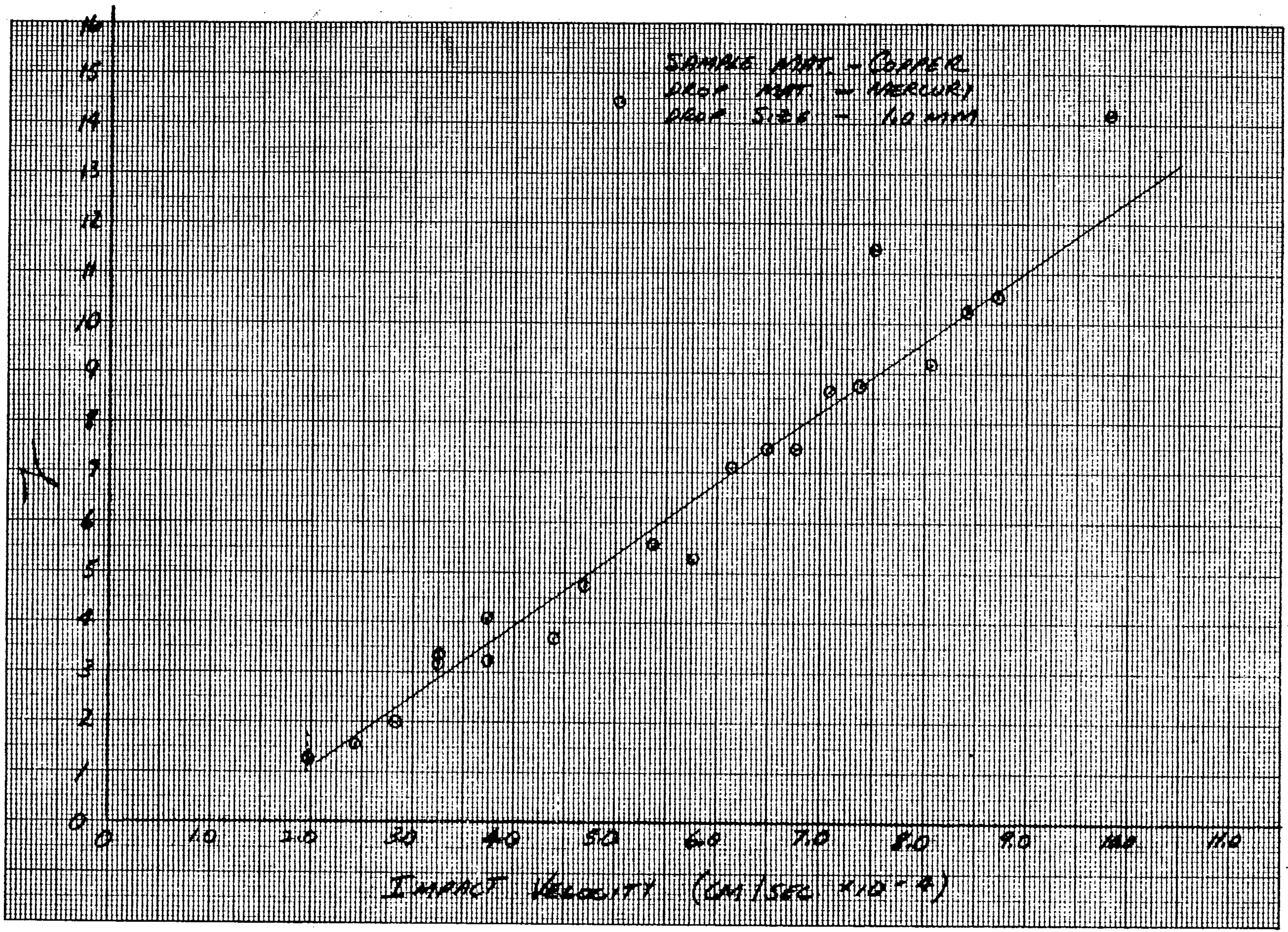

Figure 37. Gamma vs Impact Velocity - Copper - 1.0 mm Mercury

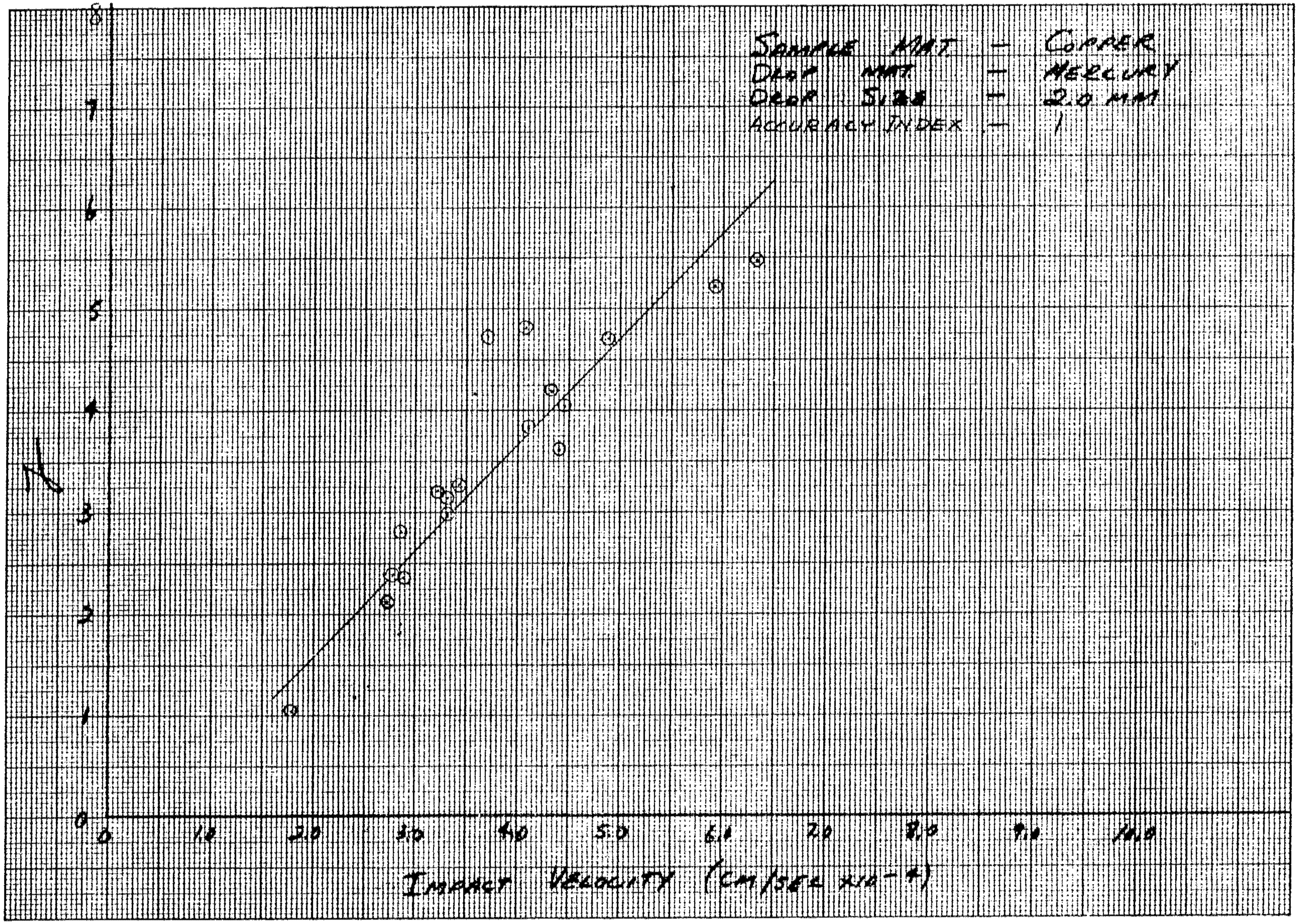

Figure 38. Gamma vs Impact Velocity - Copper - 2.0 mm Mercury

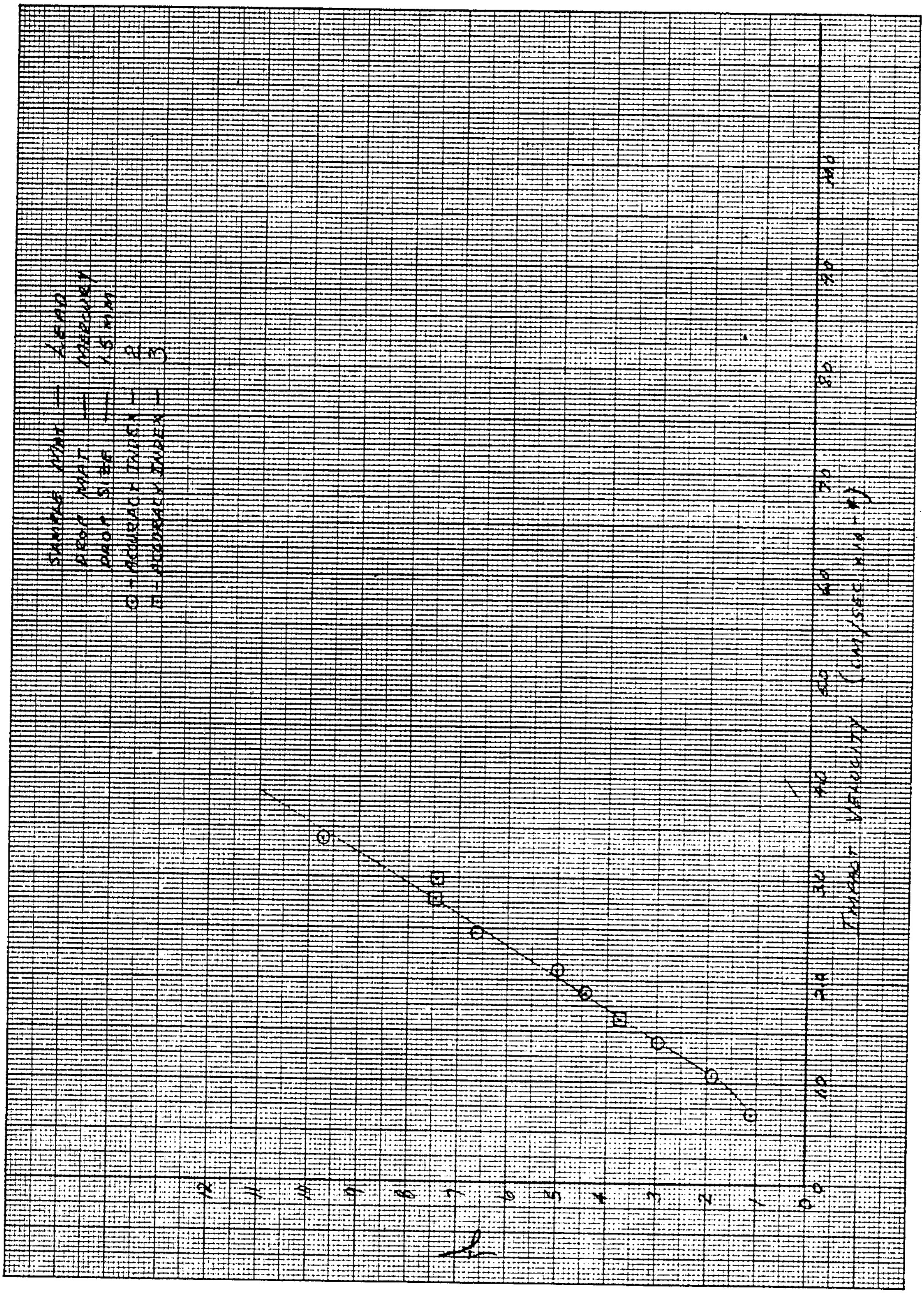

Figure 39. Gamma vs Impact Velocity - Lead - 1.5 mm Mercury

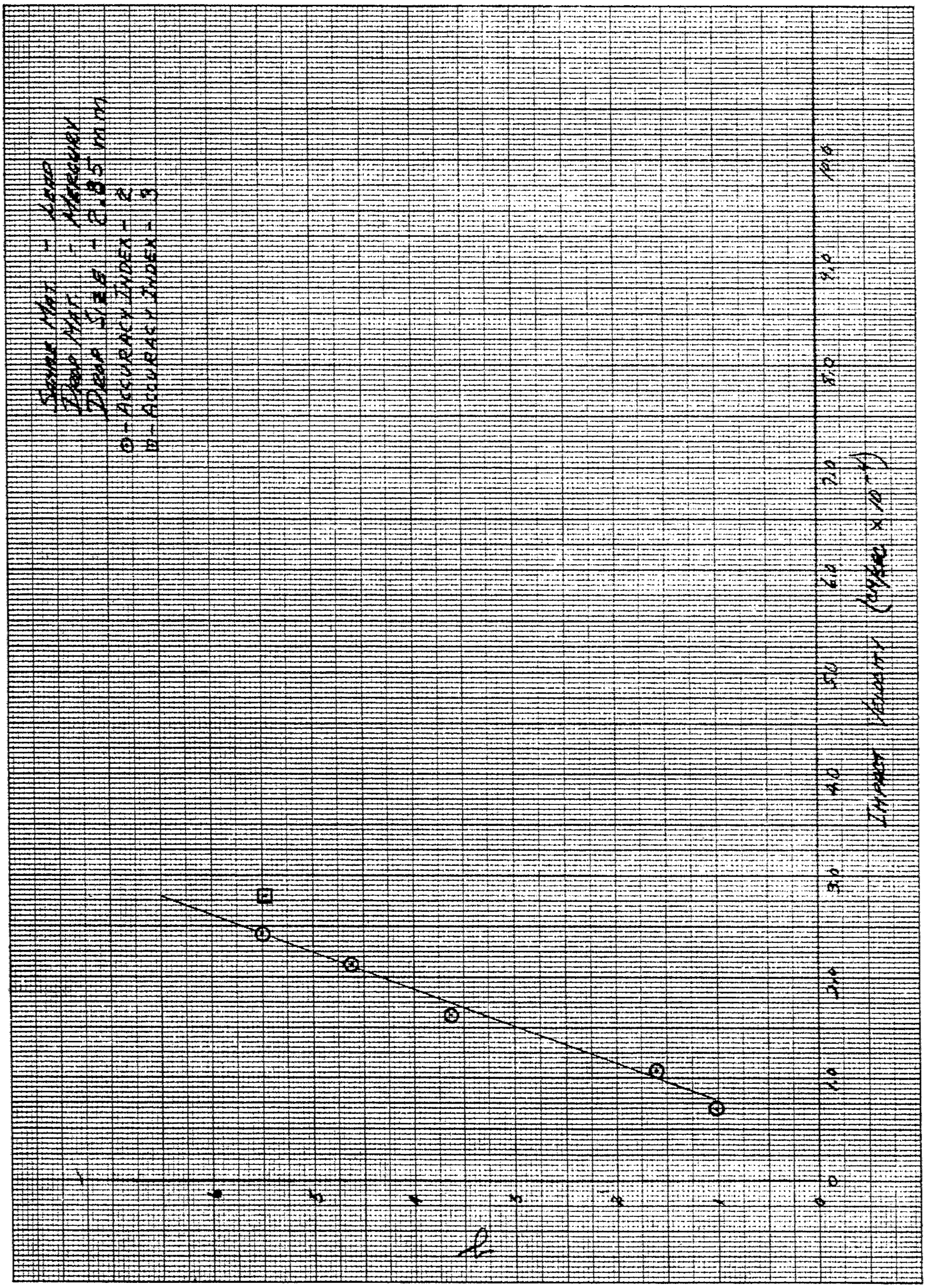

Figure 40. Gamma vs Impact Velocity - Lead - 2.85 mm Mercury

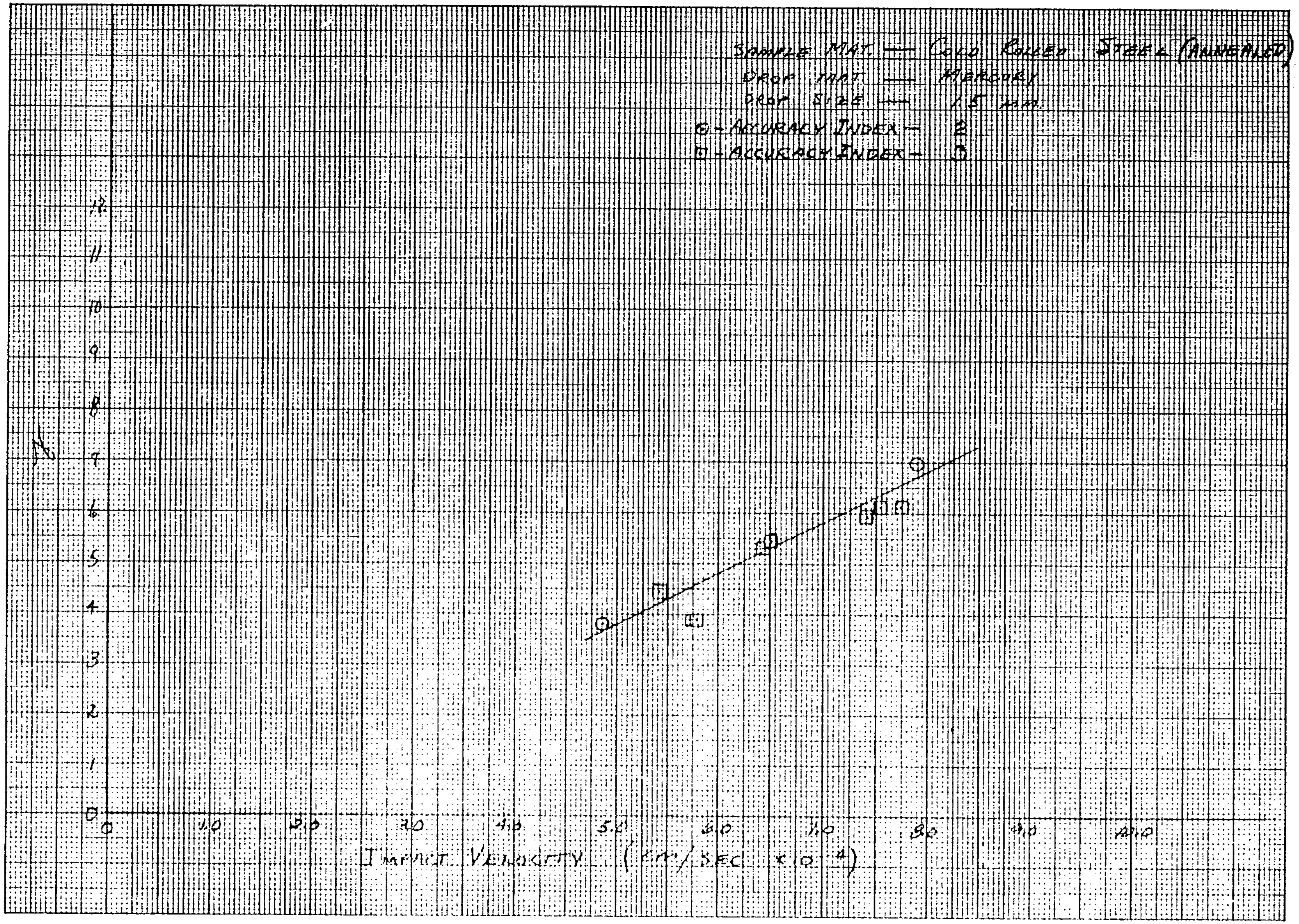

Figure 41. Gamma vs Impact Velocity - Cold Rolled Steel (Annealed) - 1.5 mm Mercury

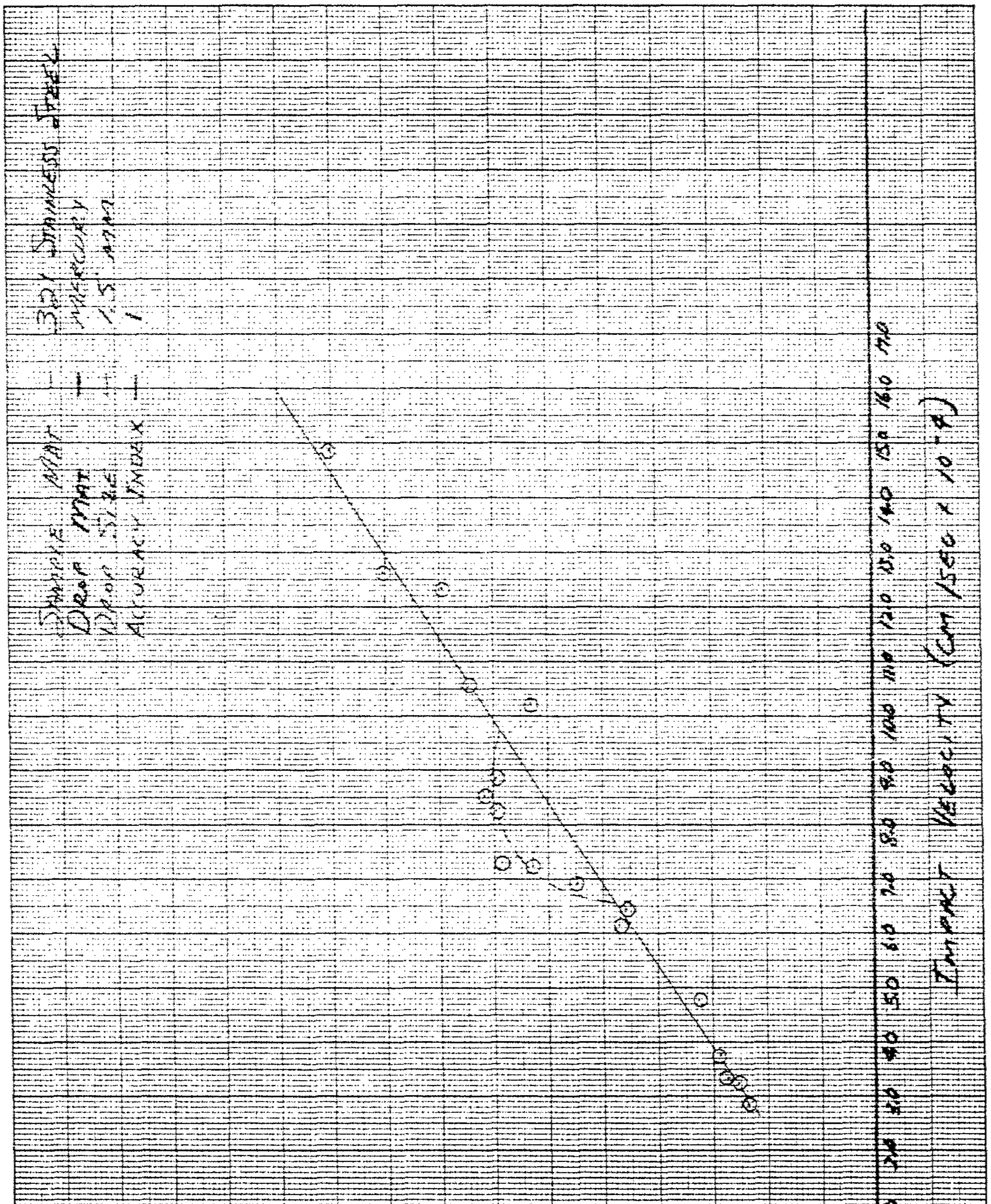

Figure 42. Gamma vs Impact Velocity - 321 Stainless Steel - 1.5 mm Mercury

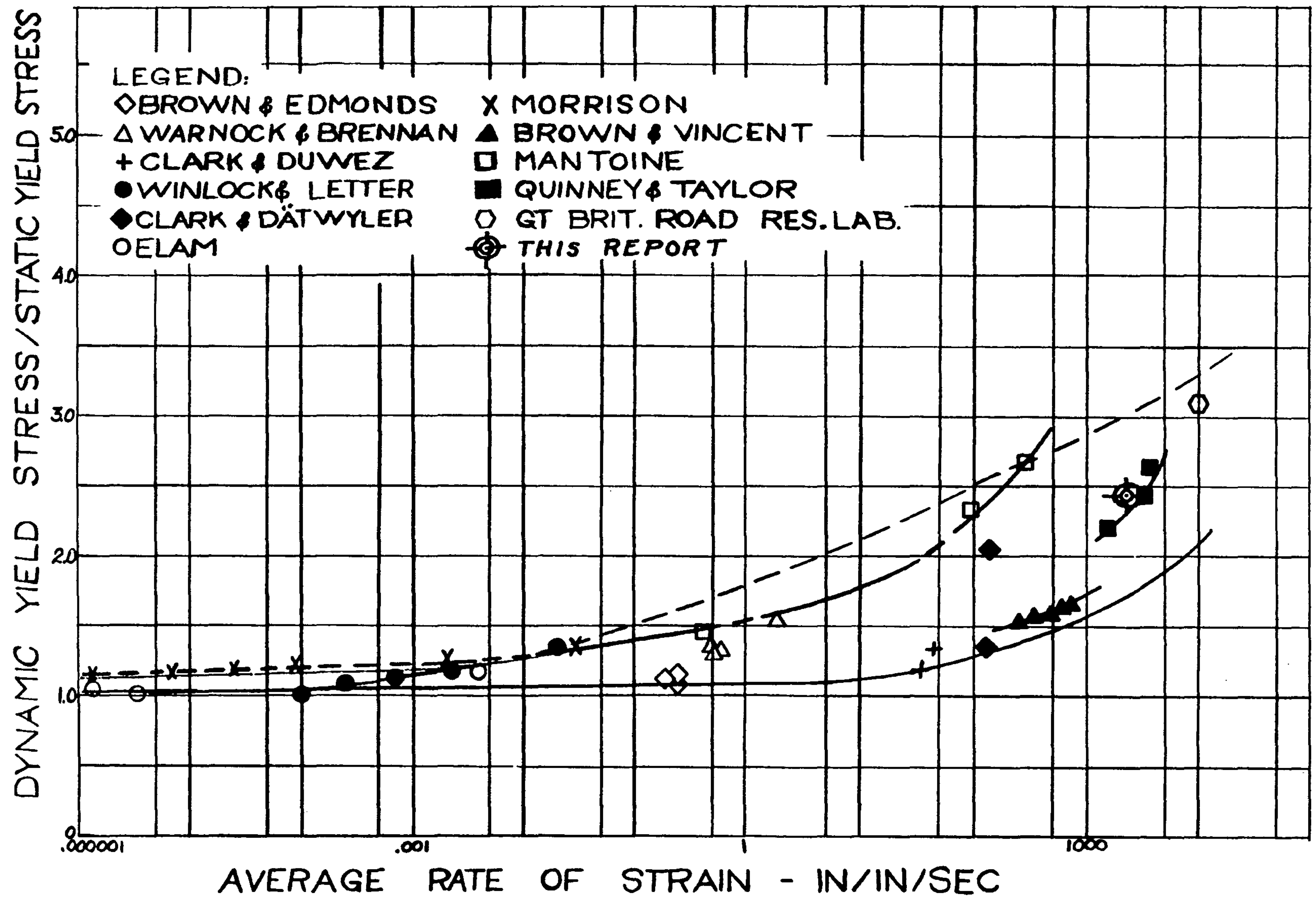

Figure 43. Dynamic Yield Stress/Static Yield Stress vs Average Rate of Strain - Mild Steel

APPENDIX I
ANGLE STUDY DATA AND CALCULATIONS

$\emptyset$	v_o (ft/sec)	x (ft) x 10^3	V_o (ft/sec)	V_o/v_o	$\frac{\sin \emptyset}{(V_o/v_o)}$
30° **	1525	0.671	692	0.454	1.102
30° **	1525	0.750	720	0.472	1.059
30° *	2050	2.88	1021	0.498	1.004
45° **	1477	1.996	1200	0.675	1.047
60° *	1105	2.00	893	0.808	1.072
60° **	1480	2.424	1360	0.919	0.944
75° *	1055	2.41	948	0.899	1.074
75° **	1500	2.875	1520	1.013	0.953
75° **	1562	3.060	1570	1.005	0.962
90° **	1525	2.850	1508	0.989	1.011
90° **	1525	2.929	1530	1.003	0.997
				Average	1.020
				or	
				Approximately	1.00

* 1.5 mm mercury drop tests
** 1.000 mm steel ball bearing tests

$\therefore$ Since $\frac{\sin \emptyset}{V_o/v_o} = 1$

$$V_o = v_o \sin \emptyset$$

or $$v_o = V_o \csc \emptyset$$

where $\emptyset$ = incidence angle (measured from line of travel)

v_o = relative velocity of drop and sample on impact

V_o = equivalent flat plate velocity (i.e., that velocity at which an equal depth indentation would be made in an equivalent flat plate specimen)

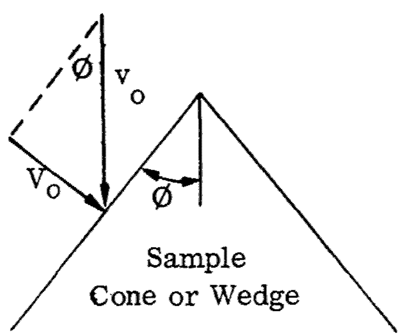

From the diagram, it is seen that the equivalent velocity is equal to the normal component of the impact velocity (i.e., $\sin \emptyset = \frac{V_o}{v_o}$).

APPENDIX II

Derivation of Equations used in the Computation of Energies and Volumes

In the following derivation it was assumed that the 10 mm diameter steel Brinell ball remained spherical during the tests with lead and polyethylene - No effect of ball deflection was included.

The volume of a spherical segment (R = 0.50 cm) is

$$V = \frac{\pi}{3}\, x^2 (3\,R - x) = \frac{\pi}{3}\, x^2 (1.500 - x).$$

It was found that the rate of change of load with penetration depth was constant during any particular test. This rate could be determined by plotting the load vs depth.

$$E_1 = \int_{x_1}^{x_2} F\,dx = \int_{x_1}^{x_2} L\,d\,x\ , \text{ where } L = \text{load.}$$

Since $$L = \int_{x_1}^{x_2} \left(\frac{dL}{dx}\right) d\,x = \left(\frac{dL}{dx}\right)_{\text{constant}} X \qquad (x_1 = 0)$$

$$\therefore \qquad E_1 \text{ (Load Varying)} = \frac{X^2}{2}\left(\frac{dL}{dx}\right)_{\text{constant}}$$

At the point where the load just becomes constant, L_o,

$$E_o = \int_o^{x_o} L_o\,d\,x = \frac{X_o^{\ 2}}{2}\left(\frac{dL}{d\,x}\right)_{\text{const.}}$$

Then $$E_2 = E_o + \int_{x_o}^{x} L_o\ d\,x$$

or $$E_2 - E_o = L_o (X - X_o)$$

Because $$L_o = X_o \left(\frac{dL}{dx}\right)_{\text{const.}}$$

$$E_2 = L_o\left(X - \frac{X_o}{2}\right)$$, where E_2 equals the damage energy when the load remains constant.

CONVAIR, San Diego, California - A STUDY OF RAIN EROSION TESTING METHODS FOR SUPERSONIC SPEEDS, by Donald E. Hurd and R. F. Holmes May 1959. 94p. incl. illus. tables. (Project 7340; Task 73400)(WADC TR 53-173 Pt VI) (Contract AF 33(616)-3421)

Unclassified report

To better understand the mechanism by which materials passing through rain at supersonic speeds are damaged, the results of numerous types of impacts on metals were analyzed. An equation which relates total energy of impacts to the volume of metal displaced was derived and found adequate to explain damage in the velocity range from less than one

(over)

UNCLASSIFIED

UNCLASSIFIED

foot per hour to greater than Mach 3. This equation together with results of incidence angle tests led to an over-all damage equation which was successfully applied to the problem of multiple drop rain damage. Principal parameters are target material tensile strength; impacting material shape and mass; angle of incidence; and the velocity of impact.

UNCLASSIFIED

UNCLASSIFIED

CONVAIR, San Diego, California - A STUDY OF RAIN EROSION TESTING METHODS FOR SUPERSONIC SPEEDS, by Donald E. Hurd and R. F. Holmes May 1959. 94p. incl. illus. tables. (Project 7340; Task 73400)(WADC TR 53-173 Pt VI) (Contract AF 33(616)-3421)

Unclassified report

To better understand the mechanism by which materials passing through rain at supersonic speeds are damaged, the results of numerous types of impacts on metals were analyzed. An equation which relates total energy of impacts to the volume of metal displaced was derived and found adequate to explain damage in the velocity range from less than one

(over)

UNCLASSIFIED

UNCLASSIFIED

foot per hour to greater than Mach 3. This equation together with results of incidence angle tests led to an over-all damage equation which was successfully applied to the problem of multiple drop rain damage. Principal parameters are target material tensile strength; impacting material shape and mass; angle of incidence; and the velocity of impact.

UNCLASSIFIED

UNCLASSIFIED

CONVAIR, San Diego, California - A STUDY OF RAIN EROSION TESTING METHODS FOR SUPERSONIC SPEEDS, by Donald E. Hurd and R. F. Holmes. May 1959. 94p. incl. illus. tables. (Project 7340; Task 73400)(WADC TR 53-173 Pt VI) (Contract AF 33(616)-3421)

Unclassified report

To better understand the mechanism by which materials passing through rain at supersonic speeds are damaged, the results of numerous types of impacts on metals were analyzed. An equation which relates total energy of impacts to the volume of metal displaced was derived and found adequate to explain damage in the velocity range from less than one

(over)

UNCLASSIFIED

UNCLASSIFIED

foot per hour to greater than Mach 3. This equation together with results of incidence angle tests led to an over-all damage equation which was successfully applied to the problem of multiple drop rain damage. Principal parameters are target material tensile strength; impacting material shape and mass; angle of incidence; and the velocity of impact.

UNCLASSIFIED

UNCLASSIFIED

CONVAIR, San Diego, California - A STUDY OF RAIN EROSION TESTING METHODS FOR SUPERSONIC SPEEDS, by Donald E. Hurd and R. F. Holmes May 1959. 94p. incl. illus. tables. (Project 7340; Task 73400)(WADC TR 53-173 Pt VI) (Contract AF 33(616)-3421)

Unclassified report

To better understand the mechanism by which materials passing through rain at supersonic speeds are damaged, the results of numerous types of impacts on metals were analyzed. An equation which relates total energy of impacts to the volume of metal displaced was derived and found adequate to explain damage in the velocity range from less than one

(over)

UNCLASSIFIED

UNCLASSIFIED

foot per hour to greater than Mach 3. This equation together with results of incidence angle tests led to an over-all damage equation which was successfully applied to the problem of multiple drop rain damage. Principal parameters are target material tensile strength; impacting material shape and mass; angle of incidence; and the velocity of impact.

UNCLASSIFIED

UNCLASSIFIED